NORTHWESTERN UNIVERSITY

Mathematical modeling of structure formation in angiogenesis

A DISSERTATION

SUBMITTED TO THE GRADUATE SCHOOL

IN PARTIAL FULFILLMENT OF THE REQUIREMENTS

for the degree

DOCTOR OF PHILOSOPHY

Field of Applied Mathematics

By

Anna Tikhomirov

EVANSTON, ILLINOIS

December 2007

ABSTRACT

Mathematical modeling of structure formation in angiogenesis

Anna Tikhomirov

Angiogenesis, the formation of blood vessels from a pre-existing vasculature, is a process whereby capillary sprouts are formed in response to chemical stimuli that can be either supplied externally or produced locally. Understanding of the fundamental mechanisms that govern angiogenesis suggests a powerful therapeutic approach that will allow to combat a variety of severe pathological conditions. The development of *in-vitro* angiogenesis provides researches with controllable tool that helps study blood vessel formation. We model endothelial cell pattern formation *in-vitro* as the first step in understanding angiogenesis and multiple factors that influence it. We formulate a mathematical model that governs endothelial cell pattern formation on a biogel surface using a five-species reaction mechanism and justify its reduction to a two-species problem. We study this simplified problem with two different forms of cell diffusion coefficient both numerically and analytically to determine whether spatially nonuniform steady patterns can appear in the system when its basic states become unstable.

We perform linear stability analysis and weakly nonlinear stability analysis near the instability threshold to describe formation of certain spatial structures observed in experiments and to determine the parameter ranges where these structures can occur. We derive amplitude equations that govern the interaction of hexagonal and stripe patterns. We also derive the Sivashinsky and Cahn-Hilliard equations.

Next we formulate a discrete-continuous mathematical model of angiogenesis *in-vivo* and perform numerical simulations of the model. The model accounts for both a continuous chemoattractant field and a discrete set of growing sprouts, propagation of which is governed by prescribed laws that involve both deterministic and random ingredients. We extend the previous model by introducing the action of repulsive factors and we show that their activity results in a larger degree of reorganization of cellular matter and in a more robust control over the size of the growing vascular network. The numerical results demonstrate new vessel growth towards the source of the growth factor and provide an insight into capillary network formation.

Acknowledgments

I would like to thank my advisor, Professor Vladimir Volpert, for giving me an opportunity to work on this project and helping me in every possible way.

I also thank Professor Alvin Bayliss for very useful discussions and help with numerical simulations, and my Ph.D. committee members, Professors Alvin Bayliss, Alexander Golovin, and Vladimir Volpert for taking time to read my thesis.

I am grateful to all ESAM faculty members whose courses I have taken: Professors David Chopp, Edward Olmstead, Moshe Matalon, Michael Miksis, Alexander Golovin, Vladimir Volpert, Mary Silber and Hermann Riecke.

I am thankful to Margo Levine, Alexander Golovin and Vladimir Volpert for helpful advises and inspiring conversations during my job search. I also thank Professors Alexander Golovin, Edward Olmstead and Vladimir Volpert for writing recommendation letters for me.

Also I would like to thank my parents, Natalia Lipilina and Edward Litvin, and my husband, Sergey, for their help and support during these five years that actually made possible my work towards the degree.

And of course, I need to thank my sons, Vsevolod and Alexander, for their love.

Table of Contents

List of Figures

CHAPTER 1

Introduction

1.1. The process of angiogenesis

New vessels inside the body originate as capillaries, which sprout from existing small vessels. This phenomenon of angiogenesis is a natural process which occurs in response to specific signals. It normally takes place during certain developmental stages of embryogenesis, healing of tissue injury (like external or internal wound) or in response to other kind of tissue offense. It also occurs in women during both the monthly reproductive cycle and during pregnancy.

In all these cases growth of new blood vessels respond to certain chemical stimuli produced by the tissue that they invade [4]. The signals are complex, but the key part is played by a protein know as vascular endothelial growth factor (VEGF). Now it is well documented that the regulation of new blood vessel growth or decay to satisfy the needs of the tissue depends on the control of VEGF production [4, 76, 93, 96]. Under normal physiological conditions VEGF production is balanced and therefore angiogenesis almost does not take place in normal tissues, except in the cases mentioned above.

However, it does occur under many pathological processes such as rheumatoid arthritis, psoriasis, cerebral ischemia, cardiovascular disease, growth of solid tumors, soft tissue sarcomas, chronic liver disease and others [20, 50, 88, 92, 141, 141, 146, 173, 175, 177, 178, 181].

Angiogenesis plays a crucial role in so many human diseases that scientists believe that angiogenic therapy will completely change the way the diseases are ultimately treated. Understanding

of the fundamental mechanisms that govern angiogenesis can provide us with a powerful therapeutic tool that will enable us to combat a variety of severe pathological conditions. Our ability to manipulate new blood vessel growth, stimulating or preventing it according to patient's needs can become a triumph of modern medicine, significantly lengthening the list of curable diseases [17, 23, 26, 35, 54, 55, 62, 70, 75, 86, 91, 92, 146, 166, 177, 187, 188]

1.2. Therapeutic applications

1.2.1. Pro-angiogenic therapy

1.2.1.1. Cardiovascular disease. Cardiac ischemia occurs when a coronary artery is partially or completely obstructed, such as due to atherosclerosis. This reduces blood flow to the heart muscle (myocardium). Cardiac ischemia can be life-threatening. A sudden, severe blockage of a coronary artery may lead to death of part of the heart muscle (heart attack). Cardiac ischemia may also cause an abnormal heart rhythm (arrhythmia), which can lead to fainting or even sudden death. People who suffer from cardiac ischemia could significantly benefit from growth of new blood vessels to the heart. One of the approaches that cardiology researchers are taking is to induce angiogenesis in the ischemic tissue. They are trying to promote new blood vessel growth to repair damaged heart and otherwise ischemic tissue [70, 87, 153].

1.2.1.2. Wound healing. Wound healing has been most closely studied in skin. Skin is composed of an outer layer called epidermis and an inner layer called dermis. The dermis contains living cells, blood vessels, nerves and protein fibers, while the epidermis consists of mostly dead cells which move upward from the dermis. The simplest situation of wound occurring in the skin is created by a cut through the epidermis into the dermis or when parts of the epidermis are removed [140].

Growth of new blood vessels is necessary to supply the damaged tissue with oxygen and nutrients so the healing could take place (see Fig.1.1).

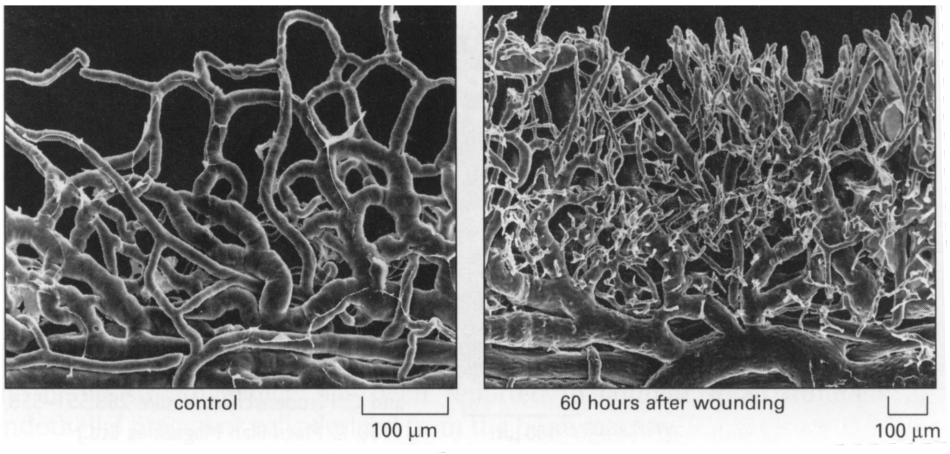

FIGURE 1.1. **New capillary formation in response to wounding.** Scanning electron microscopy of blood vessels surrounding the margin of the cornea shows the reaction to wounding. Sixty hours after wounding many new capillaries have begun to sprout towards the site of injury, which is just above the top of the picture. Their oriented outgrowth reflects a chemotactic response of the endothelial cells to an angiogenic factor released at the wound [4].

Experiments have shown that there exists a negative feedback mechanism that controls development of new capillary network [129]. When the concentration of oxygen is at low level certain chemical substances that have the capacity to stimulate new vessel growth and collagen deposition (such as VEGF and transforming growth factor- β) are released at the wound site. Many experiments have suggested that the generation of new blood vessels within the wounded area is stimulated and maintained as long as the growth factors are present. It was also found that insufficient blood supply affects the wound healing process as a whole, moreover, the rate of wound healing depends on oxygen supply [113]. Patients with delayed healing (the case of chronic wounds) suffer from infection and gangrene often necessitating limb amputation. Promoting angiogenesis in a wound could accelerate healing and circumvent the risk of amputation.

1.2.1.3. Stroke. Ischemic stroke is a leading cause of human death and disability. A stroke or ”brain attack” occurs when a blood clot blocks an artery (a blood vessel that carries blood from the heart to the body) or a blood vessel breaks, interrupting blood flow to an area of the brain. When either of these things happens, brain cells begin to die and brain damage occurs. When brain cells die during a stroke, functions controlled by that area of the brain are lost. Although stroke survivors may gain spontaneous partial functional recovery, they often suffer from sensory-motor dysfunctions, behavioral/neurological alterations, and various degrees of paralysis.

Increasing attention has been focused on potential strategies of promoting tissue repair and functional recovery in the damaged post-ischemic brain. Angiogenesis may contribute to cell survival and functional recovery of the area of insult, helping reduce neurological disabilities and preserve neurological function of the brain. The study of angiogenesis will increase the understanding of the mechanism underlying post-ischemia neurovascular plasticity and regeneration [210].

1.2.1.4. Tissue engineering. Another field where angiogenesis seems to play a central role has to do with tissue engineering and biomaterial applications. Before complete organs such as a kidney or liver can be produced, engineers must be able to manufacture the blood vessels required to properly distribute the nutrients these organs need to survive and function. Growth and functioning of the organ- or tissue-specific cells on the biomaterial is an important issue. However, in most cases a successive outcome is entirely dependent on a proper vascularization after implantation, which remains one of the major challenges in tissue engineering [110, 111, 211]. Implantation involves tissue trauma, which evokes an inflammatory response, coupled to a wound healing reaction, involving angiogenesis, fibroblast activation and local tissue remodeling. *In-vitro* studies of angiogenesis provide some insight on the regulation of the inflammatory and angiogenic response after implantation. They are an important contribution to understanding biological reactions at

the tissue-biomaterial interface thus facilitating successive tissue engineering and organ implantation [109].

1.2.2. Anti-angiogenic therapy

1.2.2.1. Eye disease. Proliferative retinopathy is a disease that affects about 60,000 diabetics and more then 10,000 premature babies in the United States each year [130]. It is a condition in which abnormal blood vessel growth in the retina impairs vision, and sometimes causes blindness. The abnormal vessel growth has been recently associated with the presence of VEGF. Studies show [74,129,131] that oxygen-starved cells produce VEGF (in particular, the oxygen-starved cells of the retina). It happens in diabetics because their capillaries often get clogged which prevents oxygen transport, and in premature infants which are born before their retinal blood vessels are fully grown. When VEGF level rises, it triggers abnormal capillary growth across the retina, which may cause damage, and sometimes permanent loss of vision. In this case many people could benefit form anti-angiogenic therapy, i.e. from medical prevention of new blood vessel growth in the retina [11, 16].

1.2.2.2. Psoriasis. Psoriasis is a common chronic dermatosis occurring in 2% of the population and associated with an inflammatory arthritis (psoriatic arthritis). Psoriatic arthritis represents the second most common diagnostic category after rheumatoid arthritis. There are a number of common pathogenic features that link the skin and the joint inflammatory processes. Angiogenesis appears to be a fundamental inflammatory response early in the pathogenesis and significant abnormalities of vascular morphology and angiogenic growth factors have been described in psoriasis and psoriatic arthritis. Recent research studies suggest [11, 120] that deregulated angiogenesis provides a primary pathogenic mechanism in psoriatic skin and arthritic joints.

1.2.2.3. Cancer. Initially, solid tumors are avascular. They do not have their own blood supply and rely on simple diffusion to provide necessary oxygen and nutrition as well as to remove tumor cell waste products. As the tumor gets bigger, diffusion through the surface is not any longer capable of supplying the entire mass of cells. As a result, some of tumor cells start to die due to starvation and hypoxia (oxygen deprivation). The tumor stops growing and reaches steady state size $\sim 1-3$ mm, in which the number of dying cells counterbalances the number of proliferating cells. Growth can resume only if the tumor becomes vascularized, i.e. permeated by a vessel network. Accumulating evidence indicates that hypoxia is one of the major triggers for angiogenesis in malignant tumors [2].

At that stage many tumors achieve rapid growth by switching on enhanced production of angiogenic signals, for example, VEGF secretion. An early response of the growing tumor to hypoxia is expression of certain chemicals that trigger VEGF production. VEGF diffuses from tumor to nearby primary vessels initiating a complicated cascade of events that results in formation of new capillaries extending from the primary vessels to the VEGF-secreting tumor as shown in Fig.1.2 [26, 59, 62, 65, 187].

Blood that starts circulating through newly formed vessels supplies the tumor with necessary nutrients and oxygen and may also serve as an easier escape route for metastatic cells [2, 4, 38, 44, 61, 169].

Thus angiogenesis is crucial for cancer invasion and understanding the mechanisms that control it will provide the basis for rational therapeutic intervention. In other words there is a hope that by blocking formation of new blood vessels through drugs it may be possible to suppress tumor growth and to prevent metastasis formation [11, 23, 54, 55, 62, 63, 84, 88, 92, 173, 208].

FIGURE 1.2. **Angiogenesis in cancer.** In this micrograph, blood vessels grow toward a sarcoma tumor (dark area at right) in a rat muscle. The oriented vessels growth reflects a chemotactic response of the endothelial cells to an angiogenic factor released by the tumor.

1.3. Main events of angiogenesis

Blood vessels penetrate every tissue in the body, and since our goal is to study new vessel formation, it is useful to gain some insight into vessel structure as well as the composition of the surrounding medium (extracellular matrix). We will start with a brief description of the extracellular matrix, then present a simplified picture of blood vessel organization and finally describe the main steps of a new vessel formation.

1.3.1. Extracellular matrix

Tissues are not made up solely of cells. A substantial part of their volume is extracellular space, which is largely filled by a intricate network of macromolecules composing the extracellular matrix (ECM). The ECM consists of a variety of proteins and polysaccharides that are secreted locally and assembled into an organized meshwork in close association with the surface of nearby cells that produce them. Among other ECM components we can name elastin, fibrillar collagens, laminins

and fibronectin [4, 103]. The ECM is not just an inert scaffold that stabilizes the physical structure of tissues, as it was once thought, but has much more active and complex role. It is in contact with the cells embedded in it and is attached to their cytoskeleton via cell adhesion molecules (CAMs) that are built into surface membrane (e.g. integrins, cadherins, see Fig.1.7) thus activating multiple cascades of events called intracellular signaling pathways. It regulates behavior, migration, proliferation, shape, survival, development and functions of the cells [105, 139, 163, 176, 204, 216].

Since blood vessels are embedded into tissues, during new vessel growth the daughter capillaries make their way through the surrounding ECM [121, 155, 163].

1.3.2. Blood vessel structure

Blood vessels are comprised of three components: (a) the basement membrane, which is a thin sheet-like structure of ECM components, primary laminins and Type IV collagen, that encircles and supports the interior of the vessel, (b) endothelial cells (ECs) which form a mono-layer of flattened and extended cells lining the lumen and resting on the inner surface of the basement membrane and (c) pericyte cells which form a periendothelial cellular network embedded within the basement membrane [4, 45, 121, 123]. Thus, endothelial cells line the entire vascular system, from the heart to the smallest capillary. ECs retain a capacity for cell division and movement. If, for example, a part of vessel wall is damaged or denuded of cells, neighboring endothelial cells proliferate and migrate in to cover the exposed surface. In most of adult tissues, ECs turn over very slowly, with a cell time ranging (for a mouse) from a couple of month (liver and lungs) to years (brain) [4, 123]. But ECs not only repair and renew the lining of already established blood vessels, they are also capable of forming new vessels.

1.3.3. New blood vessel formation

The growth of new capillaries from the pre-existing network is triggered by the presence of angiogenic growth factors in the tissue surrounding the primary blood vessel [4, 65]. There exist a number of different angiogenic growth factors, but VEGF is thought to be the major regulator of new capillary growth [76, 93, 96, 130, 131, 173, 183, 201].

It is now well accepted [5, 39, 40, 121–124, 138] that the whole process of angiogenesis can be divided into several phases that are characterized by different, overlapping genetic programs: initiation, progression, and maturation of the newly formed vascular network.

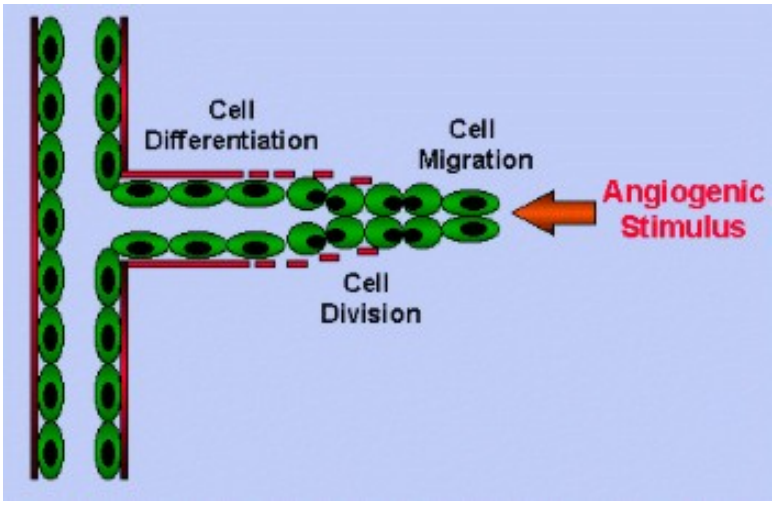

FIGURE 1.3. **Initial stages of angiogenesis.** In response to angiogenic stimulus, endothelial cells switch to an activated phenotype. They start to proliferate, release proteases that degrade the basement lamina of the parent vessel and start migration up the angiogenic stimulus gradient, forming a new capillary in that direction.

Initiation is characterized by changes in the ECs shape and permeability after VEGF molecules occupy EC surface receptors. The cells switch from the quiescent endothelial phenotype that prevails in an established vessel to an activated mesenchymal phenotype. In this state, they can be roused to proliferate with a doubling time of just a few days. There is some evidence that, where

there is a call for rapid blood vessel growth, the local population of ECs may also increase by recruitment from the blood stream, which has been reported to contain small numbers of endothelial precursor cells derived from the bone marrow. ECs produce proteolytic enzymes (proteases) which in turn degrade the basement membrane. After that, ECs proliferate and migrate through the openings in the parent vessel wall towards the source of the growth factor (Fig.1.3).

Many of the proteases belong to one of two general classes. Most are matrix metalloproteases, which depend on bound Zn^{2+} or Ca^{2+} for activity; others are serine proteases. It is known that ECs secrete matrix metalloproteases to degrade the basement membrane and adjacent ECM [72, 104, 207].

The progression phase includes further degradation of the basement membrane of the parent vessel, accompanied by migration of ECs through the created openings into the ECM that surrounds the parent vessel. The ECs form primitive blood vessels (lumens) and begin to proliferate elongating the lumen in the direction of the growth factor gradient, with proliferation occurring behind the tip of the growing capillary sprouts [76, 121–124].

Next stage involves remodeling of the primitive sprouts (loop formation) and formation of capillary network. After reaching certain distance from parent vessels the growing sprouts bifurcate, and the branches tend to incline toward each other and fuse together, by both tip-to-tip and tip-to-sprout fusion. This process, which is called anastomoses, results in capillary network formation. The frequency of branching at the front edge of the network increases as the capillary sprouts become closer to the growth factor source and this phenomenon is referred to as a ”brush border effect”. Afterwards, the new capillaries are stabilized by smooth muscle cells and pericytes that envelope the capillaries (see Fig.1.4) thus providing structural stability, the process known as vessel maturation [1, 4, 8, 123].

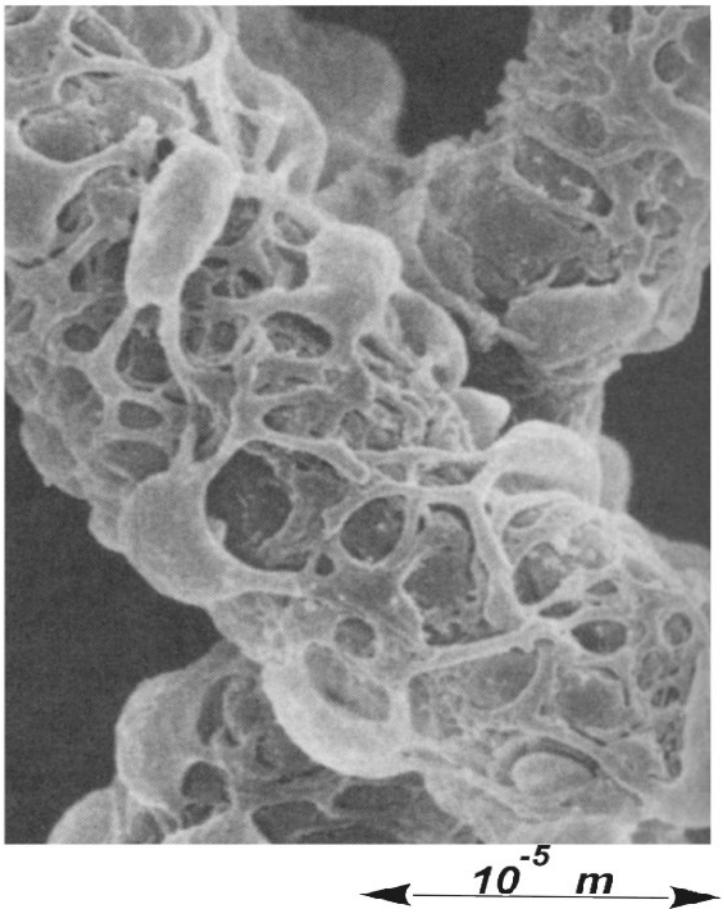

FIGURE 1.4. **Pericytes.** The scanning electron micrograph shows pericytes wrapping around a small blood vessel in the mammary gland of a cat. Pericytes are present also around capillaries, but much more sparsely distributed there [69].

1.4. Experimental study of endothelial cell migration

Now we understand that EC migration is a crucial step in the process of angiogenesis and one can control new vessel growth by influencing EC migration [12, 121].

Cell migration is a highly complicated process. A large number of theoretical, computational and experimental studies has been reported in the literature [4, 12, 52, 73, 77, 80, 82, 89, 94, 95, 116–119, 121, 132, 154, 160, 161, 179, 180, 184, 194, 199, 205].

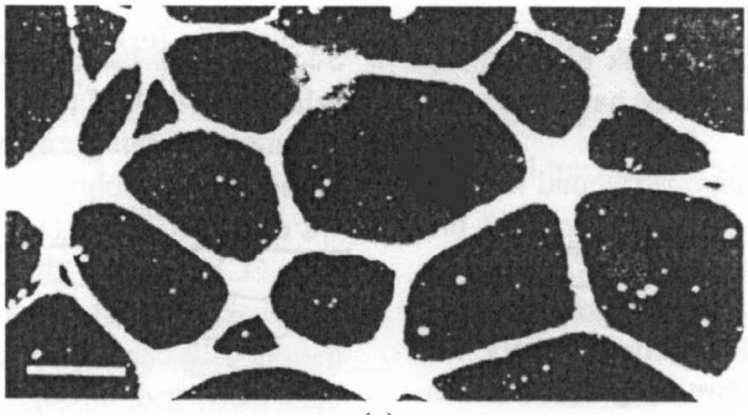

FIGURE 1.5. **Experimental angiogenesis.** Bovine aortic endothelial cells, cultured 48 h in a subconfluent monolayer on top of a layer of Matrigel, organized into a planar network of cords. Each cord (example, arrow) is comprised of many cells. Image is viewed by darkfield illumination. Bar at lower left = 200 μm.

Taking into account the great complexity of the process, a large number of various factors that affect the process and a huge amount of different outcomes that researchers can get by varying those factors, it becomes obvious that it is quite expensive, time consuming and ineffective to study cell migration *in-vivo*. So people approach the task by first studying cell migration *in-vitro* in which case experiments are faster, less expensive and much easier to control. In addition, *in-vitro* studies allow experimentalists to analyze action of different angiogenic factors separately, i.e. how one or another chemical can induce or inhibit certain stages of new vessel formation, before trying to understand more complex effects of many factor interplay [14, 112, 184].

In some of the experiments [64, 73, 184] cells are randomly seeded on the plane surface of a gel substratum and their migration and aggregation tracked by video-microscopy. It is observed that motion is directed towards the areas with higher angiogenic factor concentration, suggesting that chemotaxis plays an important role in the process.

In a time period of several hours cells spontaneously develop internal vacuoles that appear to join up from cell to cell, giving rise to a continuous multicellular network or pattern. These

patterns can have polygon-like structures as well as other geometry (Fig.1.5). Some more recent experiments show that stripe-like patterns can also occur [174]. These patterns are interpreted as the beginning of a vasculature. They determine the structure of ensuing capillary network and therefore are of interest. Typically, the patterns are not steady but rather slowly evolve in time. The form of patterns depends on experimental conditions such as the properties of the gel, initial cell and angiogenic factor concentrations as well as on other parameters of the system.

Behavior of endothelial cells cultured on biogel that resembles ECM structure can mimic some of key stages of angiogenesis (such as association in tube-like structures and subsequent capillary network formation), thus providing a powerful experimental tool for studying the possibilities of affecting different stages of angiogenesis [14, 112, 184].

The goal of our work is to propose and study a mathematical model that governs EC dynamics and exhibits pattern formation. It should be noted that the experimentally observed patterns are not necessarily spatially regular, namely, hexagons and stripes, which can be perceived as a regular counterparts of the experimental observations. These patterns can result form Turing instabilities which is the subject of this work. We anticipate that these regular patterns may in turn become unstable leading to irregular polygonal structures similar to those observed in [64, 73, 184], as seen in other problems [79]. Our study of the Turing patterns is useful as it indicates the parameter regime where the irregular structures can appear as a secondary bifurcation. Afterwards, these structures can be sought numerically (see Chapter 2).

1.5. Molecular mechanisms

It is now widely accepted that vascular growth during development and pathological conditions is strictly regulated by a complex interplay and balance of angiogenic stimuli and inhibitors [60].

The angiogenic switch is off when the effect of proangiogenic molecules is balanced by that of antiangiogenic molecules, and is on when the net balance is shifted in favor of angiogenesis. Various signals that trigger that switch have been discovered. These include metabolic stress (low oxygen concentration or hypoxia, low pH, hypoglycemia); mechanical stress (e.g., pressure generated by proliferating cells); and immune response (e.g., immune/inflammatory cells that have infiltrated the tissue). How the interplay between various mechanisms influences angiogenesis is a complex and largely unsolved question.

All the consecutive events of angiogenesis described in this introduction are carried out by means of sophisticated cell communication mechanisms that allow endothelial cells to govern their own behavior for the benefit of the process as a whole. These communication mechanisms depend heavily on both extracellular signal molecules, which are produced by cells to signal to their near neighbors and distant cells, and elaborate systems of intracellular proteins that transfer signals from cell surface to a specific target protein inside the cell (signaling pathways) which allow a cell to respond to a particular subset of signals in the cell-specific way. The extracellular signal molecules that regulate cell size and cell number are generally either soluble secreted proteins that are able to diffuse through the ECM (for example, angiogenic growth factors), proteins bound to the surface of cells, or components of ECM. Factors are protein molecules present in the ECM that bind to receptors on the cell surface. The primary result of the binding is activation of multiple intracellular responses resulting in cell proliferation, growth, differentiation, secretion of different molecules, consecutive cascade of angiogenic events or programmed cell death (apoptosis). A large number of angiogenic factors are presently identified. Many factors are quite versatile, stimulating cellular responses in numerous different cell types; while others are specific to a particular cell type. In particular, VEGF is known to be largely EC specific angiogenic factor while fibroblast growth

factor (FGF) can stimulate the proliferation of other cell types as well. The factors that promote growth and development can be divided into three major classes: mitogens, which stimulate cell division; growth factors, which stimulate cell growth; and survival factors, which promote cell survival by suppressing apoptosis. Studies have shown that VEGF alone controls several of the most important processes in ECs such as proliferation, survival and migration [76, 93].

Cell protein systems that carry out different signaling pathways include cell-surface receptor proteins which bind the signal molecules; a variety of intracellular signaling proteins (e.g. kinases, phosphatases) that distribute the signal to appropriate parts of the cell [21]; and target proteins (e.g. gene regulatory proteins, ion channels, parts of cytoskeleton) that are altered as a result of each signaling pathway, thus changing the behavior of the cell.

Action of all molecules that comprise every single signaling pathway has to be well-coordinated to allow the ultimate goal to be accomplished in a multicellular organism, for example, to have thousands of cells form a functional vascular network in the process of angiogenesis.

Of crucial importance for understanding of angiogenesis is figuring out the signal transduction systems by means of which endothelial cells become instructed to proliferate, secrete proteases, migrate, form lumens and to recruit pericytes during the new vessel maturation.

1.5.1. VEGF and its receptors

About twenty years ago the cloning and characterization of a secreted homodimer protein purified from tissue culture cells was reported that turned out to be a mitogen specific for endothelial cells and to be angiogenic *in-vivo* and therefore was named vascular endothelial growth factor (actually there is a whole family of VEGFs [4] including VEGF, placenta growth factor PGF, and VEGF -B, -C and -D [56, 202]). VEGF, also designated as VEGF-A, is the major regulator of normal and

abnormal angiogenesis, including that associated with tumors [3, 107, 183, 201].

The cellular responses to the members of the VEGF family are mediated primarily by the high affinity EC receptors VEGF receptor-1 (VEGFR-1) and VEGF receptor-2 (VEGFR-2; also called Flt-1). VEGFR-2 is considered to be the main signaling VEGF receptor in ECs [22], whereas VEGFR-1 may have a negative role either by acting as a decoy receptor or by suppressing signaling through VEGFR-2 [48, 180, 202, 212]. VEGF receptor signal trunsduction appears to rely upon the canonical pathways activated by most receptor tyrosine kinases [172], i.e as a result of ligand binding, the receptor homodimerize and becomes autophosphorylated on specific cytoplasmic tyrosine residues, which mediate the recruitment of adaptor proteins and enzymes (e.g., Grb, Nck, VRAP, Sck) and lead to early and late biological responses such as EC migration, proliferation and survival by activating Ras, Map, and protein kinase B pathways [4, 13, 15, 147, 195].

VEGF has a number of important effects in angiogenesis. VEGF was initially defined by its ability to induce vascular leak and permeability, as well as for its ability to promote vascular EC proliferation [212]. VEGF was also found to be a potent chemoattractant for ECs that stimulates cell migration in the direction of chemoattractant gradient. It also induces expression of matrix-degrading enzymes such as matrix metalloproteases (MMPs) which facilitates EC migration via alterations of ECM. Moreover, VEGF is discussed as an important survival factor for immature vessels [27, 36, 47, 57, 126].

1.5.2. Crawling

As mentioned above, ECs change their behavior, aggregate and eventually migrate along the gradient of VEGF and other secreted growth factors which diffuse through the tissue that surrounds

the parent vessel. The direction of cell migration can also be influenced by nondiffusing chemical cues attached to the ECM or to the surface of the cells [4, 13, 76, 82, 195, 212].

Two distinct steps are necessary in order that a cell can move toward the source of a chemoattractant: (i) it must orient itself properly and (ii) it must generate the necessary forces. Amoeboid cells such as ECs are large enough to detect gradients of attractants across their length, and in fact, some eukaryotic cells can respond to concentration differences as small as 2% across their length, frequently at concentrations at which molecular fluctuations, and hence noise in the signal, are significant. Cell migration is a highly complex integrated process, dependent on the actin-rich cortex beneath the plasma membrane [4, 134, 135, 143–145]. Most of the cells in adult animals migrate by crawling rather than by other means. The forces needed for cell migration are generated by the special proteins called motor proteins. These molecules bind to cytoskeleton filaments and use the energy derived from constantly repeated cycles of ATP hydrolysis to move along thus mediating sliding of cytoskeleton filaments relative to one another and the transport of cell organelles along filament tracks.

Motion of a crawling cell is generally described as a multi-step process (see Fig. 1.6) involving (i) actin polymerization at the leading edge, which leads to extension of a pseudopodia or lamellipodia (protrusions of cell leading edge that are results of actin polymerization pushing cell membrane outward), (ii) attachment of the pseudopodia or lamellipodia to the substrate or ECM via integrin-mediated adhesion sites, (iii) contraction of the cell via actin-myosin contraction (iv) release of adhesion sites at the rear, and (v) recycling of adhesion receptors and other membrane components to the front of the cell via endocytosis and vesicular transport [82, 134, 135, 143, 144, 170, 171, 185].

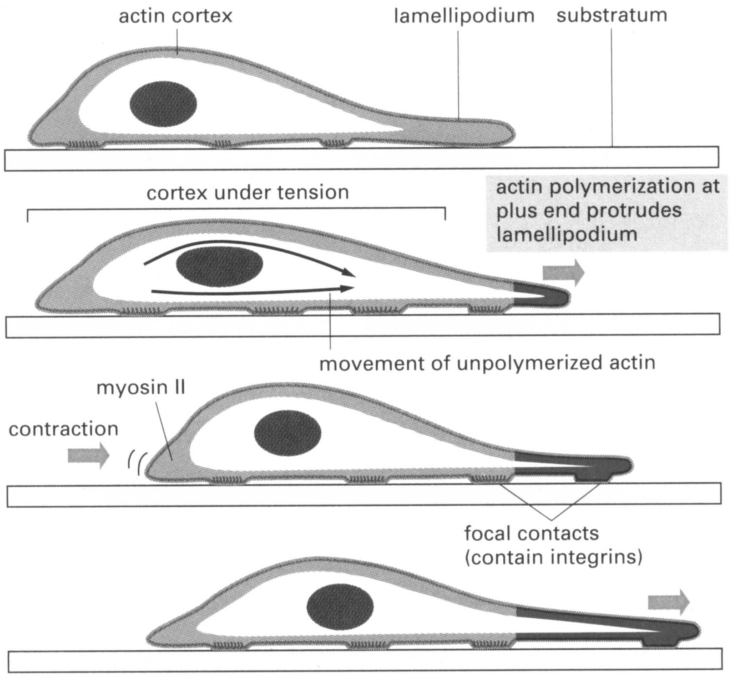

FIGURE 1.6. **A model of how forces generated in the actin-rich cortex move cell forward.** The actin polymerization and firm attachment of lamellipodium at the leading edge of the crawling cell moves the edge forward. Contraction at the rear of the cell propels the body of the cell forward to relax some of the tension (traction). New focal adhesion sites are made at the front, and old ones are disassembled at the back as the cell crawls forward. The same cycle can be repeated, moving the cell forward in stepwise fashion.

1.5.3. Integrin-mediated mechanisms

The association of cells with extracellular matrix initiates the assembly of specific cell-matrix adhesion sites, which are essential for cell migration as well as for activation of adhesion-mediated signaling events. Key mediators of both matrix attachment and signaling responses are the integrins [4, 24, 49, 97, 98, 105, 139].

The integrins are the best characterized group of cell adhesion molecules that usually span the entire phospholipid bilayer, which isolates the interior of the cell (cytoplasm) from the exterior and otherwise known as cell membrane [172].

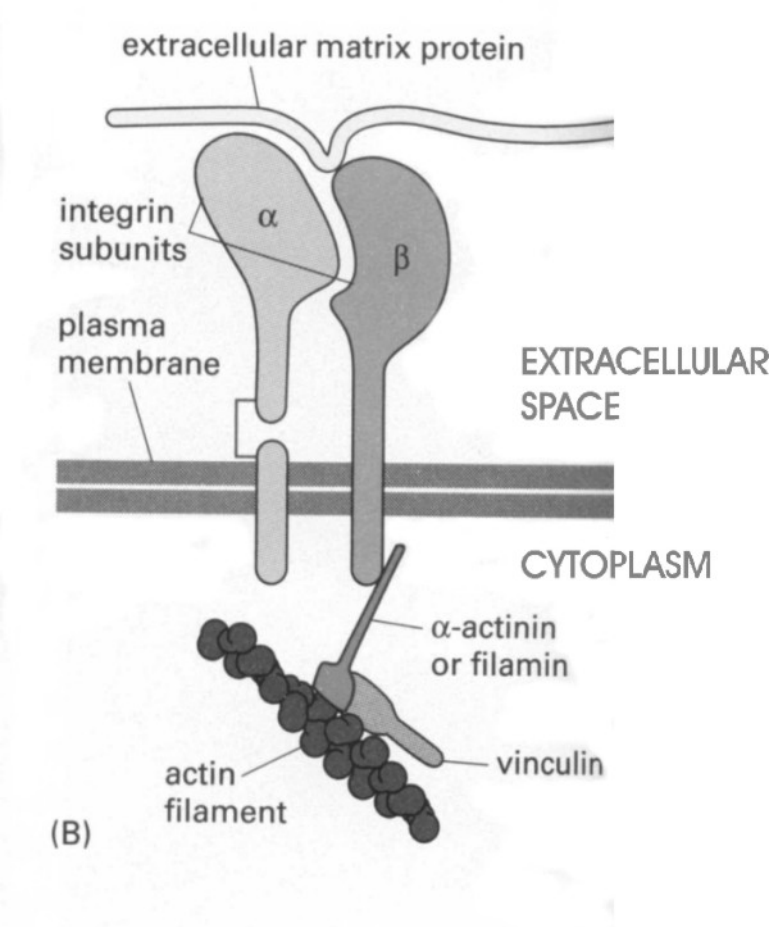

FIGURE 1.7. **The structure of focal adhesions.** Some of the proteins that form focal adhesion sites. The transmembrane adhesion protein is an integrin heterodimer, composed of an α and a β subunit. It extracellular domain binds to components of extracellular matrix, while the cytoplasmic tail of the β subunit binds indirectly to actin filaments via several intracellular anchor proteins.

These proteins are exposed on both the internal and external surfaces of the cell, so they can simultaneously interact with ECM components as well as with internal cell organelles such as cytoskeleton thus connecting the interior of the cell to the surrounding ECM (Fig.1.7).

Integrins are heterodimeric proteins that consist of an α subunit noncovalently associated with a β subunit. Following association with their ligands, integrins induce reorganization of actin cytoskeleton and associated proteins, thus allowing a specific signal carried by certain ligand penetrate inside the cell. The combination of specific subunits determines the particular ligands that

the particular integrin can bound and therefore different biological consequences among which are influence on ECs activation, migration, proliferation, differentiation and gene expression.

In addition, integrins are one of the cellular molecules families that fulfill VEGF co-receptors' function, i.e. modulate VEGF receptors' activity and specificity. In particular, integrin $\alpha_5\beta_3$ functions as co-receptor in VEGFR-2 signal transduction resulting in increased VEGFR-2 kinase activity and augmented VEGF-A mediated mitogenicity in angiogenic ECs.

The integrin $\alpha_5\beta_3$ is one of the primary integrins in ECs, and it has been shown recently that they are selectively recruited to the leading edge of cell lamellipodia [108]. This localization can promote localized adhesion and alter the overall strength of adhesion at the front (the direction of motion) as opposed to the rear. A mechanism for activation of $\alpha_5\beta_3$ by VEGF signaling, via the activation of PI3K and its downstream effectors has been suggested [33].

Since integrins bind their ligands with a low affinity, there is a certain number of them that is required to obtain enough sticking capacity to adhere to ECM, in other words, no strong adhesion can occur when integrins are diffusively distributed over the cell surface. Therefore, in the process of ECs crawling integrins have to cluster for their combined weak affinities to generate a strong enough traction force which the moving cell uses to pull itself forward. Integrin clustering gives rise to the recruitment of numerous structural and catalytically active cytoplasmic proteins, creating a complex structures called focal adhesion complexes (Fig.1.7) on the leading edge of a crawling cell [98, 216]. Cell uses them for migration, but they also fulfill multiple functional purposes, the fact known as anchorage dependence. Signaling through focal adhesions regulates a variety of cellular processes including cell growth, migration, and apoptosis [28]. Focal adhesions are dynamic structures. After forming at the cell front they remain stationary as the cell moves forward

over them, persisting until the rear of the cell catches up with them [95, 160]. Afterwards, they get disassembled and recycled to the front of the cell via endocytosis [185].

Formation and breakdown of focal adhesion complexes are regulated by many different extracellular stimuli, and not all of them are known and experimentally proved. Studies show [13, 195] that VEGF-induced endothelial cell migration is mediated by an accelerated rate of focal adhesion complex assembly and disassembly.

To summarize, VEGF triggers integrin clustering on ECs surface which leads to the formation of structurally complicated focal adhesion complexes on the leading edge of a crawling cell (in the direction of VEGF chemotactic gradient) and ultimately to cell migration up the gradient of VEGF.

1.5.4. Localized ECM remodeling

Attachment of a cell to the surrounding ECM can happen under two conditions: (i) the presence of focal adhesion sites on the cell surface by means of which it attaches to the ECM; (ii) the presence of specific attachment sites in the surrounding ECM [105, 147]. The latter are created by selected cleavage of the ECM by proteolitic enzymes called proteases [4].

An increase in growth factors such as VEGF leads to secretion of proteolytic enzymes by ECs. These enzymes degrade the ECM around the parent vessel, the process which facilitates subsequent EC migration into the extracellular space [72, 121, 123, 182, 214]. Many of the proteases implicated in angiogenesis belong to two general classes: matrix metalloproteinases (MMPs), which depend on Ca^{2+} or Zn^{2+} for activity; and serine proteases, which contain components of the PA-plasmin system. Together, these proteases cooperate to degrade ECM components such as collagen, laminin, and fibronectin. The involvement of the MMP action in the process of angiogenesis

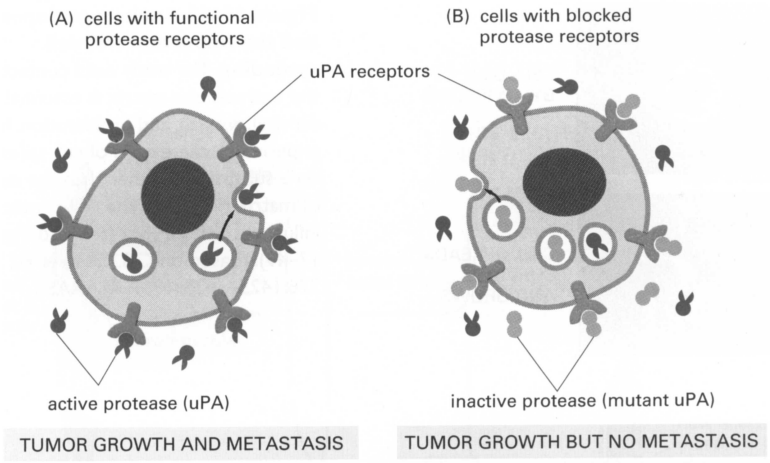

FIGURE 1.8. **Proteases confined to the cell surface and possible way of their inhibition.** (A) Proteases bind to cell surface receptors at the leading edge of a moving cell where they become active as a result of the binding and may serve to clear a pathway for cell migration. (B) Protease inhibitors block protease surface receptors thus preventing binding of proteases to the receptors and their activation. It prevents degradation of the surrounding extracellular matrix and ultimately may prevent cell migration through the matrix.

has been demonstrated both *in-vitro* and *in-vivo* using MMP-specific inhibitors [115, 207]. There are MMP family members with enzymatic activity against virtually all components of the ECM and basement membranes. Most importantly, the MMP family includes the only enzymes capable of cleaving fibrillar collagens [207].

ECM degradation allows migrating cells to clear a path through the matrix. Moreover, selective cleaving of ECM molecules can release growth factors or inhibitors, and by exposing cryptic binding sites for adhesion and destroying other adhesion sites, can dramatically alter the invasive ability of the cells.

Three main strategies are employed to ensure that the matrix degrading proteases are tightly controlled: local activation (e.g. plasminogen activation); confinement by cell-surface receptors (e.g. urokinase-type plasminogen activator uPA that binds to the receptors on the leading edge of some migrating cells thus cleaving ECM specifically in the direction of cell movement as shown

in Fig.1.8); and finally, secretion of protease-specific inhibitors (e.g. tissue inhibitors of metalloproteases TIMPs, serine protease inhibitors serpins) that may protect uninvolved matrix as well as cell-surface proteins required for cell adhesion and migration from destruction [4, 115, 207, 214].

1.5.5. Capillary lumen formation

In order to assemble into tubular structures, ECs must lose their invasive phenotype, reassociate with matrix proteins, and develop cell-cell contacts in a tubular conformation. Many *in-vitro* studies have attempted to define the different morphological steps in the formation of capillary sprouts. A commonly used method of *in vitro* angiogenesis is the growth-factor-induced formation of cord-like structures when ECs are cultured on an extracellular matrix secreted by Engelbroth-Holm-Swarm sarcoma cells, commonly known as Matrigel [213]. In these models, capillary-like lumens are developed, which closely mimic those observed within collagen matrices *in vivo* [51]. Two different types of capillary vessel formation can be distinguished, which occur independently of each other or in combination within a single sprout: sprout formation through intracellular or intercellular lumen formation.

An intracellular lumen develops through the formation of intracellular vacuoles that enlarge and coalesce in response to EC contact with collagen matrix. Vacuole formation occurs through a pinocytic process with internalization of plasma membrane and molecules from the extracellular space. The union of adjacent cellular lumens results in the formation of a continuous capillary tube, which traverses the cytoplasm of the cells, or the nucleus. In the second type, a lumen arises through a protrusion or migration of neighboring ECs from newly formed or established vessels. Here, the lumen forms via the coordinated migration of several ECs that maintain their polarity and junctional contacts [4].

1.5.6. Maturation of the neovasculature

During the process of angiogenesis, the developing vessels are leaky and dependent on VEGF for survival [18, 27, 36, 57]. Formation of a new vessel ends by acquisition of a pericyte coating (Fig.1.4) and the deposition of a basement membrane [81, 90, 123]. This allows to overcome vulnerability of the immature blood vessel preventing it from breaking or leaking. ECs recruit pericytes via the secretion of platelet-derived growth factor (PDGF), which acts as a mitogen and chemoattractant for pericyte precursors. The proposed roles for pericytes include: regulation of capillary blood flow, as smooth muscle cell precursors, phagocytosis, and the control of capillary growth [90]. Upon EC-pericyte contact, the pericytes exert an inhibitory effect on EC proliferation and maintain vessel integrity. Growth factors called angiopoietins that also interact with ECs via surface receptors [9,114,212] play a critical role in this process. These help stabilize mature vessels by promoting interaction between ECs and the newly recruited pericyte layer.

1.5.7. Angiogenesis inhibition

Since the early 70s when the importance of angiogenesis in tumor growth and metastasis was established, the discovery of the identity and biochemical mechanisms of substances that can inhibit angiogenesis has been a focal point in angiogenesis research. The concept of manipulation of the vascular bed to either increase or decrease the number of blood vessels has attracted considerable interest. There is a growing evidence that anti-angiogenic drugs will improve future therapies of a variety of human diseases. There is currently a number of angiogenesis inhibitors in clinical trials. It is important to understand the process in great detail to identify potential targets for anti-angiogenic therapy.

As follows from the above brief description, there are a number of molecular mechanisms that appear to be crucial during the early stages of angiogenesis, and by means of interfering with which angiogenesis can in principle be blocked. Namely, (i) VEGF and other growth factor interactions with their cell-surface receptors that trigger multiple intracellular signal pathways, in particular promoting survival and proliferation of immature ECs [21, 22, 27, 56]; (ii) formation of focal adhesion complexes on the leading edge of the cell [13, 76, 195]; (iii) release of proteases by ECs; (iv) localized degradation of extracellular matrix components by proteases [72, 214], creation of specific attachment sites in the extracellular matrix [216]; (v) anchorage dependence of cell growth, survival, division and migration mediated mainly by focal adhesions via intracellular signals they generate [205]; (vi) EC directional crawling through the ECM in response to chemotactic gradient of VEGF [185]. This suggests a number of anti-angiogenic strategies that can be employed to prevent angiogenesis.

- Blocking VEGF and other growth factors activity by factor-specific antibodies [3, 93].
- Blocking VEGF -receptors with receptor-specific antibodies which occupy receptors [200].
- Blocking VEGF expression [96].
- Inhibition of ECs intracellular signaling which is the result of binding of VEGF molecules to cell surface receptors. It can be done by blocking tirosine kinase activity of VEGF receptors [127].
- Inhibition of certain functions of cellular adhesion molecules, which can prevent integrins from attaching to ECM (leads to apoptosis because of anchorage dependence of ECs, i.e. they need to attach to surrounding cells and ECM in order to survive) [24, 25].
- Inhibition of ECM remodeling and blocking creation of ECM attachment sites by protease inhibitors (Fig.1.8), the strategy that often blocks cell migration [199].

- Direct inhibition of ECs activity, i.e. suppressing endothelial cell proliferation and migration induced by growth factors via impeding the downstream intracellular signaling using EC toxins [200].

The development of anti-angiogenic agents with different mechanisms of action requires powerful preclinical models for the analysis and optimization of these therapies. These studies rely on a range of *in-vitro* and *in-vivo* assays that are designed to gain information about each of the multiple events that constitute the angiogenic process [10, 101, 102, 206]. Theoretical studies (i.e. mathematical modeling) can also serve as a tool of this research. Modeling allows one to take a hypothetical mechanism and examine its consequences in the form of a mathematical model, making predictions and suggesting experiments that would verify or invalidate the model. In other words, it highlights the areas where the knowledge of biological mechanisms is deficient and suggests directions in which experimentation might lead the researchers.

This ideas are best expressed by James D. Murray [150]: ”Why use mathematics to study something as intrinsically complicated and ill-understood as development, angiogenesis, wound healing and so on? We suggest that mathematics, rather mathematical modeling, must be used if we ever hope to genuinely and realistically convert an understanding of the underlying mechanisms into a predictive science. Mathematics is required to bridge the gap between the level on which most of our knowledge is accumulating (cellular and below) and the macroscopic level of the patterns we see. ... A mathematical approach lets us explore the logic of the process. Even if the mechanisms were well understood (and they certainly are not at this stage) mathematics would be required to explore the consequences of manipulating the various parameters associated with any particular scenario.”

1.6. Review of mathematical models of angiogenesis

Different kinds of mathematical models were created in an attempt to convert the phenomena briefly described above into a mathematical model and thus to better understand the mechanisms that govern vascular network formation, especially the issue of ECs geometrical self-organization into spatial structures.

Mathematical models of tumor-induced angiogenesis fall into three major categories: (i) continuum models that treat the EC density and chemical species as continuous variables that evolve according to a reaction-diffusion system of equations [5–7, 29–32, 37–43, 43–45, 66, 118, 121–125, 128, 130, 131, 155–157, 162, 164, 165, 168, 169, 190–192, 203]; (ii) mechanochemical models that incorporate some of the mechanical effects of EC-ECM interaction on cell motion, in addition to the diffusible chemical species [58, 73, 80, 83, 94, 133, 136, 137, 148, 149, 151, 176, 184, 198, 204] and (iii) discrete, cell-based models in which cells are treated as units and move, grow, and divide according to prescribed rules [5, 40, 142, 161, 167, 193, 194].

These research groups model various stages of angiogenesis. The work ranges from describing the early stages of the process in which the collapse of vascular lamina occurs and capillary buds are formed [66, 121–123, 125, 156] to attempts to capture the formation of complex capillary networks and blood flow through them [5–7, 29, 37, 39–42, 78, 136, 157, 168, 169, 191]. Various models are used, both deterministic and stochastic, ranging from detailed biochemical pathways to overall phenomenological description of the main stages of angiogenesis.

Some models deal with *in-vivo* angiogenesis, for instance, tumor-induced or epidermal wound healing angiogenesis [5, 6, 37, 39–42, 66, 78, 94, 121–125, 128–131, 155, 156, 162, 165, 190, 191, 198, 203] and other models describe the results of *in-vitro* experiments with endothelial cell cultures grown on Matrigel [58, 73, 80, 136, 137, 148, 150, 151, 176, 184].

Below we describe in greater detail the works relevant to the present study.

A large class of continuum models including our model is based on reinforced random walk equation for endothelial cell density that governs chemotactic/diffusional motion of the ECs (cf. [159]) coupled with mass balance equations for certain species that are present in the system and affect EC behavior. The works differ by biochemical phenomena they account for and consequently by the number and properties of the chemicals involved.

In [123, 124] early stages of tumor-induced angiogenesis are studied. The authors consider initial EC aggregation and collapse of the basement membrane that opens a passage of the cells into the ECM. In [124] dynamics of ECs, growth factor and proteases is accounted for while in [123] the authors study the role of pericytes and macrophages in the initiation of angiogenesis.

Other work on the initiation, though not necessarily based on the reinforced random work equation includes [66, 156].

A large number of works are devoted to the subsequent stages of angiogenesis, namely the growth of capillaries and capillary network formation.

In [6, 191, 193] the authors model capillary network formation in absence of ECs proliferation. They account for cell random motility, chemotaxis and also haptotaxis due to the presence of two chemical stimuli: growth factor and fibronectin. This work is done in the context of tumor-induced angiogenesis.

In [5,37,39,40,42] the authors include migratory response of ECs to growth factor, EC proliferation, EC interaction with ECM molecules such as fibronectin. They also study capillary branching and loop formation. These models are not based on the reinforced random work equation, but postulate diffusion flux as consisting of random motility, chemotaxis and haptotaxis terms.

We note that these works were indispensable as a starting point of our modeling efforts. However, our model differs from the existing models by certain problems that we pose, by our treatment of cell motility, and by the dependent variables we introduce. As discussed in [138], a typical continuum model comprise equations for unknown variables that represent densities of all cell types involved in the process(e.g., ECs, pericytes, etc.) as well as the concentrations of substances influencing migration and/or proliferation, such as VEGF, proteases and angiogenic inhibitors. In our work we emphasize importance of integrin-mediated mechanisms in cell migration by including the concentration of focal adhesion sites r and the concentration of ECM active sites m into the model.

CHAPTER 2

Modeling of endothelial cell chemotactic motion

2.1. Development of the base mathematical model

The model that we propose is a reaction-diffusion model that can be used for a description of various manifestations of angiogenesis. In this chapter the model is used to describe endothelial cell (EC) pattern formation on a two-dimensional gel matrix. A detailed description of the main stages of angiogenesis is given in the previous chapter. Here we provide a brief summary of the processes that are accounted for in our mathematical model.

We study the motion of ECs that are initially plated on a gel matrix along with the growth factor. The growth factor plays multiple roles in the angiogenesis process. (A growth factor, which is frequently observed in angiogenic studies, is vascular endothelial growth factor, VEGF). First of all, the growth factor stimulates EC motility. Moreover, it triggers mitosis of ECs, induces the expression of matrix-degrading proteases by ECs, and is an important survival factor for the cells. The growth factor can be produced by endothelial cells, and it decays over a relatively short time. All these facts are reflected in our model.

Next, both the cells and the growth factor can diffuse. Diffusion of the growth factor is a relatively simple process, which we model by Fickian diffusion with a constant diffusion coefficient. Diffusion of ECs, however, is rather complex. First, there is a preferred direction of EC motion, which is the direction along the growth factor gradient (chemotaxis). In addition, diffusion of ECs involves cell-matrix adhesion, which requires the presence of (i) cell adhesion molecules

(CAMs) on the cell surface and (ii) active adhesion sites in the extracellular matrix (ECM). The best characterized group of CAMs are integrins. The integrins have to cluster to generate strong enough traction forces that pull the cell forward. These clusters give rise to focal adhesion sites on the leading edge of a crawling cell. Formation of the active sites in the ECM to which cells can attach via focal adhesions occurs through a localized degradation of the matrix components by various cell-expressed proteases. As mentioned earlier, both proteases and focal adhesion sites are produced by the cells in response to the growth factor.

Thus, our model governs the spatio-temporal behavior of the following quantities:

c – the concentration of endothelial cells, f – the growth factor concentration,

r – the concentration of focal adhesion sites, p – the protease concentration,

m – the concentration of ECM active sites available for cell adhesion.

The model has much in common with other reaction-diffusion models that can be found in the literature [138]. It differs from the existing models by the dependent variables that we employ and by the treatment of cell motility that yields a diffusion-chemotaxis equation with a variable diffusion coefficient. As discussed in [138], a typical continuum model comprise equations for unknown variables that represent densities of all cell types involved in the process(e.g., ECs, pericytes, etc.) as well as the concentrations of substances influencing migration and/or proliferation, such as VEGF, proteases and angiogenic inhibitors. In our work we emphasize the importance of integrin-mediated mechanisms in cell migration by including the concentration of focal adhesion sites r and the concentration of ECM active sites m into the model, which has not been done in other works. Below we develop the model beginning with the cell motility and growth factor diffusion equations, and continue with kinetic equations for the state variables.

2.1.1. Cell motility

We begin with a derivation of the reinforced random walk equation that governs chemotactic/diffusional behavior of the ECs (cf. [159]). Consider a population of endothelial cells that are located at the nodes of a square lattice in the (x, y)-plane (see Figure 2.1). A cell can either stay at a node or jump from the node to one of the four neighboring nodes. Let $c_{n,k}(t)$ be the probability density distribution of the endothelial cells at the grid point (nh, kh) at time t. Here h is the stepsize of the lattice. In what follows we refer to the grid point (nh, kh) as (n, k). Then the time rate of change of $c_{n,k}(t)$ is governed by the master equation:

$$\frac{\partial c_{n,k}(t)}{\partial t} = \hat{\tau}^{\Rightarrow}_{n-1,k} c_{n-1,k} + \hat{\tau}^{\Leftarrow}_{n+1,k} c_{n+1,k} + \tag{2.1}$$

$$\hat{\tau}^{\Downarrow}_{n,k+1} c_{n,k+1} + \hat{\tau}^{\Uparrow}_{n,k-1} c_{n,k-1} - [\hat{\tau}^{\Rightarrow}_{n,k} + \hat{\tau}^{\Leftarrow}_{n,k} + \hat{\tau}^{\Downarrow}_{n,k} + \hat{\tau}^{\Uparrow}_{n,k}] c_{n,k}.$$

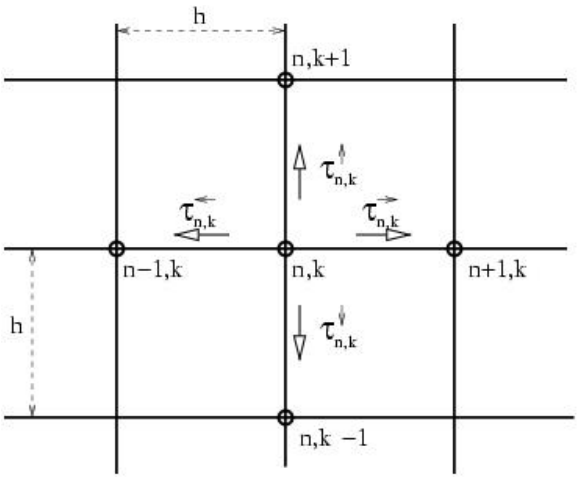

FIGURE 2.1. Schematic of the cell movement process

Here $\tau^{\Leftarrow}_{n,k}$, $\tau^{\Rightarrow}_{n,k}$, $\tau^{\Uparrow}_{n,k}$, $\tau^{\Downarrow}_{n,k}$, are the transition probability rates per unit time for a one-step move of an endothelial cell from the grid point (n, k) to grid points $(n - 1, k)$, $(n + 1, k)$, $(n, k + 1)$,

$(n, k-1)$, respectively. Thus, $c_{n,k}$ increases due to cell jumps from the grid points $(n \pm 1, k \pm 1)$ to (n, k) and decreases due to cell jumps from the grid point (n, k) to $(n \pm 1, k \pm 1)$. It is convenient to think of this conditional probability density as the density of endothelial cells. The transition probability rates $\tau^{\Leftarrow}_{n,k}$, $\tau^{\Rightarrow}_{n,k}$, $\tau^{\Uparrow}_{n,k}$, $\tau^{\Downarrow}_{n,k}$, depend on the state of the cell and the extracellular matrix adjacent to the cell. Though numerous biochemical species can affect the above state variables we presume that the readiness of the cell to sustain motion is characterized by the presence of focal adhesion sites r, while the preparedness of the matrix to support cell motion is characterized by the availability of the matrix sites m, to which the cell attaches. In addition, the polarity of the cell is accounted for by introducing the dependence of the transition rates on the growth factor concentration f. We assume that r, f and m are defined on the lattice at $1/2$-step size.

The transition rates can be represented as

$$\text{(2.2a)} \quad \hat{\tau}^{\Rightarrow}_{n,k} = \lambda(r_{n,k}, m_{n,k}) \frac{\tau(f_{n+1/2,k}, m_{n+1/2,k})}{S_{n,k}}, \quad \hat{\tau}^{\Leftarrow}_{n,k} = \lambda(r_{n,k}, m_{n,k}) \frac{\tau(f_{n-1/2,k}, m_{n-1/2,k})}{S_{n,k}},$$

$$\text{(2.2b)} \quad \hat{\tau}^{\Uparrow}_{n,k} = \lambda(r_{n,k}, m_{n,k}) \frac{\tau(f_{n,k+1/2}, m_{n,k+1/2})}{S_{n,k}}, \quad \hat{\tau}^{\Downarrow}_{n,k} = \lambda(r_{n,k}, m_{n,k}) \frac{\tau(f_{n,k-1/2}, m_{n,k-1/2})}{S_{n,k}},$$

where

$$S_{n,k} = \tau(f_{n+1/2,k}, m_{n+1/2,k}) + \tau(f_{n-1/2,k}, m_{n-1/2,k}) + \tau(f_{n,k+1/2}, m_{n,k+1/2}) + \tau(f_{n,k-1/2}, m_{n,k-1/2}).$$

Here λ characterizes the mean waiting time that the cell spends at the lattice point (n, k) before it jumps. Unlike the previous work we do not assume that the mean waiting time of the process is constant across the lattice; rather, we account for the state of the cell and the matrix as the quantities that determine the waiting time. The fractional terms on the right-hand sides of (2.2) define the

probability of jumping to one of the four adjacent locations – up, down, left, or right. We remark that the sum of these terms is equal to unity.

Substituting (2.2) into the master equation (2.1) and Taylor expanding yields

$$\frac{\partial c_{n,k}(t)}{\partial t} = \frac{h^2}{4}\left(\frac{\partial^2}{\partial x^2}+\frac{\partial^2}{\partial y^2}\right)(\lambda(r_{n,k},m_{n,k})c_{n,k}) - \frac{h^2}{4}\frac{\partial}{\partial x}\left(c_{n,k}\frac{\lambda(r_{n,k},m_{n,k})}{\tau(f_{n,k},m_{n,k})}\frac{\partial\tau(f_{n,k},m_{n,k})}{\partial x}\right)$$

$$-\frac{h^2}{4}\frac{\partial}{\partial y}\left(c_{n,k}\frac{\lambda(r_{n,k},m_{n,k})}{\tau(f_{n,k},m_{n,k})}\frac{\partial\tau(f_{n,k},m_{n,k})}{\partial y}\right)+O(h^3). \tag{2.3}$$

Next, we take the limit in (2.3) as $h\to 0$ and $\lambda\to\infty$ in such a way that

$$D = \frac{1}{4}\lim_{h\to 0,\lambda\to\infty}\lambda h^2$$

is finite, to obtain the equation

$$\frac{\partial c}{\partial t} = \frac{\partial}{\partial x}\left(\frac{\partial Dc}{\partial x} - Dc\frac{1}{\tau}\frac{\partial\tau}{\partial x}\right)+\frac{\partial}{\partial y}\left(\frac{\partial Dc}{\partial y} - Dc\frac{1}{\tau}\frac{\partial\tau}{\partial y}\right). \tag{2.4}$$

Including a logistic term in (2.4) to account for cell proliferation and apoptosis, and rewriting the terms with the derivatives we obtain

$$\frac{\partial c}{\partial t} = \text{div}\left[Dc\ \text{grad}\left(\ln\frac{Dc}{\tau}\right)\right]+K_c c(c_0-c). \tag{2.5}$$

Equation (2.5) is a reinforced random walk equation that governs chemotactic/diffusional behavior of the ECs. The equation is a modification of that in [159]. It involves a non-constant diffusion coefficient D, which depends on the state of both the matrix and the cells. The equation with a constant diffusion coefficient has been a subject of investigation in a number of works (see [125, 168] and the references therein).

The rate parameter K_c in the logistic term is taken in the form $K_c = \lambda_c(f - f_c)/(1 + \nu_c f)$ (cf. Michaelis-Menten kinetics in (2.11) below). This form reflects the fact that in order for immature ECs to survive and proliferate, a certain level of growth factor is required [46]. The cells undergo apoptosis if f falls below the critical level f_c. The quantities λ_c and ν_c in K_c are constants.

Note that since λ in (2.2) is a function of r and m, so is the diffusion coefficient D, i.e., $D = D(r, m)$. The form of the diffusion coefficient must account for the fact that diffusion is negligibly small if either r or m is small. We use an activated diffusion term of the form

$$D = D_c^0 \exp\left[-\frac{m_*}{m} - \frac{r_*}{r}\right], \quad D_c^0 = \text{const},$$

with some characteristic concentrations m_* and r_*. Another form of the diffusion coefficient is introduced and employed later. We also need to choose a specific form of τ. There are several functional forms of τ used in the literature. Typically they are not derived from the first principles but rather chosen at a phenomenological level. We use $\tau = \exp(\gamma f)$, where γ is a constant that characterizes chemotactic sensitivity of the cells (cf. [155]).

2.1.2. Cell and matrix state variables

To describe the production of proteases p and focal adhesion sites r in response to the growth factor f we assume the following overall reaction (cf. [124])

$$f + [Rec] \xrightarrow{k_1} [Rec \cdot f] \xrightarrow{k_2} [Rec] + \mu_p p + \mu_r r,$$

in which we denote the concentration of a species by the same letter as used for the species itself. Here $[Rec]$ is a free growth factor receptor, to which a growth factor molecule can bind, and $[Rec{\cdot}f]$

is the receptor occupied by a growth factor molecule. Thus, the first reaction describes binding of f to $[Rec]$ with the rate constant k_1, while the second reaction, which has the rate constant k_2, describes the secretion of μ_p molecules of protease and μ_r integrin clusters as well as the return of the receptor to its active form. Here the detailed pathways are not considered, and only the net reactions presented.

The mass balance equations governing the above reaction scheme have the form

$$\frac{\partial f}{\partial t} = -k_1 f[Rec], \tag{2.6}$$

$$\frac{\partial p}{\partial t} = \mu_p k_2 [Rec \cdot f], \tag{2.7}$$

$$\frac{\partial r}{\partial t} = \mu_r k_2 [Rec \cdot f], \tag{2.8}$$

$$\frac{\partial [Rec \cdot f]}{\partial t} = k_1 f[Rec] - k_2 [Rec \cdot f]. \tag{2.9}$$

In the last equation we use the steady-state assumption, which states that the rates of production and disappearance of the $[Rec \cdot f]$ complex are significantly higher than the rate of change of its concentration, which results in the algebraic balance

$$k_1 f[Rec] - k_2 [Rec \cdot f] = 0. \tag{2.10}$$

In mathematical terms this means that equation (2.9), appropriately nondimensionalized, will have a small parameter in front of the time derivative. We set this parameter to zero, thus considering the outer solution that is valid after a short transient period.

Introducing the total concentration $[Rec]_T$ of receptors, both occupied by f and unoccupied,

$$[Rec]_T = [Rec] + [Rec \cdot f],$$

and noting that $[Rec]_T = [Rec]_{Tc} \cdot c$, where $[Rec]_{Tc}$ is the number of receptors per cell, we can rewrite equations (2.6)–(2.8) as

$$-\frac{\partial f}{\partial t} = \frac{1}{\mu_p}\frac{\partial p}{\partial t} = \frac{1}{\mu_r}\frac{\partial r}{\partial t} = Kfc, \quad K \equiv \frac{k_1[Rec]_{Tc}}{1 + fk_1/k_2}. \tag{2.11}$$

In what follows we use the notation $\nu_f = k_1/k_2$, $\lambda_f = k_1[Rec]_{Tc}$. We can now formulate mass balance equations for p, r and f as

$$\frac{\partial p}{\partial t} = \mu_p K f c - k_p p, \tag{2.12}$$

$$\frac{\partial r}{\partial t} = \mu_r K f c - k_r r, \tag{2.13}$$

$$\frac{\partial f}{\partial t} = D_f \nabla^2 f - K f c + \delta c - \beta f. \tag{2.14}$$

Here the first term on the right-hand side of (2.12) is the rate of protease production (see (2.11)), while the second term is the rate of protease decay, e.g. due to self-cleavage. Similarly, the first term on the right-hand side of (2.13) is the rate of production of integrin clusters and, the second term is the rate of their disassembly. Equation (2.14) for the growth factor is a diffusion equation, with diffusion coefficient D_f. The second term on the right-hand side describes consumption of f according to (2.11), and the last two terms describe production of f by the endothelial cells and its decay. The quantities k_p, k_r, δ, and β in the above equations are rate constants.

Finally, the equation for the matrix adhesion sites is taken in the form

$$\frac{\partial m}{\partial t} = K_m p - k_{mr} m r. \tag{2.15}$$

Here the first term on the right-hand side is the sites production rate, proportional to the concentration of protease, with

$$K_m = \frac{\lambda_m(M-m)}{1+\nu_m(M-m)}$$

(cf. Michaelis-Menten kinetics in (2.11)). The second term is the rate of disappearance of available sites due to their occupation by integrin clusters. The quantities λ_m, ν_m, M, and k_{mr} are constants.

The system of equations derived above can be summarized as

$$\frac{\partial c}{\partial t} = \text{div}\left[Dc\ \text{grad}\left(\ln\frac{Dc}{\tau}\right)\right] + K_c(f)c(c_0-c), \tag{2.16a}$$

$$\frac{\partial f}{\partial t} = D_f\nabla^2 f - K_f(f)c + \delta c - \beta f, \tag{2.16b}$$

$$\frac{\partial p}{\partial t} = \mu_p K_f(f)c - k_p p, \tag{2.16c}$$

$$\frac{\partial r}{\partial t} = \mu_r K_f(f)c - k_r r, \tag{2.16d}$$

$$\frac{\partial m}{\partial t} = K_m(m)p - k_m m r, \tag{2.16e}$$

where

$$D = D_c^0\exp\left(-\frac{m_*}{m}-\frac{r_*}{r}\right), \quad K_c(f) = \frac{\lambda_c(f-f_c)}{1+\nu_c f},$$

$$\tau = \exp\left(\gamma f\right), \quad K_f(f) = \frac{\lambda_f f}{1+\nu_f f}, \quad K_m(m) = \frac{\lambda_m(M-m)}{1+\nu_m(M-m)}$$

and all the other parameters in (2.16) are constant.

2.1.3. Steady-state approximation

We again employ a steady-state assumption, this time with respect to the state variables p, r, and m, i.e., we assume that because the described biochemical reactions in the cell occur on a faster time

scale than the diffusion processes, eqns (2.16c)-(2.16e) can be replaced by the algebraic balances

$$\mu_p K_f(f)c - k_p p = 0, \quad \mu_r K_f(f)c - k_r r = 0, \quad K_m(m)p - k_m m r = 0$$

after a short transient period. From these algebraic equations we obtain

(2.17) $$p_s = \frac{\mu_p}{k_p} K_f(f)c, \quad r_s = \frac{\mu_r}{k_r} K_f(f)c, \quad m_s = \frac{\lambda_m M}{k_m k_p/k_r + \lambda_m}.$$

The steady-state assumption reduces the problem (2.16) to

(2.18) $$\frac{\partial c}{\partial t} = \text{div}\left[D_c \,\text{grad}\left(\ln\frac{D_c}{\tau}\right)\right] + K_c(f)c(c_0 - c),$$

(2.19) $$\frac{\partial f}{\partial t} = D_f \nabla^2 f - K_f(f)c + \delta c - \beta f,$$

where $$D_c = cD_0 \exp\left(-\frac{r_* k_r}{cK_f(f)\mu_r}\right), \quad D_0 = D_c^0 \exp\left(-\frac{m_*}{m_s}\right) = \text{const}.$$

Assuming for simplicity $\nu_c = \nu_f = 0$ in the expressions for K_f and K_c, we obtain

(2.20a) $$\frac{\partial c}{\partial t} = \nabla^2 D_c - \gamma \,\text{div}\,[D_c \,\text{grad} f] + \lambda_c(f - f_c)\, c\,(c_0 - c),$$

(2.20b) $$\frac{\partial f}{\partial t} = D_f \nabla^2 f - \lambda_f f c + \delta c - \beta f,$$

where D_c takes the form

(2.21) $$D_c = cD_0 \exp\left(-\frac{k_*}{cf}\right), \quad k_* = \frac{r_* k_r}{\lambda_f \mu_r}.$$

Below we discuss the spatially uniform steady states of the problem (2.20) and their linear stability. Then we focus on nonlinear stability analysis of one of the basic states of (2.20).

2.2. Basic states of the system

The system of equations (2.20) has three spatially uniform time-independent solutions that we refer to as the basic states and label them by a subscript s. They are

(2.22a) $$c_{s_1} = 0, \quad f_{s_1} = 0,$$

(2.22b) $$c_{s_2} = c_0, \quad f_{s_2} = \frac{\delta c_0}{\beta + \lambda_f c_0},$$

(2.22c) $$c_{s_3} = \frac{\beta f_c}{\delta - \lambda_f f_c}, \quad f_{s_3} = f_c.$$

Linear stability analysis of the basic states that is given below demonstrates that the first basic state is always stable, while the other two basic states may be either stable or unstable depending on the parameters of the system. We are particularly interested in the Turing instability, i.e., the instability that is caused by diffusion of the species. Turing instability of the second and third basic states occurs if

$$\gamma > \frac{k_*}{c_0 f_{s2}^2} + \frac{\delta k_*}{\beta f_{s2}^3} + \frac{\delta c_0}{\beta f_{s2}^2}, \qquad \gamma < \frac{k_*}{c_{s3} f_c^2} + \frac{\delta k_*}{\beta f_c^3} + \frac{\delta c_{s3}}{\beta f_c^2},$$

respectively. We are interested in the situation when the endothelial cells are very sensitive to the factor gradient, i.e., the sensitivity parameter γ is large. Thus, in what follows we focus on the second basic state for which the Turing instability occurs for large γ.

2.3. Nondimensionalization

We nondimensionalize the system of equations using

$$\tilde{c} = \frac{c - c_{s2}}{c_{s2}}, \ \tilde{f} = \frac{f - f_{s2}}{f_{s2}}, \ \tilde{x} = \frac{x}{l_*}, \ \tilde{y} = \frac{y}{l_*}, \ \tilde{t} = \frac{t}{t_*}, \ t_* = \frac{1}{\lambda_c c_0 f_{s2}}, \ l_*^2 = D_0 e^{-g} t_*, \ g = \frac{k_*}{f_{s2} c_{s2}},$$

to obtain

$$\frac{\partial \tilde{c}}{\partial \tilde{t}} = \nabla^2 \widetilde{D_c} - \omega \text{ div } [\widetilde{D_c} \text{ grad} \tilde{f}] - (1 - q_c + \tilde{f})(\tilde{c} + \tilde{c}^2), \tag{2.23a}$$

$$\frac{\partial \tilde{f}}{\partial \tilde{t}} = \widetilde{D_f} \nabla^2 \tilde{f} - (z + \zeta)\tilde{f} + \zeta \tilde{c} - z\tilde{f}\tilde{c}, \tag{2.23b}$$

with the basic state becoming $(\tilde{f}, \tilde{c}) = (0, 0)$ and

$$\omega = \gamma f_{s2}, \quad q_c = f_c / f_{s2}, \quad z = t_* \lambda_f c_{s2}, \quad \zeta = t_* \beta,$$

$$\widetilde{D_f} = \frac{D_f}{D_0} e^g, \qquad \widetilde{D_c} = (1 + \tilde{c}) \exp \left[g \frac{\tilde{c} + \tilde{f} + \tilde{c}\tilde{f}}{(1 + \tilde{c})(1 + \tilde{f})} \right]. \tag{2.24}$$

2.4. Analytical results

2.4.1. Linear stability analysis

We begin the linear stability analysis with linearizing the system (2.23) about the trivial steady state. We use the following linearization of $\widetilde{D_c}$ in (2.24),

$$\widetilde{D_c} = 1 + (1 + g)\tilde{c} + g\tilde{f} + \ldots, \tag{2.25}$$

to obtain

$$\frac{\partial \tilde{c}}{\partial \tilde{t}} = (1 + g)\nabla^2 \tilde{c} + (g - w)\nabla^2 \tilde{f} + (q_c - 1)\tilde{c}, \tag{2.26a}$$

$$\frac{\partial \tilde{f}}{\partial \tilde{t}} = \widetilde{D_f} \nabla^2 \tilde{f} + \zeta \tilde{c} - (z + \zeta)\tilde{f}. \tag{2.26b}$$

Substituting the normal mode solution

$$\begin{pmatrix} \tilde{c} \\ \tilde{f} \end{pmatrix} = \begin{pmatrix} a \\ b \end{pmatrix} e^{\sigma\tilde{t}+i\alpha_x\tilde{x}+i\alpha_y\tilde{y}},$$

where σ is the growth rate of the perturbation and (α_x, α_y) is the wave vector, we obtain the dispersion relation of the form

$$\sigma^2 + \left[\alpha^2(\widetilde{D_f} + g + 1) + z + \zeta + 1 - q_c\right]\sigma + \widetilde{D_f}\left[\alpha^4(1+g) + \alpha^2(1-q_c)\right]$$

$$+\alpha^2\left[\zeta(1+2g-\omega) + z(g+1)\right] + (\zeta+z)(1-q_c) = 0,$$

where α is the wavenumber of the perturbation, $\alpha^2 = \alpha_x^2 + \alpha_y^2$. We consider $q_c < 1$, in which case instability occurs as real σ changes the sign from negative to positive as parameters of the problem vary. The stability boundary corresponds to $\sigma = 0$. The neutral stability curve (Fig. 2.2), which can be written in the form

$$\widetilde{D_f} = -\frac{\alpha^2\left[\zeta(1+2g-\omega) + z(g+1)\right] + (\zeta+z)(1-q_c)}{\alpha^4(1+g) + \alpha^2(1-q_c)},$$

has a maximum $(\alpha_{cr}, \widetilde{D_f}_{cr})$, where

$$\widetilde{D_f}_{cr} = \frac{z+\zeta}{1-q_c}(\xi-1)^2(1+g), \quad \alpha_{cr}^2 = \frac{1-q_c}{(\xi-1)(1+g)}, \quad \xi = \left[\frac{\zeta(\omega-g)}{(1+g)(z+\zeta)}\right]^{1/2}, \tag{2.27}$$

provided that $\xi > 1$.

The eigenvector (a, b) for $\sigma = 0$, $\alpha = \alpha_{cr}$, and $\widetilde{D_f} = \widetilde{D_f}_{cr}$ is given by

$$a = \alpha_{cr}^2\widetilde{D_f} + z + \zeta, \quad b = \zeta.$$

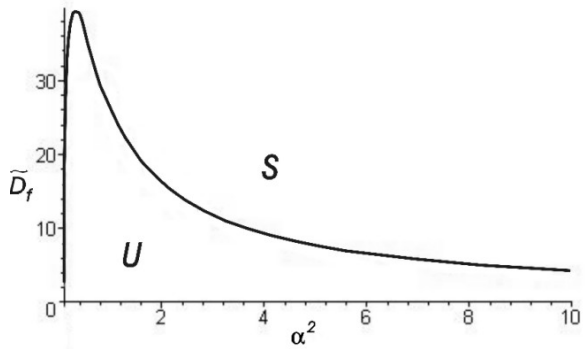

FIGURE 2.2. Neutral stability curve in the $(\alpha^2, \widetilde{D_f})$ plane. The stability region lies above the curve. Here $\zeta = 12$, $\omega = 6$, $z = 1$, $g = 0.5$, and $q_c = 0.5$.

The steady state (2.22b) is stable for $\widetilde{D_f} > \widetilde{D_{f\,cr}}$ and unstable otherwise. This result has a clear biological interpretation. If there is a local increase in the concentration of the growth factor, it will result in factor gradients and, therefore, in cell movement and EC aggregation at this location. These cells will release the growth factor thus providing positive feedback that leads to pattern formation. If, on the other hand, the diffusion coefficient of the factor is sufficiently large, factor gradients will vanish and cell aggregation will not occur.

To enhance our understanding of the model it is useful to analyze the dependence of $\widetilde{D_{f\,cr}}$ on the nondimensional parameters of the model. We consider the following parameter groups that appear as a result of nondimensionalization of (2.20)

$$\omega = \gamma f_{s2}, \quad q_c = f_c/f_{s2}, \quad z = t_* \lambda_f c_{s2}, \quad \zeta = t_* \beta.$$

2.4.1.1. ω – chemotactic sensitivity of ECs. It is clear from the expressions (2.27) that $\widetilde{D_{f\,cr}}$ increases with ω. It completely agrees with our understanding of ω as a measure of chemotactic sensitivity of the endothelial cells. Indeed, if there is a local increase in the concentration of the growth factor, the nearby cells start moving in that direction and the rate of their motion increases with ω as can also be seen directly from the first equation in (2.23). Thus, the larger is the ω, the

larger threshold value of $\widetilde{D_{f\,cr}}$ is needed to suppress the growth factor fluctuations and return the system to the steady state.

2.4.1.2. q_c – the EC proliferation/apoptosis parameter. The reason why q_c is called proliferation/apoptosis parameter can be understood by looking at the logistic term in the first equation in (2.20). If there is a local increase in the growth factor concentration, which in turn leads to an increase of the EC concentration at the same spot, then $c > c_0$, $f > f_c$ and the logistic term is negative, i.e. apoptosis takes place and the local EC density decreases. In this case an increase in f_c (which corresponds to an increase in q_c) means that apoptosis rate slows down, i.e. smaller number of cells are dying and more cells respond to the chemotactic stimulus by migrating up the growth factor gradient. Thus the larger is q_c, the smaller $\widetilde{D_f}$ is needed to suppress this growth factor fluctuation. This phenomenological understanding agrees with (2.27) from which $\widetilde{D_{f\,cr}}$ increases as q_c decreases, $0 < q_c < 1$.

2.4.1.3. z – the rate of the growth factor consumption by ECs. Computing partial derivative of $\widetilde{D_{f\,cr}}$ with respect to z we get

$$\frac{\partial \widetilde{D_{f\,cr}}}{\partial z} = \frac{1+g}{1-q_c}(1-\xi) < 0$$

since $0 < q_c < 1$ and $\xi > 1$ (see (2.27)). This fact is in agreement with our understanding that if the rate of consumption of the growth factor increases, then a smaller $\widetilde{D_f}$ is needed to eliminate random growth factor fluctuations and prevent instability.

2.4.1.4. ζ – the rate of growth factor decay. Computing the partial derivative of $\widetilde{D_{f\,cr}}$ with respect to ζ we obtain

$$\frac{\partial \widetilde{D_{f\,cr}}}{\partial \zeta} = \frac{1+g}{1-q_c}(\xi-1)\left[\xi\left(1+\frac{z}{\zeta}\right)-1\right] > 0$$

since $0 < q_c < 1$ and $\xi > 1$. This also agrees with our understanding of the process. Indeed, as we see from the second equation in (2.23), if a cell density fluctuation becomes larger then the growth factor fluctuation, it leads to an increase in the growth factor density. In this case a larger $\widetilde{D_f}$ is needed to suppress fluctuations and to prevent an instability development.

2.4.2. Weakly nonlinear analysis: stripes and hexagons

We now focus on the weakly nonlinear analysis of the system (2.23) in order to understand pattern formation near the instability threshold. In this section we study the appearance of hexagons and stripes.

Let small parameter ε characterize the magnitude of the bifurcating solution. We introduce the slow time $T = \varepsilon^2 \tilde{t}$ and expand both unknowns $\tilde{c}$ and $\tilde{f}$ as well as the bifurcation parameter $\widetilde{D_f}$ as

$$\tilde{c} = \varepsilon c_1 + \varepsilon^2 c_2 + \varepsilon^3 c_3 + \dots, \quad \tilde{f} = \varepsilon f_1 + \varepsilon^2 f_2 + \varepsilon^3 f_3 + \dots, \quad \widetilde{D_f} = \widetilde{D_{f\,cr}} - \varepsilon^2 \mu. \tag{2.28}$$

Here $\tilde{c}$, c_j, $\tilde{f}$, f_j $(j = 1, 2, 3)$ are functions of T, $\tilde{x}$, and $\tilde{y}$. In what follows we use the following expansion of $\widetilde{D_c}$ about $\tilde{c} = \tilde{f} = 0$

$$\widetilde{D_c} \approx 1 + (1+g)\,\tilde{c} + g\tilde{f} + \frac{1}{2}g^2\tilde{c}^2 + \left(\frac{1}{2}g^2 - g\right)\tilde{f}^2 + g^2\tilde{c}\tilde{f} + \tag{2.29}$$

$$\left(\frac{1}{6}g^3 - \frac{1}{2}g^2\right)\tilde{c}^3 + \left(\frac{1}{6}g^3 - g^2 + g\right)\tilde{f}^3 + \left(\frac{1}{2}g^3 - \frac{3}{2}g^2\right)\tilde{c}\tilde{f}^2 + \left(\frac{1}{2}g^3 - g^2\right)\tilde{c}^2\tilde{f} + \dots.$$

Substituting the expansions (2.28) into the system of equations (2.23) and collecting like powers of ε we obtain at orders ε^j $(j = 1, 2, 3)$ the sequence of problems

$$-\frac{\partial c_j}{\partial \tilde{t}} + (g+1)\widetilde{\nabla}^2 c_j + (g-\omega)\widetilde{\nabla}^2 f_j - (1-q)c_j = R_{cj} \tag{2.30a}$$

(2.30b) $$-\frac{\partial f_j}{\partial \tilde{t}} + \widetilde{D}_{f\,cr}\widetilde{\nabla}^2 f_j - (z+\zeta)f_j + \zeta c_j = R_{fj}.$$

Here the right-hand sides for $j = 1, 2$ are given by

$$R_{c1} = R_{f1} = 0, \quad R_{f2} = z f_1 c_1,$$

$$R_{c2} = -\widetilde{\nabla}^2 \left[\frac{1}{2}g^2 c_1^2 + \left(\frac{1}{2}g^2 - g\right) f_1^2 + g^2 c_1 f_1\right] +$$

$$w(g+1)\widetilde{\nabla} f_1 \cdot \widetilde{\nabla} c_1 + w[(g+1)c_1 + g f_1]\widetilde{\nabla}^2 f_1 + wg(\widetilde{\nabla} f_1)^2 + c_1 f_1 + (1-q_c)c_1^2.$$

The right-hand sides R_{c3}, R_{f3} are presented in Appendix.

At $O(\varepsilon)$ we obtain the linearized system (2.26b). We seek solution in the form

(2.31) $$\begin{pmatrix} c_1 \\ f_1 \end{pmatrix} = (L_1 e_1 + L_2 e_2 + L_3 e_3 + c.c.) \begin{pmatrix} a \\ b \end{pmatrix},$$

where

(2.32) $$e_1 = \exp(i\alpha_{cr}\tilde{x}), \quad e_{2,3} = \exp\left[i\alpha_{cr}\left(-\frac{\tilde{x}}{2} \pm \frac{\sqrt{3}}{2}\tilde{y}\right)\right],$$

and $c.c.$ denotes complex conjugate terms. Here the amplitudes L_1, L_2, L_3 are functions of the slow time T. We choose this form of the solution, with the three normal modes, because we want to describe the appearance of both hexagons and stripes as well as their interaction.

Next we turn to the $O(\varepsilon^2)$ problem. The right-hand sides R_{c2} and R_{f2} can be written in the form

$$R_{c2} = K_1 E_1 + K_2 E_2 + K_3 E_3 + K_4 E_4, \quad R_{f2} = zab(E_1 + E_2 + 2E_3 + 2E_4),$$

where

$$E_1 = L_1^2 e_1^2 + L_2^2 e_2^2 + L_3^2 e_3^2 + c.c., \quad E_2 = 2(|L_1|^2 + |L_2|^2 + |L_3|^2),$$

$$E_3 = L_1 L_2^* e_1 e_2^* + L_1 L_3^* e_1 e_3^* + L_2 L_3^* e_2 e_3^* + c.c., \quad E_4 = L_1 L_2 e_3^* + L_1 L_3 e_2^* + L_2 L_3 e_1^* + c.c.,$$

the asterisk denotes the complex conjugate, and the coefficients K_1, K_2, K_3, K_4 are given in Appendix. We remark that the terms $K_4 E_4$ are secular terms that appear in the $O(\varepsilon^2)$ problem due to the resonance interaction of the modes (2.32). These secular terms are considered to be small and will contribute to the solvability condition at $O(\varepsilon^3)$ [209].

Then the solution of the $O(\varepsilon^2)$ problem is given by

$$\begin{pmatrix} c_2 \\ f_2 \end{pmatrix} = E_1 \begin{pmatrix} c_{21} \\ f_{21} \end{pmatrix} + E_2 \begin{pmatrix} c_{22} \\ f_{22} \end{pmatrix} + E_3 \begin{pmatrix} c_{23} \\ f_{23} \end{pmatrix},$$

where the coefficients c_{2j}, f_{2j} are given in Appendix.

Elimination of secular terms in the $O(\varepsilon^3)$ problem via the orthogonality conditions of the right-hand side (R_{c3}, R_{f3}) to the solutions of the adjoint homogeneous problem given by

$$\begin{pmatrix} \zeta \\ (1+g)\alpha_{cr}^2 + 1 - q_c \end{pmatrix} e_j, \quad j = 1, 2, 3$$

results in the following system of equation for the amplitudes L_1, L_2, L_3

(2.33a) $$\frac{dL_1}{dT} = \mu C_1 L_1 + C_2 L_2^* L_3^* + C_3 L_1 |L_1|^2 + C_4 L_1 (|L_2|^2 + |L_3|^2),$$

(2.33b) $$\frac{dL_2}{dT} = \mu C_1 L_2 + C_2 L_1^* L_3^* + C_3 L_2 |L_2|^2 + C_4 L_2 (|L_1|^2 + |L_3|^2),$$

(2.33c) $$\frac{dL_3}{dT} = \mu C_1 L_3 + C_2 L_1^* L_2^* + C_3 L_3 |L_3|^2 + C_4 L_3 (|L_1|^2 + |L_2|^2).$$

The quadratic terms in the equations come from the secular terms in the $O(\varepsilon^2)$ problem. The coefficients C_k, $k = 1, 2, 3, 4$ are real and depend on the parameters of the problem. They are given in Appendix.

2.4.3. Analysis of the amplitude equations: stripes and hexagons

We consider steady states of the system (2.33). Specifically, we are interested in the steady states that describe hexagons and stripes in the original system. We briefly list below the well known general results concerning these patterns [209], and then relate these results to the problem at hand. Hexagonal patterns correspond to

$$L_1 = L_2 = L_3 = L_h,$$

where L_h is a solution of the quadratic equation

$$(C_3 + 2C_4)L_h^2 + C_2 L_h + \mu C_1 = 0.$$

Stripes parallel to the y-axis correspond to

$$L_1 = L_s, \quad L_2 = L_3 = 0, \quad L_s = \sqrt{-\frac{\mu C_1}{C_3}}.$$

We first discuss the stripes. Linear stability analysis of the stripes as a stationary solution of the system (2.33) results in the following values for the growth rate σ of perturbations:

$$\sigma_1 = -2\mu C_1, \quad \sigma_2 = 0, \quad \sigma_{3,4} = C_2 L_s - (C_3 - C_4)L_s^2, \quad \sigma_{5,6} = -C_2 L_s - (C_3 - C_4)L_s^2.$$

Since the coefficient C_1 is always positive, we conclude that

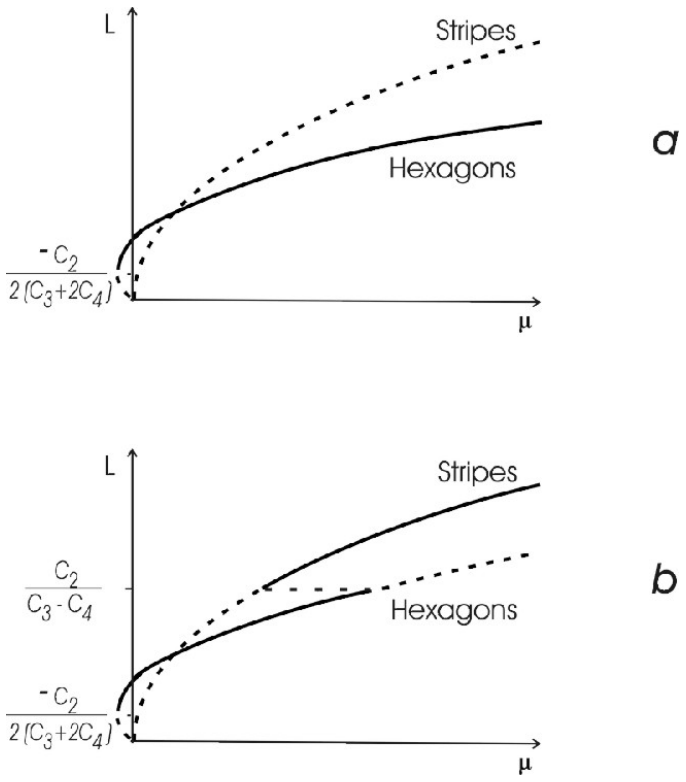

FIGURE 2.3. Bifurcation diagram in $(\mu, |L|)$ plane.
Case a : $C_3 + 2C_4 < 0$, $C_2 > 0$, and $C_3 < 0$, $C_3 - C_4 < 0$;
Case b : $C_3 + 2C_4 < 0$, $C_2 > 0$, $C_3 - C_4 > 0$, $C_3 + C_4 < 0$ and $C_3 < 0$.

- if $C_3 > 0$ the stripes are subcritical (i.e., they exist for $\mu < 0$) and are unstable;
- if $C_3 < 0$ the stripes are supercritical ($\mu > 0$);
- the supercritical stripes are unstable for all L_s if $C_3 - C_4 < 0$ (Fig. 2.3 a);
- the supercritical stripes are stable for $L_s > |C_2|/(C_3 - C_4)$ if $C_3 - C_4 > 0$ (Fig. 2.3 b).

Linear stability analysis of the hexagons as a stationary solution of the system (2.33) results in the following values for the growth rate σ of perturbations:

$$\sigma_1 = C_2 L_h + 2(C_3 + 2C_4)L_h^2, \quad \sigma_{2,3} = 2[-C_2 L_h + (C_3 - C_4)L_h^2], \quad \sigma_4 = -3C_2 L_h, \quad \sigma_{5,6} = 0.$$

Again, keeping in mind the fact that the coefficient $C_1 > 0$, we conclude that

- for $C_3 + 2C_4 > 0$ there exist only subcritical hexagonal patterns that are always unstable (more precisely, there exist supercritical hexagons in this case if $C_2 < 0$, but they are unstable anyway);
- for $C_3 + 2C_4 < 0$ there exist supercritical hexagonal patterns;
- the supercritical hexagonal patterns are stable for $L_h > -C_2/[2(C_3 + 2C_4)]$ if the three conditions $C_3 + 2C_4 < 0$, $C_2 > 0$, and $C_3 - C_4 < 0$ are simultaneously met (Fig. 2.3 a). If, however, the first two conditions on the coefficients are satisfied, but $C_3 - C_4 > 0$, then there exist stable hexagons only if $C_3 + C_4 < 0$. In this case the amplitudes L_h of the stable hexagons satisfy $-C_2/[2(C_3 + 2C_4)] < L_h < C_2/(C_3 - C_4)$ (Fig. 2.3 b);
- the supercritical hexagonal patterns are always unstable if either $C_2 < 0$ or $C_3 - C_4 > 0$ and $C_3 + C_4 > 0$.

From the above results it follows that stable stripes and hexagons can coexist in the system if $C_2 > 0$ and $C_4 < C_3 < 0$. In this case the system will exhibit stable hexagons with amplitudes L_h in the range $-C_2/[2(C_3 + 2C_4)] < L_h < C_2/(C_3 - C_4)$ and stable stripes with amplitudes $L_s > C_2/(C_3 - C_4)$. There is a region of bistability of the two patterns, which occurs for

$$-\frac{C_2^2 C_3}{C_1(C_3 - C_4)^2} < \mu < -\frac{C_2^2(2C_3 + C_4)}{C_1(C_3 - C_4)^2}.$$

These result are summarized in the bifurcation diagram, where solid lines stand for stable states of the system and dotted lines show unstable states (Fig. 2.3).

2.4.4. Parameter sensitivity: stripes and hexagons

We next turn to a discussion of the patterns that occur in the angiogenesis problem depending on the parameters of the system. The parameters that we vary are ζ, ω, and z. It is useful to recall

the biological meaning of these parameters. Parameter ζ can be interpreted as a nondimensional rate of decay of the growth factor. There are means to control ζ, e.g., by introducing decoy soluble growth factor receptors that reduce the concentration of active growth factor, which can be treated as an increase in ζ. Parameter ω characterizes the chemotactic sensitivity of the endothelial cells. It can also be controlled, e.g., by inhibiting the growth factor receptors. Parameter z is related to the rate of intracellular activity, which results, e.g., in production of proteases and formation of integrin clusters.

Figures 2.4 show the dependence of the coefficient C_2 as well as $C_3 - C_4$ and $C_3 + 2C_4$ on ζ for different values of z and ω.

We first observe that for small ζ, i.e., for a very slow decay of the growth factor, $C_3 - C_4 < 0$, $C_3 + 2C_4 > 0$, and $C_2 > 0$ (in fact, $C_2 > 0$ for all parameter values we considered). The signs of these quantities mean that hexagons are subcritical, unstable, and therefore cannot occur in this case. The stripes appear supercritically, but they are also unstable. The resulting behavior of the original system is not described by the amplitude equations, and can be quite complex, e.g., chaotic.

For intermediate values of ζ, $C_3 + 2C_4 < 0$ and $C_2 > 0$ while the sign of $C_3 - C_4$ depends on the other parameters. For smaller ω and z, i.e., for reduced chemotactic sensitivity and lower biochemical activity of the cells $C_3 - C_4 > 0$, which means that both stable hexagons and stripes exist for some values of the diffusion coefficient of the growth factor, and moreover, for some values of the diffusion coefficient they coexist. For larger ω and z only stable hexagons can be observed.

For large values of ζ, $C_3 + 2C_4 < 0$ and $C_2 > 0$, and the previous scenario repeats – both hexagons and stripes can be observed unless z is increased, in which case only hexagons survive.

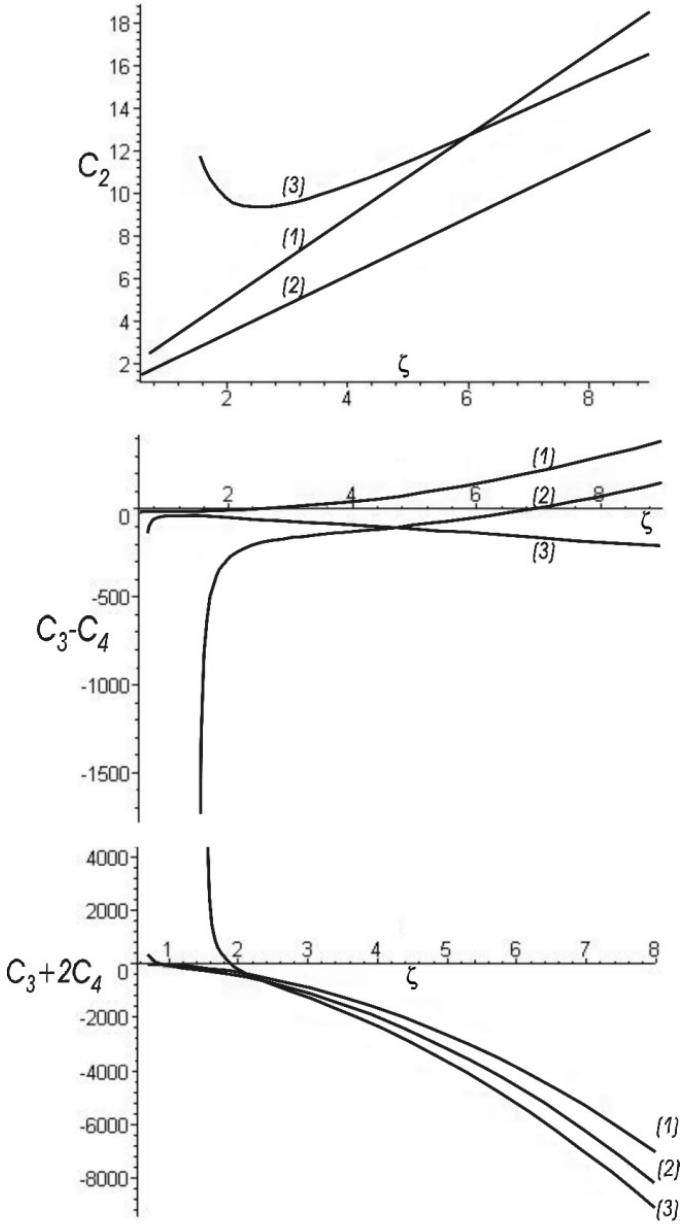

FIGURE 2.4. The quantities C_2, C_3-C_4 and C_3+2C_4 as functions of ζ for different parameter values. Here $q = 0.5$, $g = 1$ for all the curves, and $\omega = 6$, $z = 1$ for curves (1), $\omega = 7$, $z = 1$ for curves (2), $\omega = 7$, $z = 3$ for curves (3)

The above observations can be useful as they demonstrate the trends that may be expected as parameters of the biological system are varied in experiments. These results can be summarized as follows. No steady patterns can be observed if the rate of decay of the growth factor is small.

Increasing the rate of decay of the growth factor (e.g., by introducing decoy soluble growth factor receptors) allows one to observe steady patterns if the diffusion coefficient of the growth factor is sufficiently small. These patterns are hexagons and stripes. Most often hexagons are observed. In order for the stripes to occur the chemotactic sensitivity of the endothelial cells and/or their biochemical activity has to be reduced.

2.4.5. Weakly nonlinear analysis: squares

We again perform the weakly nonlinear analysis of the systems (2.23) with the cell diffusion coefficient taken in the form (2.21). This time we study occurrence of square patterns near the instability threshold.

We again introduce the slow time $T = \varepsilon^2 \tilde{t}$ and expand both unknowns $\tilde{c}$ and $\tilde{f}$ as well as the bifurcation parameter $\widetilde{D_f}$ as

$$\tilde{c} = \varepsilon c_1 + \varepsilon^2 c_2 + \varepsilon^3 c_3 + \dots, \quad \tilde{f} = \varepsilon f_1 + \varepsilon^2 f_2 + \varepsilon^3 f_3 + \dots, \quad \widetilde{D_f} = \widetilde{D_f}_{cr} - \varepsilon^2 \mu, \tag{2.34}$$

$\tilde{c}$, c_j, $\tilde{f}$, f_j $(j = 1, 2, 3)$ being functions of $\tilde{t}$, T, $\tilde{x}$, $\tilde{y}$.

Substituting the expansions (2.34), (2.29) into the system of equations (2.23) and collecting like powers of ε we obtain at orders ε^j $(j = 1, 2, 3)$ the same sequence of problems as before

$$-\frac{\partial c_j}{\partial \tilde{t}} + (g+1)\widetilde{\nabla}^2 c_j + (g-\omega)\widetilde{\nabla}^2 f_j - (1-q)c_j = R_{cj}, \tag{2.35a}$$

$$-\frac{\partial f_j}{\partial \tilde{t}} + \widetilde{D_f}_{cr}\widetilde{\nabla}^2 f_j - (z+\zeta)f_j + \zeta c_j = R_{fj}. \tag{2.35b}$$

Here the right-hand sides for $j = 1, 2$ are given by

$$R_{c1} = R_{f1} = 0, \quad R_{f2} = z f_1 c_1. \quad R_{c2} = -\widetilde{\nabla}^2 \left[\frac{1}{2} g^2 c_1^2 + \left(\frac{1}{2} g^2 - g \right) f_1^2 + g^2 c_1 f_1 \right] +$$

$$w(g+1)\widetilde{\nabla} f_1 \cdot \widetilde{\nabla} c_1 + w[(g+1)c_1 + g f_1]\widetilde{\nabla}^2 f_1 + wg(\widetilde{\nabla} f_1)^2 + c_1 f_1 + (1 - q_c)c_1^2,$$

The right-hand sides R_{c3}, R_{f3} are presented in Appendix. At $O(\varepsilon)$ we have obtained the linearized system (2.26b). We seek solution in the form

$$\begin{pmatrix} c_1 \\ f_1 \end{pmatrix} = (L_1 e_1 + L_2 e_2 + c.c.) \begin{pmatrix} a \\ b \end{pmatrix}, \tag{2.36}$$

where $e_1 = \exp(i\alpha_{cr}\tilde{x}), \quad e_2 = \exp(i\alpha_{cr}\tilde{y})$, and $c.c.$ denotes the complex conjugate terms. Here the amplitudes L_1, L_2 are functions of the slow time T. We choose this form of the solution, with the two normal modes, because we want to describe the appearance of square patterns.

Next we turn to the $O(\varepsilon^2)$ problem. The right-hand sides R_{c2} and R_{f2} can be written in the form

$$R_{c2} = K_1 E_1 + K_2 E_2 + K_3 E_3, \quad R_{f2} = zab(E_1 + E_2 + 2E_3),$$

where

$$E_1 = L_1^2 e_1^2 + L_2^2 e_2^2 + c.c., \quad E_2 = 2(|L_1|^2 + |L_2|^2), \quad E_3 = L_1 L_2 e_1 e_2 + L_1^* L_2 e_1^* e_2 + c.c.,$$

the asterisk denotes the complex conjugate, and the coefficients K_1, K_2, K_3 are given in Appendix. The solution of the $O(\varepsilon^2)$ problem is given by

$$\begin{pmatrix} c_2 \\ f_2 \end{pmatrix} = E_1 \begin{pmatrix} c_{21} \\ f_{21} \end{pmatrix} + E_2 \begin{pmatrix} c_{22} \\ f_{22} \end{pmatrix} + E_3 \begin{pmatrix} c_{23} \\ f_{23} \end{pmatrix},$$

where the coefficients c_{2j}, f_{2j} are given in Appendix.

Elimination of secular terms in the $O(\varepsilon^3)$ problem via the orthogonality conditions of the right-hand side (R_{c3}, R_{f3}) to the solutions of the adjoint homogeneous problem given by

$$\begin{pmatrix} \zeta \\ (1+g)\alpha_{cr}^2 + 1 - q_c \end{pmatrix} e_j, \quad j = 1, 2$$

results in the following system of equation for the amplitudes L_1, L_2

$$\frac{dL_1}{dT} = \mu C_1 L_1 + C_3 L_1 |L_1|^2 + C_4 L_1 |L_2|^2, \tag{2.37a}$$

$$\frac{dL_2}{dT} = \mu C_1 L_2 + C_3 L_2 |L_2|^2 + C_4 L_2 |L_1|^2. \tag{2.37b}$$

The coefficients C_k, $k = 1, 3, 4$ are real and depend on the parameters of the problem. They are given in Appendix.

2.4.6. Analysis of the amplitude equations: squares

Below we consider steady states of the system (2.37), specifically, we are interested in the steady states that describe squares in the original system. We briefly list below well known general results concerning these patterns [209], and then relate these results to the problem at hand. Square patterns correspond to $L_1 = L_2 = L_{sq}$, where L_{sq} is a solution of the quadratic equation

$$(C_3 + C_4) L_{sq}^2 + \mu C_1 = 0.$$

The linear stability analysis of the system (2.37) results in the following values for the growth rate σ of perturbations:

$$\sigma_1 = \sigma_2 = 0, \quad \sigma_3 = -\mu C_1, \quad \sigma_4 = 2(C_3 - C_4) L_{sq}^2.$$

Since the coefficient C_1 is always positive, we conclude that

- for $C_3 + C_4 > 0$ there exist only subcritical square patterns that are always unstable;
- for $C_3 + C_4 < 0$ there exist supercritical square patterns;
- the supercritical square patterns are stable if $C_3 - C_4 < 0$
- the supercritical square patterns are unstable if $C_3 - C_4 > 0$.

2.4.7. Parameter sensitivity: squares

We next turn to a discussion of the square patterns that can occur in the angiogenesis problem depending on the parameters of the system. The parameters that we vary are ζ, ω, and q_c. It is useful to recall the biological meaning of these parameters. Parameter ζ can be interpreted as a nondimensional rate of decay of the growth factor. There are means to control ζ, e.g., by introducing decoy soluble growth factor receptors that reduce the concentration of active growth factor, which can be treated as an increase in ζ. Parameter ω characterizes the chemotactic sensitivity of the endothelial cells. It can also be controlled, e.g., by inhibiting the growth factor receptors. Parameter $q_c = f_c/f_{s2}$ is the endothelial cell proliferation/apoptosis parameter (see (2.20a)). This parameter reflects cell sensitivity to the presence of the growth factor in the system and the growth factor level necessary for cell metabolic needs in order to avoid apoptosis.

Figures 2.5 show the dependence of the coefficient combinations $C_3 + C_4$ and $C_3 - C_4$ on ζ for different values of q_c. These dependencies have the same character when ω is slightly increased, i.e. the appearance of square patterns does not depend on chemotactic sensitivity of endothelial cells.

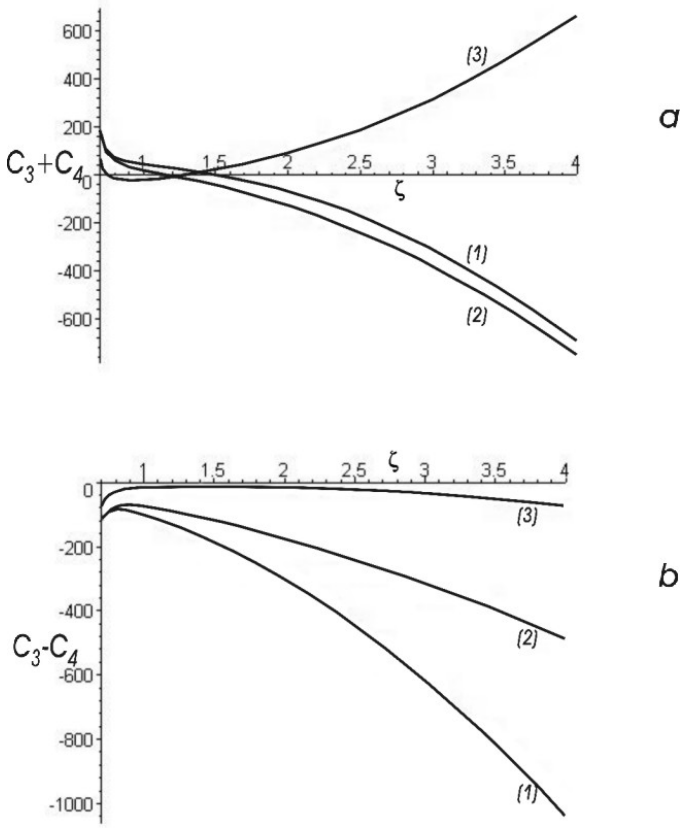

FIGURE 2.5. The quantities $C_3 + C_4$ and $C_3 - C_4$ as functions of ζ for different parameter values. Here $\omega = 6$, $g = 1$, $z = 1$ for all curves, and $q_c = 0.1$, for curves (1), $q_c = 0.5$, for curves (2), $q_c = 0.9$ for curves (3)

We first observe that for small ζ, i.e., for a very slow decay of the growth factor, $C_3 - C_4 < 0$, $C_3 + C_4 > 0$. The signs of these quantities mean that squares are subcritical, unstable, and therefore cannot occur in this case. The resulting behavior of the original system is not described by the amplitude equations, and can be quite complex, e.g., chaotic.

For intermediate values of ζ, $C_3 - C_4 < 0$ while the sign of $C_3 + C_4$ depends on q_c. For smaller q_c, i.e., for reduced sensitivity of the cells to the presence of the growth factor $C_3 + C_4 > 0$, which means that squares are subcritical and unstable but as q_c increases, $C_3 + C_4$ changes sign and becomes negative indicating the existence of stable supercritical squares in the system.

For large values of ζ, $C_3 - C_4 < 0$ while the sign of $C_3 + C_4$ depends on q_c. For smaller q_c, i.e. for reduced sensitivity of the cells to the presence of the growth factor $C_3 + C_4 < 0$ which means that stable supercritical squares exist in the system. For larger q_c, $C_3 + C_4$ turns positive which means that squares become subcritical and unstable.

The above observations can be useful as they demonstrate the trends that may be expected as parameters of the biological system are varied in experiments. These results can be summarized as follows. No steady patterns can be observed if the rate of decay of the growth factor is small. Increasing the rate of decay of the growth factor (e.g., by introducing decoy soluble growth factor receptors) allows one to observe steady square patterns if endothelial cell sensitivity to the presence of the growth factor is sufficiently large. Further increasing the rate of decay of the growth factor we observe steady square patterns if endothelial cell sensitivity to the presence of the growth factor decreases.

2.5. Coexistence of hexagons, stripes and square patterns

If we go back and summarize the results obtained in subsections 2.4.6 and 2.4.3 we can make the following conclusions about system behavior at certain chosen parameter values:

- Stable supercritical stripes and stable supercritical square patterns never coexist in the system;
- Stable supercritical hexagonal patterns and stable supercritical stripes can coexist for $-C_2/[2(C_3 + 2C_4)] < L_{h,s} < C_2/(C_3 - C_4)$ if all the conditions $C_3 + 2C_4 < 0$, $C_2 > 0$, $C_3 < 0$, $C_3 - C_4 > 0$ and $C_3 + C_4 < 0$ are simultaneously met (Fig. 2.3 b);

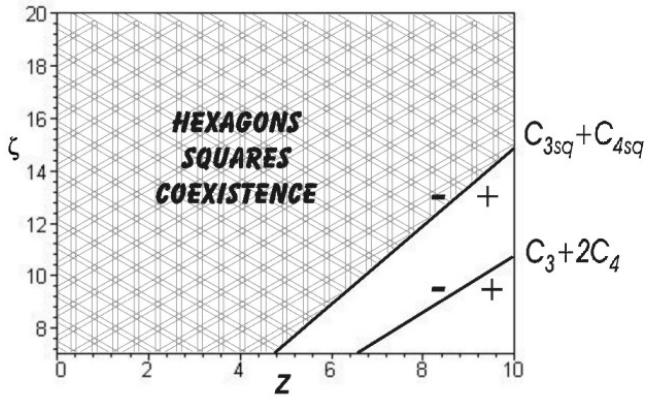

FIGURE 2.6. Zero contour plots of quantities $C_3 + 2C_4$ and $C_{3sq} + C_{4sq}$ in $z - \zeta$ plane for $\omega = 6$, $g = 1$, $q_c = 0.1$. For the chosen range of z and ζ $C_2 > 0$ and $C_3 - C_4 < 0$.
Subscript 'sq' indicates coefficients of the amplitude equations derived for squares (2.37).

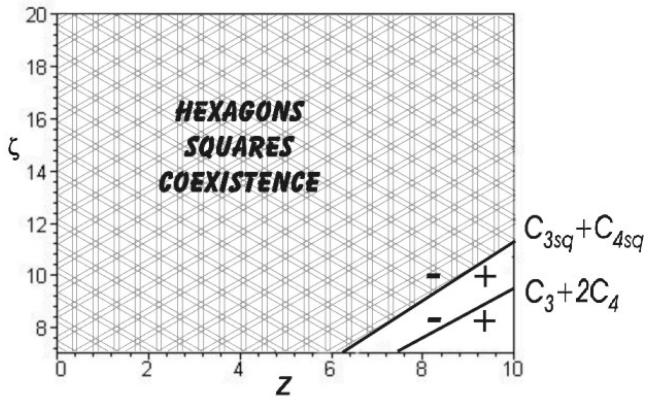

FIGURE 2.7. Zero contour plots of quantities $C_3 + 2C_4$ and $C_{3sq} + C_{4sq}$ in $z - \zeta$ plane for $\omega = 6$, $g = 1$, $q_c = 0.5$. For the chosen range of z and ζ $C_2 > 0$, $C_3 - C_4 < 0$ and $C_{3sq} - C_{4sq} < 0$
Subscript 'sq' indicates coefficients of the amplitude equations derived for squares (2.37).

- Stable supercritical hexagonal patterns and stable supercritical stripes can coexist for $L_h > -C_2/[2(C_3 + 2C_4)]$ if all the conditions $C_2 > 0$, $C_3 + 2C_4 < 0$, $C_3 - C_4 < 0$ and $C_3 + C_4 < 0$ are simultaneously met.

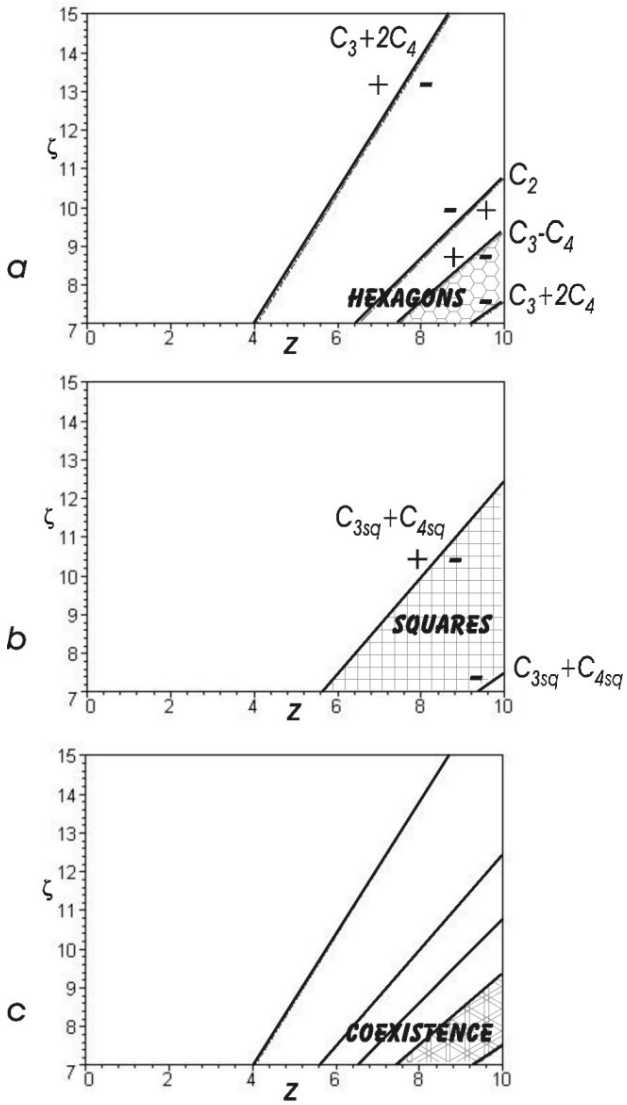

FIGURE 2.8. Area of existence for hexagons, stripes and their coexistence in $z-\zeta$ plane for $\omega = 6$, $g = 1$, $q_c = 0.9$.
a) Zero contour plots of quantities C_2, $C_3 + 2C_4$, $C_3 - C_4$ and $C_3 - C_4$.
b) Zero contour plot for $C_{3sq}+C_{4sq}$. For the chosen range of z and ζ $C_{3sq}-C_{4sq} < 0$. Subscript 'sq' indicates coefficients of the amplitude equations derived for squares (2.37).
c) $z-\zeta$ region where stable supercritical hexagonal and square patterns coexist.

Coexistence of stable supercritical hexagons and squares for different parameter values is demonstrated on the Fig. 2.6, 2.7, 2.8.

2.6. Endothelial cell system in the absence of cell proliferation

We are also interested in the case when endothelial cells are not allowed to proliferate. If EC mitosis is prevented the growth of capillaries is drastically reduced and results only in a restricted network being formed ([186]). Study of this particular case provides an underlying insight into mechanisms of cell migration which are crucial for understanding angiogenesis ([6]). In terms of our mathematical model it means that we put $\lambda_c = 0$ in the first equation of the system (2.20). We obtain the system of equations

$$\frac{\partial c}{\partial t} = \nabla^2(D_c) - \gamma \text{ div } [D_c \text{ grad} f], \tag{2.38a}$$

$$\frac{\partial f}{\partial t} = D_f \nabla^2 f - \lambda_f f c + \delta c - \beta f, \tag{2.38b}$$

where D_c has the same form (2.21) as before.

2.6.1. Basic states of the system and nondimensionalization

The system of equations (2.38) has a one-parameter family of spatially uniform time-independent solutions that we refer to as the basic states and label them by a subscript s. They are

$$c_s = \text{constant}, \quad f_s = \frac{\delta c_s}{\beta + \lambda_f c_s}. \tag{2.39}$$

It is convenient to nondimensionalize the system of equations using the basic state (2.39) as the reference quantities. Specifically, the following nondimensional variables are introduced

$$\tilde{c} = \frac{c - c_s}{c_s}, \quad \tilde{f} = \frac{f - f_s}{f_s}, \quad \tilde{x} = \frac{x}{l_*}, \quad \tilde{y} = \frac{y}{l_*}, \quad \tilde{t} = \frac{t}{t_*},$$

where

$$t_* = \frac{f_s}{\delta c_s}, \quad l_*^2 = D_0 t_* e^{-g}, \quad g = \frac{k_*}{f_s c_s}.$$

We obtain

$$\frac{\partial \tilde{c}}{\partial \tilde{t}} = \nabla^2(\widetilde{D_c}) - \omega \text{ div } [\widetilde{D_c} \text{ grad} \tilde{f}], \tag{2.40a}$$

$$\frac{\partial \tilde{f}}{\partial \tilde{t}} = \widetilde{D_f}\nabla^2 \tilde{f} - \tilde{f} + (1-z)\tilde{c} - z\tilde{f}\tilde{c}, \tag{2.40b}$$

with

$$\omega = \gamma f_s, \quad z = t_* \lambda_f c_s \equiv \frac{\lambda_f c_s}{\beta + \lambda_f c_s} < 1, \quad \widetilde{D_f} = \frac{D_f e^g}{D_0}, \ \widetilde{D_c} = (1+\tilde{c}) \exp\left[g \frac{\tilde{c} + \tilde{f} + \tilde{c}\tilde{f}}{(1+\tilde{c})(1+\tilde{f})} \right].$$

2.6.2. Linear stability analysis

Next, we perform linear stability analysis of the basic state $\tilde{c} = 0$, $\tilde{f} = 0$ of the problem (2.40). Linearizing (2.40) about the trivial basic state, we obtain

$$\frac{\partial \tilde{\tilde{c}}}{\partial \tilde{t}} = (1+g)\nabla^2 \tilde{\tilde{c}} + (g-\omega)\nabla^2 \tilde{\tilde{f}}, \tag{2.41a}$$

$$\frac{\partial \tilde{\tilde{f}}}{\partial \tilde{t}} = \widetilde{D_f}\nabla^2 \tilde{\tilde{f}} - \tilde{\tilde{f}} + (1-z)\tilde{\tilde{c}}. \tag{2.41b}$$

Substituting the normal mode solution

$$\begin{pmatrix} \tilde{\tilde{c}} \\ \tilde{\tilde{f}} \end{pmatrix} = \begin{pmatrix} a \\ b \end{pmatrix} e^{\sigma \tilde{t} + i\alpha_x \tilde{x} + i\alpha_y \tilde{y}},$$

where σ is the growth rate of the perturbation and (α_x, α_y) is the wave vector, into (2.40), yields

$$\begin{pmatrix} -\alpha^2(1+g)-\sigma & -(g-\omega)\alpha^2 \\ 1-z & -\widetilde{D_f}\alpha^2-1-\sigma \end{pmatrix} \begin{pmatrix} a \\ b \end{pmatrix} = 0,$$

where $\alpha^2 = \alpha_x^2 + \alpha_y^2$. Setting the determinant of the above matrix equal zero we obtain the dispersion relation

$$\sigma^2 + \left[\alpha^2(\widetilde{D_f}+g+1)+1\right]\sigma + \alpha^2\left[(g+1)(\widetilde{D_f}\alpha^2+1)+(g-\omega)(1-z)\right] = 0.$$

There are two roots of the quadratic equation, $\sigma_\pm(\alpha)$. It is easy to check that Re$(\sigma_-(\alpha)) < 0$ for all α and parameter values. The real part of the other root, $\sigma_+(\alpha)$, can be either positive or negative, depending on parameter values. Specifically, if

$$\omega < \omega_{cr} \equiv \frac{g+1}{1-z} + g, \tag{2.42}$$

then Re$(\sigma_+(\alpha)) < 0$ for all α. If, however, $\omega > \omega_{cr}$, then there is a range of α given by

$$0 < \alpha < \alpha_{cr},$$

for which Re$(\sigma_+(\alpha)) > 0$ (see Fig. 2.9). The quantity α_{cr} is determined by

$$\alpha_{cr}^2 = \frac{1}{\widetilde{D_f}}\left[\frac{(\omega-g)(1-z)}{g+1} - 1\right] = \frac{1}{\widetilde{D_f}}\frac{1-z}{g+1}\,(\omega-\omega_{cr}). \tag{2.43}$$

It has to be noted that for ω slightly above ω_{cr} the maximum of the growth rate $\sigma_+(\alpha)$ is attained at $\alpha = \alpha_{cr}/\sqrt{2}$ and is equal to

$$\sigma_{max} = \frac{1}{4}\widetilde{D_f}\,(g+1)\,\alpha_{cr}^4. \tag{2.44}$$

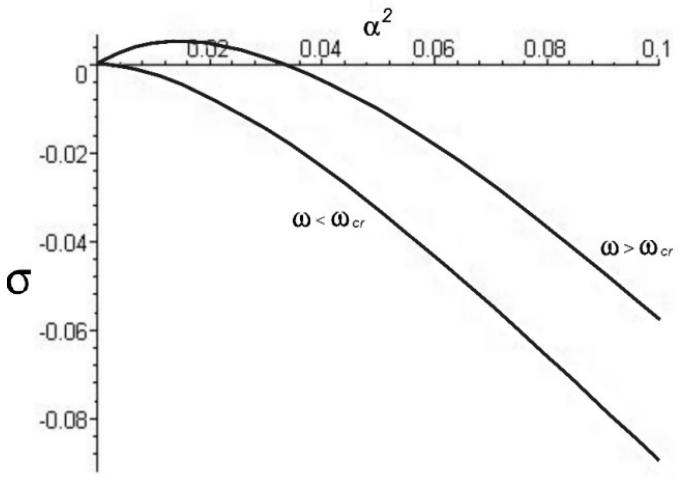

FIGURE 2.9. The quantity σ as a function of α_{cr}^2 for two different values of ω. Here $z = 0.5$, $g = 0.5$, $\widetilde{D_f} = 15$, $\omega_{cr} = 3.5$, $\omega_1 = 3.4$, $\omega_2 = 5$, $\alpha_{cr} = 0.036$

2.6.3. Long-wave analysis: Sivashinsky equation

We consider ω close to the critical value ω_{cr},

$$\omega = \omega_{cr} + \mu\varepsilon^2.$$

Then the results of linear stability analysis suggest the following scalings:

$$\chi = \varepsilon\tilde{x}, \quad \eta = \varepsilon\tilde{y}, \quad T = \varepsilon^4\tilde{t},$$

which transform the system (2.40) into

(2.45a) $$\varepsilon^4\frac{\partial\tilde{c}}{\partial T} = \varepsilon^2\nabla^2_{\chi,\eta}(\widetilde{D_c}) - (\omega_{cr} + \mu\varepsilon^2)\varepsilon^2\,\nabla_{\chi,\eta}\cdot[\widetilde{D_c}\,\nabla_{\chi,\eta}\tilde{f}],$$

(2.45b) $$\varepsilon^4\frac{\partial\tilde{f}}{\partial T} = \varepsilon^2\widetilde{D_f}\nabla^2_{\chi,\eta}\tilde{f} - \tilde{f} + (1-z)\tilde{c} - z\tilde{f}\tilde{c}.$$

Here we retain the same notations $\tilde{c}$ and $\tilde{f}$ for the solution that depends on the slow variables χ, η and T.

We introduce the following notations for quadratic and cubic parts of the Taylor expansion (2.29) for $\widetilde{D_c}$, namely

(2.46a) $$a(\tilde{c},\tilde{f}) = \frac{1}{2}g^2\tilde{c}^2 + \left(\frac{1}{2}g^2 - g\right)\tilde{f}^2 + g^2\tilde{c}\tilde{f},$$

(2.46b)
$$b(\tilde{c},\tilde{f}) = \left(\frac{1}{6}g^3 - \frac{1}{2}g^2\right)\tilde{c}^3 + \left(\frac{1}{6}g^3 - g^2 + g\right)\tilde{f}^3 + \left(\frac{1}{2}g^3 - \frac{3}{2}g^2\right)\tilde{c}\tilde{f}^2 + \left(\frac{1}{2}g^3 - g^2\right)\tilde{c}^2\tilde{f}.$$

Then the system (2.45) can be rewritten in the form:

(2.47a) $$\varepsilon^4\frac{\partial\tilde{c}}{\partial T} = \varepsilon^2\nabla^2_{\chi,\eta}[(1+g)\tilde{c} + (g-\omega_{cr})\tilde{f}] + \varepsilon^2\nabla^2_{\chi,\eta}[a(\tilde{c},\tilde{f})] +$$

$$\varepsilon^2\nabla^2_{\chi,\eta}[b(\tilde{c},\tilde{f})] - \omega_{cr}\nabla\cdot\{([(1+g)\tilde{c} + (g-\omega_{cr})\tilde{f}] + a(\tilde{c},\tilde{f})\nabla\tilde{f}\} - \mu\varepsilon^4\nabla^2_{\chi,\eta}\tilde{f} - \omega^2_{cr}\varepsilon^2\nabla\cdot(\tilde{f}\nabla\tilde{f}),$$

(2.47b) $$\varepsilon^4\frac{\partial\tilde{f}}{\partial T} = \varepsilon^2\widetilde{D_f}\nabla^2_{\chi,\eta}\tilde{f} - \tilde{f} + (1-z)\tilde{c} - z\tilde{f}\tilde{c}.$$

We expand both unknowns $\tilde{c}$ and $\tilde{f}$ as

$$\tilde{c}(\chi,\eta,T) = \varepsilon^2 c_2(\chi,\eta,T) + \varepsilon^4 c_4(\chi,\eta,T) + \varepsilon^6 c_6(\chi,\eta,T) + \ldots,$$

$$\tilde{f}(\chi,\eta,T) = \varepsilon^2 f_2(\chi,\eta,T) + \varepsilon^4 f_4(\chi,\eta,T) + \varepsilon^6 f_6(\chi,\eta,T) + \ldots.$$

Substituting the expansions for $\tilde{c}$, $\tilde{f}$ into (2.47) and collecting like powers of ε we obtain at order $O(\varepsilon^2)$ a linear algebraic relation between c_2 and f_2,

(2.48) $$f_2 = (1-z)c_2.$$

At orders $O(\varepsilon^4)$ and $O(\varepsilon^6)$ we obtain

(2.49a) $$\nabla^2_{\chi,\eta}\left[(1+g)c_2+(g-\omega_{cr})f_2\right]=0,$$

(2.49b) $$-f_4+(1-z)c_4=-\widetilde{D_f}\nabla^2_{\chi,\eta}f_2+zc_2f_2,$$

and

(2.50a) $$-\frac{\partial c_2}{\partial T}+\nabla^2_{\chi,\eta}\left[(1+g)c_4+(g-\omega_{cr})f_4+a(c_2,f_2)\right]-$$

$$\omega_{cr}\nabla_{\chi,\eta}\cdot\{[(1+g)c_2+(g-\omega_{cr})f_2]\nabla_{\chi,\eta}f_2\}-\mu\nabla^2_{\chi,\eta}f_2-\omega^2_{cr}\nabla_{\chi,\eta}\cdot(f_2\nabla f_2)=0,$$

(2.50b) $$-f_6+(1-z)c_6=\frac{\partial f_2}{\partial T}-\widetilde{D_f}\nabla^2_{\chi,\eta}f_4+z(c_2f_4+c_4f_2),$$

respectively. From (2.42) and (2.48) it follows that (2.49a) is satisfied, while (2.49b) allows one to determine f_4 as

(2.51) $$f_4=(1-z)\widetilde{D_f}\nabla^2_{\chi,\eta}c_2+(1-z)c_4-z(1-z)c_2^2.$$

Substituting (2.42), (2.48) and (2.51) into (2.50a) and simplifying, we finally obtain the equation

(2.52) $$\frac{\partial c_2}{\partial T}=-(1+g)\widetilde{D_f}\nabla^4_{\chi,\eta}c_2-\mu(1-z)\nabla^2_{\chi,\eta}c_2+\left[z-\frac{1}{2}+g(4z-z^2-3)\right]\nabla^2_{\chi,\eta}(c_2^2).$$

Equation (2.52) is known as the Sivashinsky equation. It describes the weakly nonlinear evolution of instabilities in a large class of systems, including the dewetting of a one-layer thin liquid film [158], the long-wave deformational Marangoni instability of a liquid film [71], the morphological instability of directional solidification fronts with small segregation coefficient [189]. It is

the generic nonlinear evolution equation in systems with broken up-down symmetry that exhibits a long-wave instability with the Goldstone mode caused by a conservation law (in our case - conservation of mass) [152]. Equation (37) is characterized by a subcritical instability and exhibits the blow-up in a finite time in the form of a cusp as was proved in [19]. The blow-up occurs for any sign of the coefficient of the nonlinear term (provided the coefficient is not equal to zero); this sign determines the direction of the developing cusp (up or down), since Eq. (2.52) is invariant with respect to the transformation $c_2 \to -c_2$ with the simultaneous change of the sign of the nonlinear term. In our case the blow-up can be interpreted as the formation of regions with no cells, although the weakly nonlinear approximation breaks down in this case.

The weakly nonlinear analysis can also give a prediction about the parameter region in which a different behavior, other than the blow-up, can occur. Indeed, Eq. (2.52) is derived under the assumption that all the terms in the equation are of the same order. This is not necessarily true because the coefficient of the nonlinear term can vanish. Near the surface in the parameter space where the coefficient is zero, Eq. (2.52) is not valid since higher-order nonlinearities become important and should be accounted for. In this case a different scaling should be used for the weakly-nonlinear analysis. We shall now proceed with the weakly-nonlinear analysis under the assumption that the coefficient is equal to zero.

2.6.4. Long-wave analysis: Cahn-Hilliard equation

We consider now the case when the coefficient of the nonlinear term in the Sivashinsky equation (2.52) is equal to zero, i.e.

$$z - \frac{1}{2} + g(-z^2 + 4z - 3) = 0.$$

In this case we derive the Cahn-Hilliard equation. We again consider ω close to the critical value ω_{cr} given by (2.42),

$$\omega = \omega_{cr} + \mu\varepsilon^2,$$

but now we also assume

(2.53) $$g = \frac{z - \frac{1}{2}}{z^2 - 4z + 3}.$$

As before, introducing the following scalings

$$\chi = \varepsilon\tilde{x}, \quad \eta = \varepsilon\tilde{y}, \quad T = \varepsilon^4\tilde{t},$$

and substituting Taylor expansion (2.29) for $\widetilde{D_c}$ with the corresponding notations for the quadratic and cubic parts (2.46), we transform the system (2.45) into

(2.54a) $$\varepsilon^4\frac{\partial\tilde{c}}{\partial T} = \varepsilon^2\nabla^2_{\chi,\eta}[(1+g)\tilde{c} + (g-\omega_{cr})\tilde{f}] + \varepsilon^2\nabla^2_{\chi,\eta}[a(\tilde{c},\tilde{f})] + \varepsilon^2\nabla^2_{\chi,\eta}[b(\tilde{c},\tilde{f})]$$

$$-\omega_{cr}\nabla\cdot\{([(1+g)\tilde{c} + (g-\omega_{cr})\tilde{f}] + a(\tilde{c},\tilde{f})\nabla\tilde{f}\} - \mu\varepsilon^4\nabla^2_{\chi,\eta}\tilde{f} - \omega^2_{cr}\varepsilon^2\nabla\cdot(\tilde{f}\nabla\tilde{f}),$$

(2.54b) $$\varepsilon^4\frac{\partial\tilde{f}}{\partial T} = \varepsilon^2\widetilde{D_f}\nabla^2_{\chi,\eta}\tilde{f} - \tilde{f} + (1-z)\tilde{c} - z\tilde{f}\tilde{c}.$$

Here we retain the same notations $\tilde{c}$ and $\tilde{f}$ for the solution that depends on the slow variables χ, η and T. We use a different expansion of $\tilde{c}$ and $\tilde{f}$, namely

$$\tilde{c}(\chi,\eta,T) = \varepsilon c_1(\chi,\eta,T) + \varepsilon^2 c_2(\chi,\eta,T) + \varepsilon^3 c_3(\chi,\eta,T) + \varepsilon^4 c_4(\chi,\eta,T) + \varepsilon^5 c_5(\chi,\eta,T) + \ldots,$$

$$\tilde{f}(\chi,\eta,T) = \varepsilon f_1(\chi,\eta,T) + \varepsilon^2 f_2(\chi,\eta,T)\varepsilon^3 f_3(\chi,\eta,T) + \varepsilon^4 f_4(\chi,\eta,T) + \varepsilon^5 f_5(\chi,\eta,T) + \ldots.$$

Substituting the expansions for ω_{cr}, $\tilde{c}$, $\tilde{f}$ into (2.54) and collecting like powers of ε we obtain at order $O(\varepsilon)$ a linear algebraic relation between c_1 and f_1,

(2.55) $$f_1 = (1-z)c_1.$$

At orders $O(\varepsilon^2)$ and $O(\varepsilon^3)$ we obtain

(2.56) $$f_2 = (1-z)c_2 - zf_1c_1.$$

(2.57a) $$\nabla^2_{\chi,\eta}\left[(1+g)c_1 + (g-\omega_{cr})f_1\right] = 0,$$

(2.57b) $$f_3 = (1-z)c_3 - zc_2f_1 - zc_1f_2 + \widetilde{D_f}\nabla^2_{\chi,\eta}f_1.$$

Substituting (2.42) into (2.57a) we can easily see that this equation is satisfied.

At $O(\varepsilon^4)$ we obtain

(2.58a) $$\nabla^2_{\chi,\eta}\left[(1+g)c_2 + (g-\omega_{cr})f_2\right] + \nabla^2_{\chi,\eta}[a(c_1,f_1)] -$$

$$\omega_{cr}\nabla\cdot\left[(1+g)c_1 + (g-\omega_{cr})f_1\right]\nabla f_1 - \omega^2_{cr}\nabla\cdot(f_1\nabla f_1) = 0,$$

(2.58b) $$f_4 = (1-z)c_4 - zc_1f_3 - zc_2f_2 - zc_3f_1 + \widetilde{D_f}\nabla^2_{\chi,\eta}f_2.$$

Let us show that the first equation (2.58a) is satisfied. Using (2.56) and (2.42) it simplifies to

$$-(g-\omega_{cr})\nabla^2_{\chi,\eta}(zf_1c_1) + \nabla^2_{\chi,\eta}[a(c_1,f_1)] - \omega^2_{cr}\nabla\cdot(f_1\nabla f_1) = 0.$$

Then using (2.55) and simplifying we get

$$\left[z(1+g)+a(1,1-z)-\frac{1}{2}\omega_{cr}^2(1-z)^2\right]\nabla_{\chi,\eta}^2(c_1^2)=0,$$

which is satisfied due to (2.53).

At $O(\varepsilon^5)$ we obtain the following equation for c_1:

(2.59)
$$\frac{\partial c_1}{\partial T}=\nabla_{\chi,\eta}^2[(1+g)c_3+(g-\omega_{cr})f_3]+\nabla_{\chi,\eta}^2[b(c_1,f_1)]+$$

$$\nabla_{\chi,\eta}^2[g^2c_1c_2+(g^2-2g)f_1f_2+g^2c_1f_2+g^2c_2f_1]-$$

$$\omega_{cr}\nabla_{\chi,\eta}\cdot\{[(1+g)c_2+(g-\omega_{cr})f_2+a(c_1,f_1)]\nabla_{\chi,\eta}f_1\}-$$

$$\mu\nabla_{\chi,\eta}^2f_1-\omega_{cr}^2\nabla\cdot(f_1\nabla f_2)-\omega_{cr}^2\nabla\cdot(f_2\nabla f_1).$$

Simplifying this expression we finally obtain

(2.60)
$$\frac{\partial c_1}{\partial T}=-\frac{z^2-3z+5/2}{z^2-4z+3}\widetilde{D_f}\nabla_{\chi,\eta}^4c_1-\mu(1-z)\nabla_{\chi,\eta}^2c_1+Q\nabla_{\chi,\eta}^2(c_1^3),$$

where

$$Q=-z^2(1+g)+gz(1-z)[2(1-g)+z(g-2)]+b(1,1-z)-$$

$$\frac{1}{3}\omega_{cr}(1-z)[a(1,1-z)+z(1+g)]+\omega_{cr}^2z(1-z)^2=\frac{9z^2-19z+6}{6(z-3)}$$

is shown in Fig. 2.10. Equation (2.60) is the Cahn-Hilliard equation that describes spinodal decomposition of phase separating systems [34]. It exhibits the formation of a spatial structure with

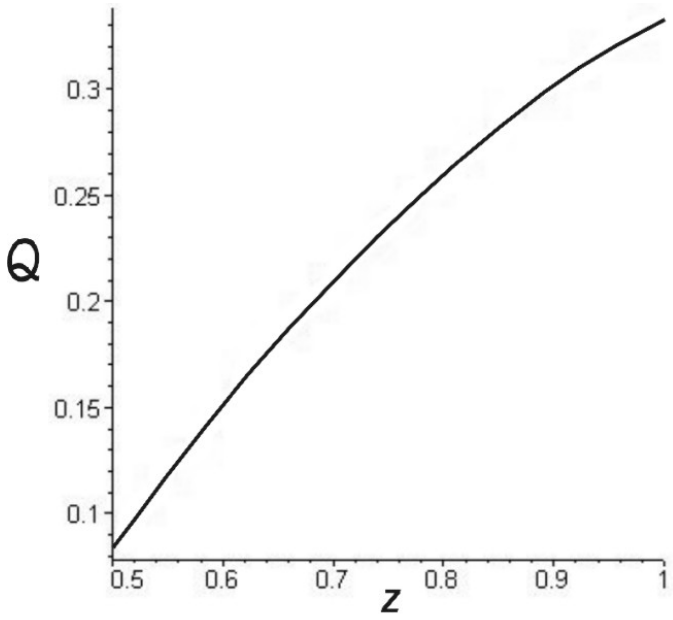

FIGURE 2.10. Dependence of the coefficient Q of the Cahn-Hilliard equation (2.60) on z.

a saturated amplitude and a characteristic wavelength that coarsens in time. This structure has the form of a labyrinth pattern. Note that this dynamics can be observed only for $Q > 0$ that holds in certain regions in the parameter space. In the parameter regions for which $Q < 0$, solutions of (2.60) blow up in a finite time and do not describe any saturated structures.

2.7. Analysis of the base model with a different form of D_c

Consider the same system of equations (2.20) as before, but with a different form of the cell diffusion coefficient, namely

$$D_c = cD_0 \exp\left(-\frac{k_* c}{f}\right). \tag{2.61}$$

This form of the diffusion coefficient addresses the experimental observation that as c increases, i.e., the environment becomes more crowded, diffusion of cells is hampered.

2.7.1. Steady states and nondimensionalization

In this case the system has the same three spatially uniform steady states as before

$$c_{s_1} = 0, \quad f_{s_1} = 0, \tag{2.62}$$

$$c_{s_2} = c_0, \quad f_{s_2} = \frac{\delta c_0}{\beta + \lambda_f c_0}, \tag{2.63}$$

$$c_{s_3} = \frac{\beta f_c}{\delta - \lambda_f f_c}, \quad f_{s_3} = f_c. \tag{2.64}$$

We again nondimensionalize using steady state (2.63) as a reference quantity

$$\tilde{c} = \frac{c - c_{s2}}{c_{s2}}, \;\; \tilde{f} = \frac{f - f_{s2}}{f_{s2}}, \;\; \tilde{x} = \frac{x}{l_*}, \;\; \tilde{y} = \frac{y}{l_*},$$

$$\tilde{t} = \frac{t}{t_*}, \;\; t_* = \frac{1}{\lambda_c c_0 f_{s2}}, \;\; l_*^2 = D_0 e^{-g} t_*, \quad g = \frac{k_* c_{s2}}{f_{s2}},$$

which yields the following nondimensional system of equations

$$\frac{\partial \tilde{c}}{\partial \tilde{t}} = \nabla^2 \widetilde{D_c} - \omega \text{ div } [\widetilde{D_c} \text{ grad} \tilde{f}] - (1 - q_c + \tilde{f})(\tilde{c} + \tilde{c}^2), \tag{2.65a}$$

$$\frac{\partial \tilde{f}}{\partial \tilde{t}} = \widetilde{D_f} \nabla^2 \tilde{f} - (z + \zeta)\tilde{f} + \zeta \tilde{c} - z \tilde{f} \tilde{c}, \tag{2.65b}$$

with the basic state becoming $(\tilde{f}, \tilde{c}) = (0, 0)$ and

$$\omega = \gamma f_{s2}, \quad q_c = f_c / f_{s2}, \quad z = t_* \lambda_f c_{s2}, \quad \zeta = t_* \beta,$$

$$\widetilde{D_f} = \frac{D_f}{D_0} e^g, \quad \widetilde{D_c} = (1 + \tilde{c}) \exp\left[g \frac{\tilde{f} - \tilde{c}}{1 + \tilde{f}} \right]. \tag{2.66}$$

2.7.2. Linear stability analysis

The linearized form of $\widetilde{D_c}$ is

$$\widetilde{D_c} = 1 + (1-g)\tilde{c} + g\tilde{f}, \tag{2.67}$$

and the linearized system is given by

$$\frac{\partial \tilde{\tilde{c}}}{\partial \tilde{t}} = (1-g)\nabla^2\tilde{\tilde{c}} + (g-w)\nabla^2\tilde{\tilde{f}} + (q_c - 1)\tilde{\tilde{c}}, \tag{2.68a}$$

$$\frac{\partial \tilde{\tilde{f}}}{\partial \tilde{t}} = \widetilde{D_f}\nabla^2\tilde{\tilde{f}} + \zeta\tilde{\tilde{c}} - (z+\zeta)\tilde{\tilde{f}}, \tag{2.68b}$$

where $\tilde{\tilde{c}}$ and $\tilde{\tilde{f}}$ are small deviations of nondimensional $\tilde{c}$ and $\tilde{f}$ from the trivial steady state.

Proceeding with the linear stability analysis in the same way as before we get the dispersion relation of the form

$$\sigma^2 + \left[\alpha^2(\widetilde{D_f} + 1 - g) + z + \zeta + 1 - q_c\right]\sigma + \widetilde{D_f}\left[\alpha^4(1-g) + \alpha^2(1-q_c)\right]$$

$$+\alpha^2\left[\zeta(1-\omega) + z(1-g)\right] + (\zeta + z)(1-q_c) = 0,$$

where σ and α are the growth rate and the wavenumber of the perturbation, respectively. We again consider $q_c < 1$ and arrive at the following expression for the neutral stability curve

$$\widetilde{D_f} = -\frac{\alpha^2\left[\zeta(1-\omega) + z(1-g)\right] + (\zeta+z)(1-q_c)}{\alpha^4(1-g) + \alpha^2(1-q_c)},$$

which has a maximum at $(\alpha_{cr}, \widetilde{D_f}_{cr})$ where

$$\widetilde{D_f}_{cr} = \frac{z+\zeta}{1-q_c}(\xi-1)^2(1-g), \quad \xi = \left[\frac{\zeta(\omega-g)}{(1-g)(z+\zeta)}\right]^{1/2}, \quad \alpha_{cr}^2 = \frac{1-q_c}{(\xi-1)(1-g)}, \tag{2.69}$$

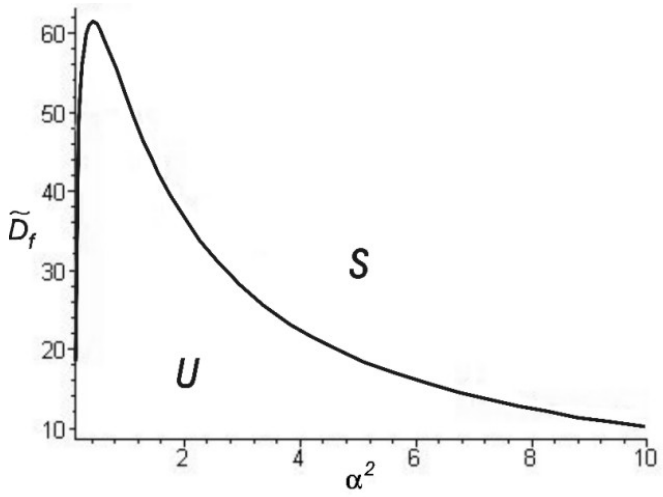

FIGURE 2.11. Neutral stability curve in the $(\alpha^2, \widetilde{D_f})$ plane. The stability region lies above the curve. Here $\zeta = 12$, $\omega = 6$, $z = 1$, $g = 0.5$, and $q_c = 0.5$.

provided that $\xi > 1$ and $0 < g < 1$.

The eigenvector (a, b) for $\sigma = 0$, $\alpha = \alpha_{cr}$, and $\widetilde{D_f} = \widetilde{D_f}_{cr}$ is given by the same values of a and b as in the previous case, namely

$$\begin{pmatrix} a \\ b \end{pmatrix} = \begin{pmatrix} \alpha_{cr}^2 \widetilde{D_f} + z + \zeta \\ \zeta \end{pmatrix}.$$

The steady state (2.63) is stable for $\widetilde{D_f} > \widetilde{D_f}_{cr}$ and unstable otherwise (see Fig. 2.11).

This result has a clear biological interpretation. If there is a local increase in the concentration of the growth factor, it will result in factor gradients and, therefore, in cell movement and their aggregation at that location. These cells will release the growth factor thus providing positive feedback leading to pattern formation. If on the other hand the diffusion coefficient of the factor is sufficiently large, factor gradients will vanish and cell aggregation will not occur.

To enhance our understanding of the model it is also useful to analyze dependencies of $\widetilde{D_f}_{cr}$ on the nondimensional parameters of the model. We will consider the following parameter complexes

that appear as a result of nondimensionalization of (2.20) with D_c taken in the form (2.61)

$$\omega = \gamma f_{s2}, \quad q_c = f_c/f_{s2}, \quad z = t_* \lambda_f c_{s2}, \quad \zeta = t_* \beta.$$

2.7.2.1. ω **- the chemotactic sensitivity of the endothelial cells.** It is clear from the expressions (2.69) that $\widetilde{D_{f\,cr}}$ increases as ω increases. It completely agrees with our understanding of ω as a measure of chemotactic sensitivity of the endothelial cells. Indeed, if there is a local increase in the concentration of the growth factor, the nearby cells start moving in that direction and the rate of their motion increases with ω as it can also be seen directly from the first equation in (2.65). Thus, the larger is ω, the larger threshold value of $\widetilde{D_{f\,cr}}$ is needed to suppress the growth factor fluctuation and let the system return to the steady state.

2.7.2.2. q_c **- the endothelial cell proliferation/apoptosis parameter.** The reason why q_c is called proliferation/apoptosis parameter can be understood by looking at the logistic term in the first equation in (2.20). If there is a local increase in the growth factor concentration which in turn leads to endothelial cell concentration increase at the same spot, then we can say that $c > c_0$, $f > f_c$ and the logistic term is negative, i.e. apoptosis takes place and local endothelial cell density reduces. In this case the increase in f_c (which corresponds to the increase in q_c) means that apoptosis rate slows down, i.e. smaller number of cells are dying and more cells respond to the chemotactic stimulus by migrating up the growth factor gradient. So, the smaller is q_c, the larger $\widetilde{D_{f\,cr}}$ is needed to suppress this growth factor fluctuation preventing an instability development. This phenomenological understanding agrees with (2.69) from which $\widetilde{D_{f\,cr}}$ increases as q_c decreases, $0 < q_c < 1$.

2.7.2.3. z - the rate of the growth factor consumption by endothelial cells. Computing partial derivative of $\widetilde{D_{f\,cr}}$ with respect to z we get

$$\frac{\partial \widetilde{D_{f\,cr}}}{\partial z} = \frac{1-g}{1-q_c}(1-\xi) < 0$$

since $0 < q_c < 1$, $0 < g < 1$ and $\xi > 1$ (see (2.69)). This fact is in agreement with our understanding that if the rate of consumption of growth factor increases then a smaller $\widetilde{D_{f\,cr}}$ is required in the system to eliminate random growth factor fluctuations and prevent instability.

2.7.2.4. ζ - the rate of decay of the growth factor. Computing partial derivative of $\widetilde{D_{f\,cr}}$ with respect to ζ we get

$$\frac{\partial \widetilde{D_{f\,cr}}}{\partial \zeta} = \frac{1-g}{1-q_c}(\xi-1)\left[\xi\left(1+\frac{z}{\zeta}\right)-1\right] > 0$$

since $0 < q_c < 1$, $0 < g < 1$ and $\xi > 1$. This as well agrees with our understanding of the process. As we see from the second equation in (2.65), if the cell density fluctuation becomes larger then the growth factor fluctuation, it leads to the increase in the growth factor density. In this case a larger $\widetilde{D_{f\,cr}}$ is required to suppress fluctuations and to prevent the instability development.

2.7.3. Weakly nonlinear analysis and amplitude equations: stripes and hexagons

We use standard asymptotic expansions

(2.70) $$\tilde{c} = \varepsilon c_1 + \varepsilon^2 c_2 + \varepsilon^3 c_3 + \ldots, \quad \tilde{f} = \varepsilon f_1 + \varepsilon^2 f_2 + \varepsilon^3 f_3 + \ldots, \quad \widetilde{D_f} = \widetilde{D_{f\,cr}} - \varepsilon^2 \mu.$$

Here $\tilde{c}$, c_j, $\tilde{f}$, f_j $(j = 1, 2, 3)$ are functions of $\tilde{t}$, T, $\tilde{x}$, $\tilde{y}$.

Taylor expansion of $\widetilde{D_c}$ (2.66) near the trivial steady state yields the following expression

(2.71) $$\widetilde{D_c} \approx 1 + (1-g)\,\tilde{c} + g\tilde{f} + \left(\frac{1}{2}g^2 - g\right)\tilde{c}^2 + \left(\frac{1}{2}g^2 - g\right)\tilde{f}^2 + (2g - g^2)\tilde{c}\tilde{f} +$$

$$\left(\frac{1}{2}g^2 - \frac{1}{6}g^3\right)\tilde{c}^3 + \left(\frac{1}{6}g^3 - g^2 + g\right)\tilde{f}^3 + \left(-\frac{1}{2}g^3 + \frac{5}{2}g^2 - 2g\right)(\tilde{c}\tilde{f}^2 + \tilde{c}^2\tilde{f}).$$

Substituting expansions (2.70) and (2.71) into the system (2.65) and collecting like powers of ε we get the following system of equations at orders ε^j $(j = 1, 2, 3)$

(2.72a) $$-\frac{\partial c_j}{\partial \tilde{t}} + (1-g)\widetilde{\nabla}^2 c_j + (g-\omega)\widetilde{\nabla}^2 f_j - (1-q_c)c_j = R_{cj}$$

(2.72b) $$-\frac{\partial f_j}{\partial \tilde{t}} + \widetilde{D_{f\,cr}}\widetilde{\nabla}^2 f_j - (z+\zeta)f_j + \zeta c_j = R_{fj}.$$

Here the right-hand sides for $j = 1, 2$ are given by

$$R_{c1} = R_{f1} = 0, \quad R_{f2} = z f_1 c_1,$$

$$R_{c2} = -\widetilde{\nabla}^2\left[\left(\frac{1}{2}g^2 - g\right)(c_1 - f_1)^2\right] +$$

$$w(1-g)\widetilde{\nabla} f_1 \widetilde{\nabla} c_1 + w[(1-g)c_1 + g f_1]\widetilde{\nabla}^2 f_1 + wg(\widetilde{\nabla} f_1)^2 + c_1 f_1 + (1-q_c)c_1^2.$$

Right hand sides R_{c3} and R_{f3} are too cumbersome and are given in Appendix.

Doing exactly the same calculations as described in the subsection 2.4.2 and eliminating secular terms in the $O(\varepsilon^3)$ problem via the orthogonality conditions of the right-hand side (R_{c3}, R_{f3}) to

the solutions of the adjoint homogeneous problem given by

$$\begin{pmatrix} \zeta \\ (1-g)\alpha_{cr}^2 + 1 - q_c \end{pmatrix} e_j, \quad j = 1, 2, 3$$

results in the following system of equation for the amplitudes L_1, L_2, L_3

$$\frac{dL_1}{dT} = \mu C_1 L_1 + C_2 L_2^* L_3^* + C_3 L_1 |L_1|^2 + C_4 L_1 (|L_2|^2 + |L_3|^2), \tag{2.73a}$$

$$\frac{dL_2}{dT} = \mu C_1 L_2 + C_2 L_1^* L_3^* + C_3 L_2 |L_2|^2 + C_4 L_2 (|L_1|^2 + |L_3|^2), \tag{2.73b}$$

$$\frac{dL_3}{dT} = \mu C_1 L_3 + C_2 L_1^* L_2^* + C_3 L_3 |L_3|^2 + C_4 L_3 (|L_1|^2 + |L_2|^2). \tag{2.73c}$$

The quadratic terms in the equations come from the secular terms in the $O(\varepsilon^2)$ problem. The coefficients C_k, $k = 1, 2, 3, 4$ are real and depend on the parameters of the problem. They are also given in Appendix.

2.7.4. Weakly nonlinear analysis and amplitude equations: squares

We again perform the weakly nonlinear analysis of the systems (2.65) with the cell diffusion coefficient taken in the form (2.61). This time we study the occurrence of square patterns near the instability threshold.

We again introduce the slow time $T = \varepsilon^2 \tilde{t}$ and expand both unknowns $\tilde{c}$ and $\tilde{f}$ as well as the bifurcation parameter $\widetilde{D_f}$ as

$$\tilde{c} = \varepsilon c_1 + \varepsilon^2 c_2 + \varepsilon^3 c_3 + \ldots, \quad \tilde{f} = \varepsilon f_1 + \varepsilon^2 f_2 + \varepsilon^3 f_3 + \ldots, \quad \widetilde{D_f} = \widetilde{D_{f_{cr}}} - \varepsilon^2 \mu, \tag{2.74}$$

with $\tilde{c}$, c_j, $\tilde{f}$, f_j $(j = 1, 2, 3)$ being functions of $\tilde{t}$, T, $\tilde{x}$, $\tilde{y}$.

Substituting the expansions (2.74), (2.71) into the system of equations (2.65) and collecting like powers of ε we obtain at orders ε^j $(j = 1, 2, 3)$ the same sequence of problems as before

(2.75a) $$-\frac{\partial c_j}{\partial \tilde{t}} + (1-g)\widetilde{\nabla}^2 c_j + (g-\omega)\widetilde{\nabla}^2 f_j - (1-q_c)c_j = R_{cj},$$

(2.75b) $$-\frac{\partial f_j}{\partial \tilde{t}} + \widetilde{D_{f\,cr}}\widetilde{\nabla}^2 f_j - (z+\zeta)f_j + \zeta c_j = R_{fj}.$$

Here the right-hand sides for $j = 1, 2$ are given by

$$R_{c1} = R_{f1} = 0, \quad R_{f2} = z f_1 c_1,$$

$$R_{c2} = -\widetilde{\nabla}^2 \left[\left(\frac{1}{2} g^2 - g \right) (c_1 - f_1)^2 \right] +$$

$$w(1-g)\widetilde{\nabla} f_1 \widetilde{\nabla} c_1 + w[(1-g)c_1 + g f_1]\widetilde{\nabla}^2 f_1 + wg(\widetilde{\nabla} f_1)^2 + c_1 f_1 + (1-q_c)c_1^2.$$

The right-hand sides R_{c3}, R_{f3} are presented in Appendix.

Repeating all the calculations described in the subsection 2.4.5 and eliminating secular terms in the $O(\varepsilon^3)$ problem via the orthogonality conditions of the right-hand side (R_{c3}, R_{f3}) to the solutions of the adjoint homogeneous problem given by

$$\begin{pmatrix} \zeta \\ (1-g)\alpha_{cr}^2 + 1 - q_c \end{pmatrix} e_j, \quad j = 1, 2$$

results in the following system of equation for the amplitudes L_1, L_2

(2.76a) $$\frac{dL_1}{dT} = \mu C_1 L_1 + C_3 L_1 |L_1|^2 + C_4 L_1 |L_2|^2,$$

(2.76b) $$\frac{dL_2}{dT} = \mu C_1 L_2 + C_3 L_2 |L_2|^2 + C_4 L_2 |L_1|^2,$$

The coefficients C_k, $k = 1, 3, 4$ are real and depend on the parameters of the problem. They are given in Appendix.

2.7.5. Parameter sensitivity study: stripes, hexagons, squares

We next discuss the patterns that occur in the angiogenesis problem depending on the parameters of the system. The parameters that we vary are ζ, ω, and z. It is useful to recall the biological meaning of these parameters. The parameter ζ can be interpreted as a nondimensional rate of decay of the growth factor. There are means to control ζ, e.g., by introducing decoy soluble growth factor receptors that reduce the concentration of active growth factor, which can be treated as an increase in ζ. The parameter ω characterizes the chemotactic sensitivity of the endothelial cells. It can also be controlled, e.g., by inhibiting the growth factor receptors. The parameter z is related to the rate of intracellular activity, which results, e.g., in production of proteases and formation of integrin clusters.

Figures 2.12 show the dependence of the coefficient C_2 as well as coefficient combinations $C_3 - C_4$ and $C_3 + 2C_4$ on ζ for different values of z and ω. To analyze these figures it is useful to recall the conclusions derived from the study of amplitude equations in subsection 2.4.3.

- for $C_3 + 2C_4 > 0$ there exist only subcritical hexagonal patterns that are always unstable (more precisely, there exist supercritical hexagons in this case if $C_2 < 0$, but they are unstable anyway);
- for $C_3 + 2C_4 < 0$ there exist supercritical hexagonal patterns;
- the supercritical hexagonal patterns are stable for $L_h > -C_2/[2(C_3 + 2C_4)]$ if the three conditions $C_3 + 2C_4 < 0$, $C_2 > 0$, and $C_3 - C_4 < 0$ are simultaneously met (Fig. 2.3a).

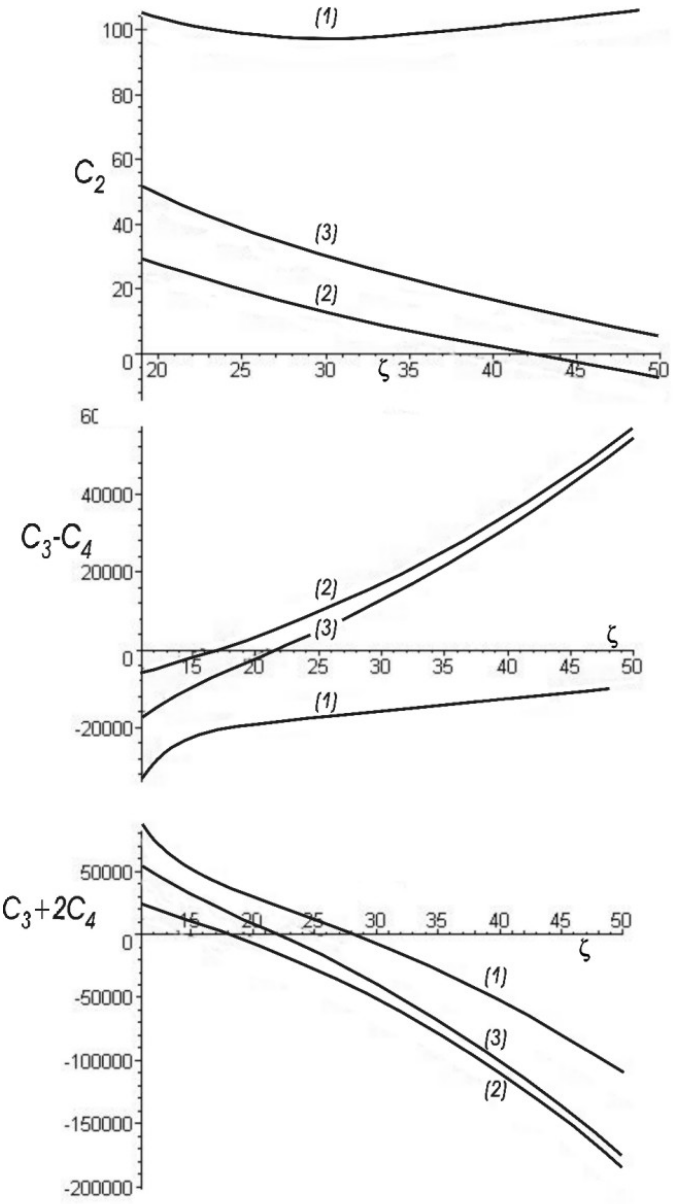

FIGURE 2.12. The quantities C_2, $C_3 - C_4$ and $C_3 + 2C_4$ as a function of ζ for different parameter values. Here $q = 0.25$, $g = 0.8$ for all curves, and $\omega = 1.5$, $z = 15$ for curves (1), $\omega = 2$, $z = 15$ for curves (2), $\omega = 2$, $z = 20$ for curves (3)

If, however, the first two conditions on the coefficients are satisfied, but $C_3 - C_4 > 0$, then there exist stable hexagons only if $C_3 + C_4 < 0$. In this case the amplitudes L_h of the stable hexagons satisfy $-C_2/[2(C_3 + 2C_4)] < L_h < C_2/(C_3 - C_4)$ (Fig. 2.3 b);

- the supercritical hexagonal patterns are always unstable if either $C_2 < 0$ or $C_3 - C_4 > 0$ and $C_3 + C_4 > 0$.

We first observe that for relatively small ζ, i.e., for a slower decay of the growth factor,$C_2 > 0$, $C_3 - C_4 < 0$ and $C_3 + 2C_4 > 0$. The signs of these quantities mean that hexagons are subcritical, unstable, and therefore cannot occur in this case. The stripes appear supercritically, but they are also unstable. The resulting behavior of the original system is not described by the amplitude equations, and can be quite complex, e.g., chaotic.

For intermediate values of ζ, $C_2 > 0$, $C_3 + 2C_4 < 0$ while the sign of $C_3 - C_4$ depends on the other parameters. For smaller ω, i.e., for reduced chemotactic sensitivity of the cells, which means that stable supercritical hexagons appear in the system. For larger ω, $C_3 - C_4 > 0$, indicating that stable supercritical hexagons and stripes can coexist providing $C_3 + C_4 < 0$ and $C_3 < 0$.

For large values of ζ, $C_3 + 2C_4 < 0$ but C_2 and $C_3 - C_4 > 0$ can have different signs depending on ω and z. For smaller ω and z, $C_2 > 0$ and $C_3 - C_4 < 0$, indicating the presence of stable supercritical hexagons. However, for larger ω and small z, $C_2 < 0$ which means that supercritical hexagons are unstable. Finally, if z is also increased, we observe $C_2 > 0$ and $C_3 - C_4 > 0$, indicating that stable supercritical hexagons and stripes can coexist providing $C_3 + C_4 < 0$ and $C_3 < 0$.

Next we discuss the appearance of square patterns.

Figures 2.13 show the dependence of the coefficient $C_3 - C_4$ and $C_3 + C_4$ on ζ for different values of z and ω. To analyze these figures we recall the conclusions derived from the study of amplitude equations in subsection 2.4.6.

- for $C_3 + C_4 > 0$ there exist only subcritical square patterns that are always unstable;
- for $C_3 + C_4 < 0$ there exist supercritical square patterns;

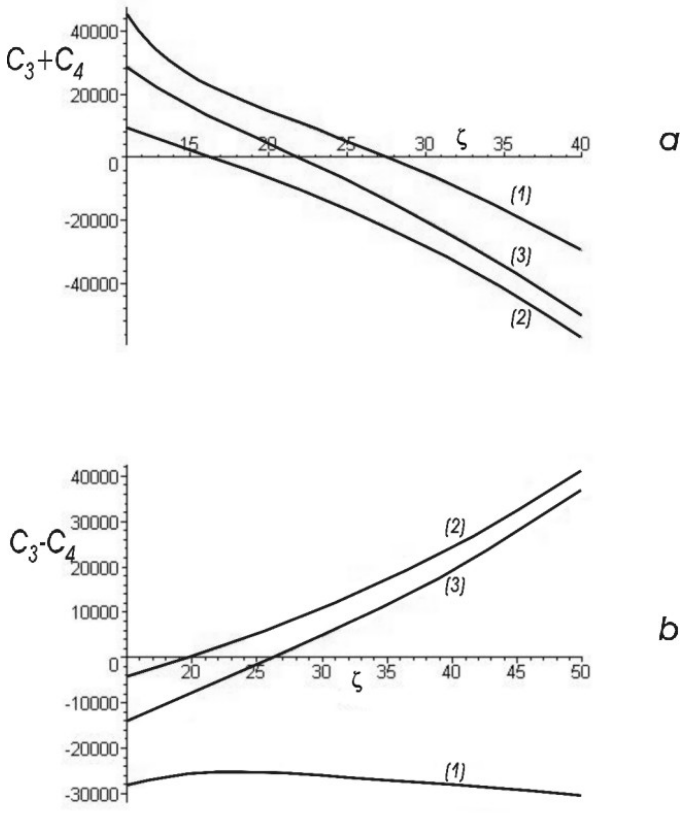

FIGURE 2.13. The quantities $C_3 - C_4$ and $C_3 - C_4$ as a function of ζ for different parameter values. Here $q = 0.25$, $g = 0.8$ for all three curves, and $\omega = 1.5$, $z = 15$ for curves (1), $\omega = 2$, $z = 15$ for curves (2), $\omega = 2$, $z = 20$ for curves (3).

- the supercritical square patterns are stable if $C_3 - C_4 < 0$
- the supercritical square patterns are unstable if $C_3 - C_4 > 0$.

We observe that for small ω, i.e., for reduced cell chemotactic sensitivity, $C_3 - C_4 < 0$ and $C_3 + C_4$ changes sign depending on ζ. This means that stable supercritical squares exist only for relatively large ζ (i.e. rate of growth factor decay) where $C_3 + C_4 < 0$.

For larger values of ω and z there exist only narrow ζ regions where the conditions $C_3 - C_4 < 0$ and $C_3 + C_4 < 0$ are simultaneously satisfied meaning that the existence of stable supercritical square patterns is very sensitive to the rate of decay of the growth factor.

The above observations can be useful as they demonstrate the trends that may be expected as parameters of the biological system are varied in experiments. These results can be summarized as follows. No steady patterns can be observed if the rate of decay of the growth factor is small. Increasing the rate of decay of the growth factor (e.g., by introducing decoy soluble growth factor receptors) allows one to observe steady patterns. These patterns are hexagons, stripes and squares. In order for the stripes to occur the chemotactic sensitivity of the endothelial cells and/or their biochemical activity has to be increased. As we increase the chemotactic sensitivity of endothelial cells, the square patterns become very sensitive to the rate of decay of the growth factor.

2.8. Coexistence of hexagons, stripes and square patterns.

We recall the results obtained from the study of amplitude equations obtained for hexagons and stripes:

- Stable supercritical stripes and stable supercritical square patterns never coexist in the system;
- Stable supercritical hexagonal patterns and stable supercritical stripes can coexist for $-C_2/[2(C_3+2C_4)] < L_{h,s} < C_2/(C_3-C_4)$ if all the conditions $C_3+2C_4<0$, $C_2>0$, $C_3<0$, $C_3-C_4>0$ and $C_3+C_4<0$ are simultaneously met (Fig. 2.3 b);
- Stable supercritical hexagonal patterns and stable supercritical stripes can coexist for $L_h > -C_2/[2(C_3+2C_4)]$ if all the conditions $C_2>0$, $C_3+2C_4<0$, $C_3-C_4<0$ and $C_3+C_4<0$ are simultaneously met.

Coexistence of stable supercritical hexagons and squares for different parameter values is demonstrated in Figs 2.14, 2.15, and 2.16.

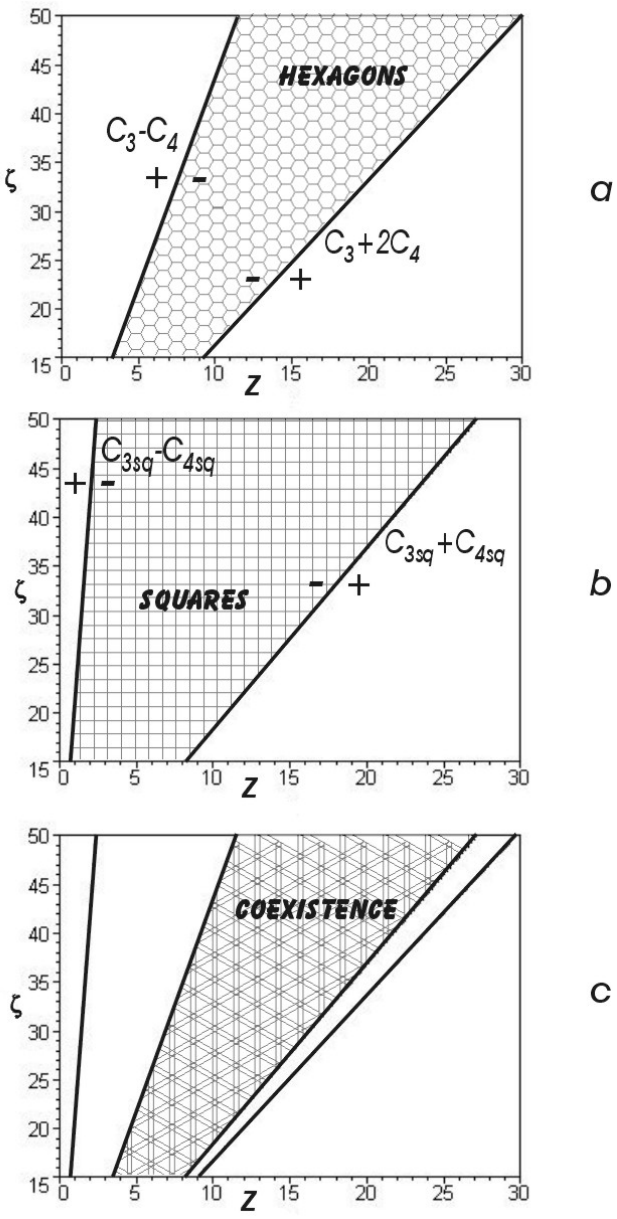

FIGURE 2.14. Zero contour plots of the coefficient combinations that determine existence and stability of supercritical hexagonal and square patterns for certain parameter values. Here $\omega = 1.5$, $q_{cr} = 0.25$, $g = 0.8$.
a) Region of existence of stable supercritical hexagons.
b) Region of existence of stable supercritical squares. Subscript 'sq' indicates coefficients of the amplitude equations derived for squares (2.76).
c) Region of hexagons - squares coexistence.

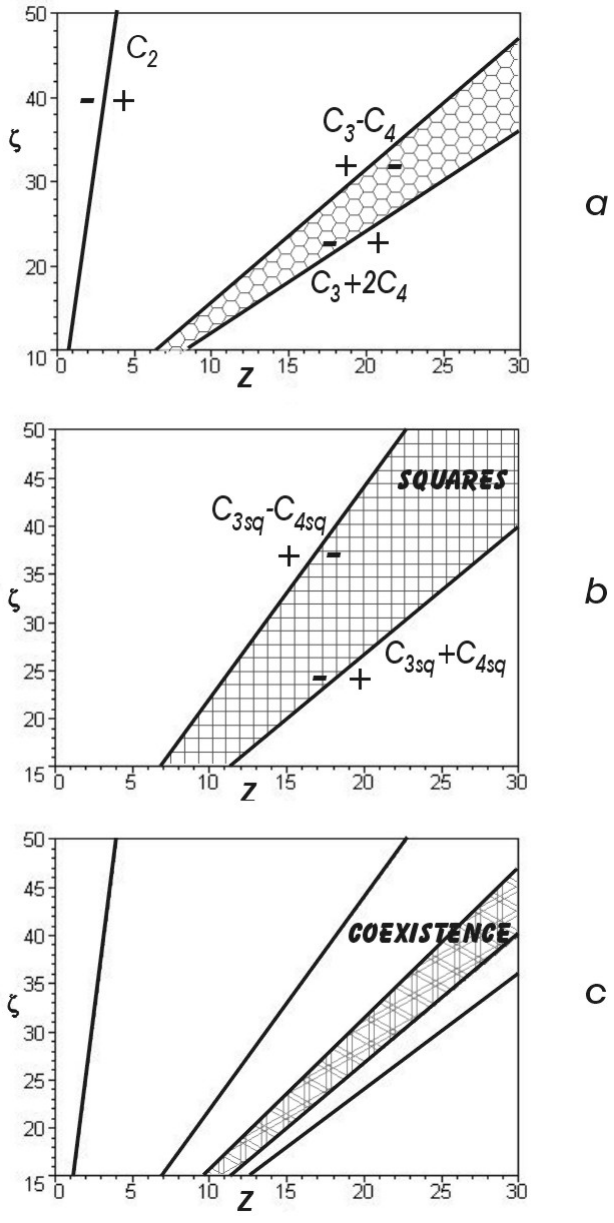

FIGURE 2.15. Zero contour plots of the coefficient combinations that determine existence and stability of supercritical hexagonal and square patterns for certain parameter values. Here $\omega = 1.75$, $q_{cr} = 0.25$, $g = 0.8$.
a) Region of existence of stable supercritical hexagons.
b) Region of existence of stable supercritical squares. Subscript 'sq' indicates coefficients of the amplitude equations derived for squares (2.76).
c) Region of hexagons - squares coexistence.

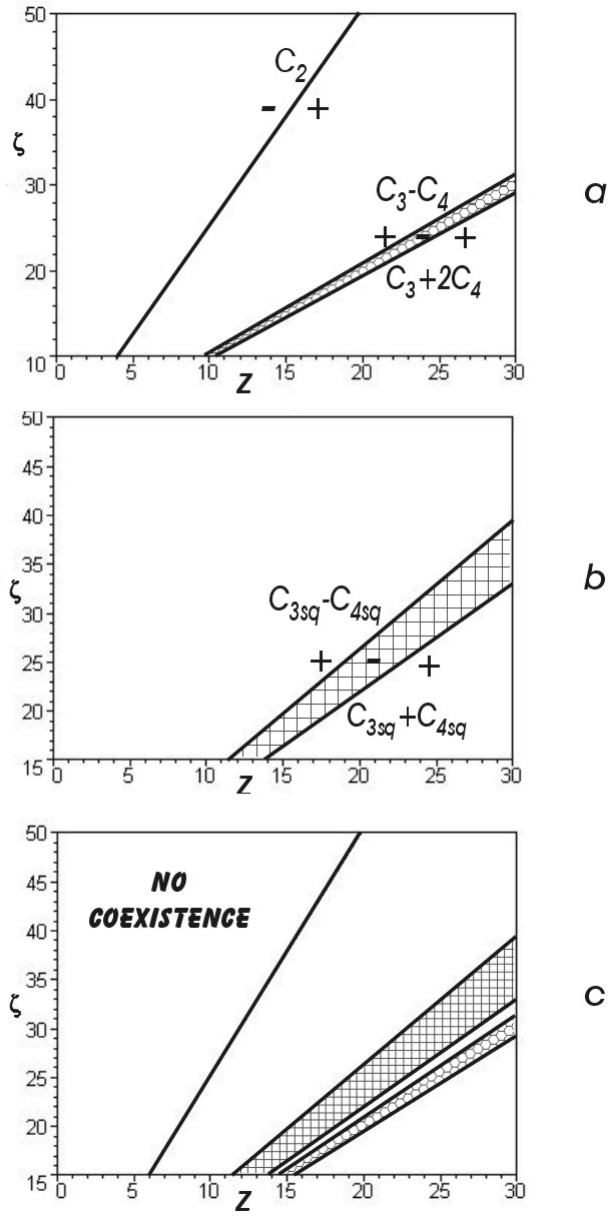

FIGURE 2.16. Zero contour plots of the coefficient combinations that determine existence and stability of supercritical hexagonal and square patterns for certain parameter values. Here $\omega = 2.0$, $q_{cr} = 0.25$, $g = 0.8$.
a) Region of existence of stable supercritical hexagons.
b) Region of existence of stable supercritical squares. Subscript 'sq' indicates coefficients of the amplitude equations derived for squares (2.76).
c) No hexagons - squares coexistence.

2.9. Analysis of the base model with a new diffusion coefficient in the absence of endothelial cell proliferation

We again consider the system

$$\frac{\partial c}{\partial t} = \nabla^2(D_c) - \gamma \text{ div } [D_c \text{ grad} f], \tag{2.77a}$$

$$\frac{\partial f}{\partial t} = D_f \nabla^2 f - \lambda_f f c + \delta c - \beta f, \tag{2.77b}$$

with the cell diffusion coefficient in the form (2.61).

2.9.1. Steady states and nondimensionalization

The system of equations (2.77) has a one-parameter family of spatially uniform time-independent solutions that we refer to as the basic states and label them by a subscript s. They are

$$c_s = \text{constant}, \quad f_s = \frac{\delta c_s}{\beta + \lambda_f c_s}. \tag{2.78}$$

We nondimensionalize the system of equations using the basic state (2.78) as the reference quantities. Specifically, the following nondimensional variables are introduced

$$\tilde{c} = \frac{c - c_s}{c_s}, \;\; \tilde{f} = \frac{f - f_s}{f_s}, \;\; \tilde{x} = \frac{x}{l_*}, \;\; \tilde{y} = \frac{y}{l_*}, \;\; \tilde{t} = \frac{t}{t_*}, \;\; t_* = \frac{f_s}{\delta c_s}, \;\; l_*^2 = D_0 t_* e^{-g}, \;\; g = \frac{k_*}{f_s c_s}.$$

We obtain

$$\frac{\partial \tilde{c}}{\partial \tilde{t}} = \nabla^2(\widetilde{D_c}) - \omega \text{ div } [\widetilde{D_c} \text{ grad} \tilde{f}], \tag{2.79a}$$

$$\frac{\partial \tilde{f}}{\partial \tilde{t}} = \widetilde{D_f} \nabla^2 \tilde{f} - \tilde{f} + (1 - z)\tilde{c} - z\tilde{f}\tilde{c}, \tag{2.79b}$$

with

$$\omega = \gamma f_s, \quad z = t_* \lambda_f c_s \equiv \frac{\lambda_f c_s}{\beta + \lambda_f c_s} < 1, \quad \widetilde{D_f} = \frac{D_f e^g}{D_0}, \quad \widetilde{D_c} = (1+\tilde{c}) \exp\left[g \frac{\tilde{f} - \tilde{c}}{1+\tilde{f}} \right].$$

2.9.2. Linear stability analysis

We now perform linear stability analysis of the basic state $\tilde{c} = 0$, $\tilde{f} = 0$ of the problem (2.79). Linearizing (2.79) about it's trivial basic state, we obtain

(2.80a) $$\frac{\partial \tilde{\tilde{c}}}{\partial \tilde{t}} = (1-g)\nabla^2 \tilde{\tilde{c}} + (g-\omega)\nabla^2 \tilde{\tilde{f}},$$

(2.80b) $$\frac{\partial \tilde{\tilde{f}}}{\partial \tilde{t}} = \widetilde{D_f} \nabla^2 \tilde{\tilde{f}} - \tilde{\tilde{f}} + (1-z)\tilde{\tilde{c}}.$$

Substituting the normal mode solution

$$\begin{pmatrix} \tilde{\tilde{c}} \\ \tilde{\tilde{f}} \end{pmatrix} = \begin{pmatrix} a \\ b \end{pmatrix} e^{\sigma \tilde{t} + i\alpha_x \tilde{x} + i\alpha_y \tilde{y}},$$

where σ is the growth rate of the perturbation and (α_x, α_y) is the wave vector, into (2.40), yields

$$\begin{pmatrix} -\alpha^2(1-g) - \sigma & -(g-\omega)\alpha^2 \\ 1-z & -\widetilde{D_f}\alpha^2 - 1 - \sigma \end{pmatrix} \begin{pmatrix} a \\ b \end{pmatrix} = 0,$$

where $\alpha^2 = \alpha_x^2 + \alpha_y^2$. Setting the determinant of the above matrix equal zero we obtain the dispersion relation

$$\sigma^2 + \left[\alpha^2(\widetilde{D_f} + 1 - g) + 1 \right] \sigma + \alpha^2 \left[(1-g)(\widetilde{D_f}\alpha^2 + 1) + (g-\omega)(1-z) \right] = 0.$$

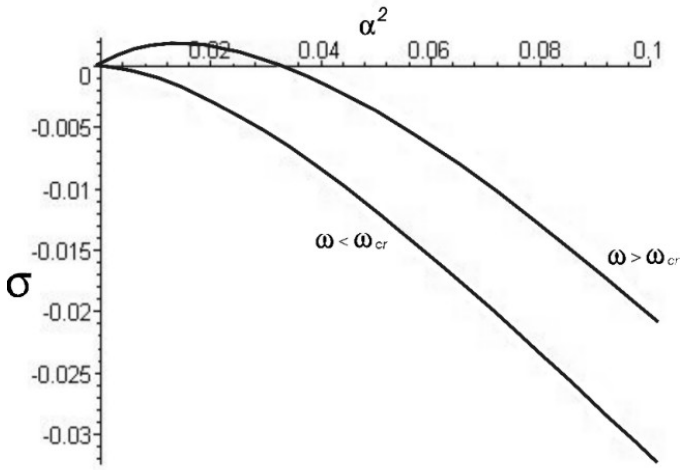

FIGURE 2.17. The quantity σ as a function of α_{cr}^2 for two different values of ω. Here $z = 0.5$, $g = 0.5$, $\widetilde{D_f} = 15$, $\omega_{cr} = 1.5$, $\omega_1 = 1.4$, $\omega_2 = 2$, $\alpha_{cr} = 0.036$

There are two roots of the quadratic equation, $\sigma_{\pm}(\alpha)$. It is easy to check that Re$(\sigma_{-}(\alpha)) < 0$ for all α and all parameter values assuming $g < 1$. The real part of the other root, $\sigma_{+}(\alpha)$, is negative for all α if

$$\omega < \omega_{cr} \equiv \frac{1-g}{1-z} + g. \tag{2.81}$$

For $\omega > \omega_{cr}$ there is a range of α given by $0 < \alpha < \alpha_{cr}$, for which Re$(\sigma_{+}(\alpha)) > 0$ (see Fig 2.17).

The quantity α_{cr} is determined by

$$\alpha_{cr}^2 = \frac{1}{\widetilde{D_f}} \left[\frac{(\omega - g)(1-z)}{1-g} - 1 \right] = \frac{1}{\widetilde{D_f}} \frac{1-z}{1-g} \, (\omega - \omega_{cr}). \tag{2.82}$$

For ω slightly above ω_{cr} the maximum of the growth rate $\sigma_{+}(\alpha)$ is attained at $\alpha = \alpha_{cr}/\sqrt{2}$ and is equal to

$$\sigma_{max} = \frac{1}{4} \widetilde{D_f} \, (1-g) \, \alpha_{cr}^4. \tag{2.83}$$

2.9.3. Long-wave analysis: Sivashinsky equation

We consider ω close to the critical value ω_{cr},

$$\omega = \omega_{cr} + \mu\varepsilon^2.$$

Then the results of linear stability analysis suggest the following scalings:

$$\chi = \varepsilon\tilde{x}, \quad \eta = \varepsilon\tilde{y}, \quad T = \varepsilon^4\tilde{t},$$

which transform the system (2.79) into

(2.84a) $$\varepsilon^4\frac{\partial\tilde{c}}{\partial T} = \varepsilon^2\nabla^2_{\chi,\eta}(\widetilde{D_c}) - (\omega_{cr} + \mu\varepsilon^2)\varepsilon^2\ \nabla_{\chi,\eta}\cdot[\widetilde{D_c}\ \nabla_{\chi,\eta}\tilde{f}],$$

(2.84b) $$\varepsilon^4\frac{\partial\tilde{f}}{\partial T} = \varepsilon^2\widetilde{D_f}\nabla^2_{\chi,\eta}\tilde{f} - \tilde{f} + (1-z)\tilde{c} - z\tilde{f}\tilde{c}.$$

Here we retain the same notations $\tilde{c}$ and $\tilde{f}$ for the solution that depends on the slow variables χ, η and T.

We introduce the following notations for quadratic and cubic parts of the Taylor expansion (2.71) for $\widetilde{D_c}$

(2.85a) $$a(\tilde{c},\tilde{f}) = \left(\frac{1}{2}g^2 - g\right)(\tilde{c}-\tilde{f})^2,$$

(2.85b) $$b(\tilde{c},\tilde{f}) = \left(-\frac{1}{6}g^3 + \frac{1}{2}g^2\right)\tilde{c}^3 + \left(\frac{1}{6}g^3 - g^2 + g\right)\tilde{f}^3 + \left(-\frac{1}{2}g^3 + \frac{5}{2}g^2 - 2g\right)(\tilde{c}\tilde{f}^2 + \tilde{c}^2\tilde{f}).$$

Then the system (2.84) can be rewritten in the form:

(2.86a) $$\varepsilon^4\frac{\partial\tilde{c}}{\partial T} = \varepsilon^2\nabla^2_{\chi,\eta}[(1-g)\tilde{c} + (g-\omega_{cr})\tilde{f}] + \varepsilon^2\nabla^2_{\chi,\eta}[a(\tilde{c},\tilde{f})] + \varepsilon^2\nabla^2_{\chi,\eta}[b(\tilde{c},\tilde{f})] -$$

$$\omega_{cr}\nabla\cdot\{([(1-g)\tilde{c}+(g-\omega_{cr})\tilde{f}]+a(\tilde{c},\tilde{f})\nabla\tilde{f}\}-\mu\varepsilon^4\nabla^2_{\chi,\eta}\tilde{f}-\omega^2_{cr}\varepsilon^2\nabla\cdot(\tilde{f}\nabla\tilde{f}),$$

(2.86b) $$\varepsilon^4\frac{\partial\tilde{f}}{\partial T}=\varepsilon^2\widetilde{D_f}\nabla^2_{\chi,\eta}\tilde{f}-\tilde{f}+(1-z)\tilde{c}-z\tilde{f}\tilde{c}.$$

We expand both unknowns $\tilde{c}$ and $\tilde{f}$ as

$$\tilde{c}(\chi,\eta,T)=\varepsilon^2c_2(\chi,\eta,T)+\varepsilon^4c_4(\chi,\eta,T)+\varepsilon^6c_6(\chi,\eta,T)+\ldots,$$

$$\tilde{f}(\chi,\eta,T)=\varepsilon^2f_2(\chi,\eta,T)+\varepsilon^4f_4(\chi,\eta,T)+\varepsilon^6f_6(\chi,\eta,T)+\ldots.$$

Substituting the expansions into (2.86) and collecting like powers of ε we obtain at order $O(\varepsilon^2)$ a linear algebraic relation between c_2 and f_2,

(2.87) $$f_2=(1-z)c_2.$$

At orders $O(\varepsilon^4)$ and $O(\varepsilon^6)$ we obtain

(2.88a) $$\nabla^2_{\chi,\eta}\left[(1-g)c_2+(g-\omega_{cr})f_2\right]=0,$$

(2.88b) $$-f_4+(1-z)c_4=-\widetilde{D_f}\nabla^2_{\chi,\eta}f_2+zc_2f_2,$$

and

(2.89a) $$-\frac{\partial c_2}{\partial T}+\nabla^2_{\chi,\eta}\left[(1-g)c_4+(g-\omega_{cr})f_4+a(c_2,f_2)\right]-$$

$$\omega_{cr}\nabla_{\chi,\eta}\cdot\{[(1-g)c_2+(g-\omega_{cr})f_2]\nabla_{\chi,\eta}f_2\}-\mu\nabla^2_{\chi,\eta}f_2-\omega^2_{cr}\nabla\cdot(f_2\nabla f_2)=0,$$

(2.89b) $$-f_6+(1-z)c_6=\frac{\partial f_2}{\partial T}-\widetilde{D_f}\nabla^2_{\chi,\eta}f_4+z(c_2f_4+c_4f_2),$$

respectively. From (2.81) and (2.87) it follows that (2.88a) is satisfied, while (2.88b) allows one to determine f_4 as

$$f_4 = (1-z)\widetilde{D_f}\nabla^2_{\chi,\eta}c_2 + (1-z)c_4 - z(1-z)c_2^2. \tag{2.90}$$

Substituting (2.81), (2.87) and (2.90) into (2.89a) and simplifying, we finally obtain the Sivashinsky equation

$$\frac{\partial c_2}{\partial T} = (g-1)\widetilde{D_f}\nabla^4_{\chi,\eta}c_2 - \mu(1-z)\nabla^2_{\chi,\eta}c_2 + \left[z - \frac{1}{2} - gz^2\right]\nabla^2_{\chi,\eta}(c_2^2). \tag{2.91}$$

2.9.4. Long-wave analysis: Cahn-Hilliard equation

Next we consider the case when the coefficient of the nonlinear term in the Sivashinsky equation (2.91) is equal to zero, i.e.

$$z - \frac{1}{2} - gz^2 = 0.$$

In this case we derive Cahn-Hilliard equation. We again consider ω close to the critical value ω_{cr} given by (2.81), $\omega = \omega_{cr} + \mu\varepsilon^2$, but now we also assume

$$g = \frac{z - \frac{1}{2}}{z^2}. \tag{2.92}$$

As before, introducing $\chi = \varepsilon\tilde{x}$, $\eta = \varepsilon\tilde{y}$, $T = \varepsilon^4\tilde{t}$, and substituting Taylor expansion (2.71) for $\widetilde{D_c}$ with the corresponding notations for the quadratic and cubic parts (2.85), we transform the system (2.79) into

$$\varepsilon^4\frac{\partial\tilde{c}}{\partial T} = \varepsilon^2\nabla^2_{\chi,\eta}[(1-g)\tilde{c} + (g-\omega_{cr})\tilde{f}] + \varepsilon^2\nabla^2_{\chi,\eta}[a(\tilde{c},\tilde{f})] + \varepsilon^2\nabla^2_{\chi,\eta}[b(\tilde{c},\tilde{f})] - \tag{2.93a}$$

$$\omega_{cr}\nabla\cdot\{([(1-g)\tilde{c}+(g-\omega_{cr})\tilde{f}]+a(\tilde{c},\tilde{f})\nabla\tilde{f}\}-\mu\varepsilon^4\nabla^2_{\chi,\eta}\tilde{f}-\omega^2_{cr}\varepsilon^2\nabla\cdot(\tilde{f}\nabla\tilde{f})$$

(2.93b) $$\varepsilon^4\frac{\partial\tilde{f}}{\partial T}=\varepsilon^2\widetilde{D_f}\nabla^2_{\chi,\eta}\tilde{f}-\tilde{f}+(1-z)\tilde{c}-z\tilde{f}\tilde{c}.$$

Here we retain the same notations $\tilde{c}$ and $\tilde{f}$ for the solution that depends on the slow variables χ, η and T. We use a different expansion of $\tilde{c}$ and $\tilde{f}$, namely

$$\tilde{c}(\chi,\eta,T)=\varepsilon c_1(\chi,\eta,T)+\varepsilon^2c_2(\chi,\eta,T)+\varepsilon^3c_3(\chi,\eta,T)+\varepsilon^4c_4(\chi,\eta,T)+\varepsilon^5c_5(\chi,\eta,T)+\ldots,$$

$$\tilde{f}(\chi,\eta,T)=\varepsilon f_1(\chi,\eta,T)+\varepsilon^2f_2(\chi,\eta,T)\varepsilon^3f_3(\chi,\eta,T)+\varepsilon^4f_4(\chi,\eta,T)+\varepsilon^5f_5(\chi,\eta,T)+\ldots.$$

Substituting the expansions for ω_{cr}, $\tilde{c}$, $\tilde{f}$ into (2.93) and collecting like powers of ε we obtain at order $O(\varepsilon)$ a linear algebraic relation between c_1 and f_1,

(2.94) $$f_1=(1-z)c_1.$$

At orders $O(\varepsilon^2)$ and $O(\varepsilon^3)$ we obtain

(2.95) $$f_2=(1-z)c_2-zf_1c_1,$$

(2.96a) $$\nabla^2_{\chi,\eta}\left[(1-g)c_1+(g-\omega_{cr})f_1\right]=0,$$

(2.96b) $$f_3=(1-z)c_3-zc_2f_1-zc_1f_2+\widetilde{D_f}\nabla^2_{\chi,\eta}f_1.$$

Substituting (2.81) into (2.96a) we can easily see that this equation is satisfied.

At $O(\varepsilon^4)$ we obtain

(2.97a) $$\nabla^2_{\chi,\eta}\left[(1-g)c_2+(g-\omega_{cr})f_2\right]+\nabla^2_{\chi,\eta}[a(c_1,f_1)]-$$

$$\omega_{cr}\nabla\cdot\left[(1-g)c_1+(g-\omega_{cr})f_1\right]\nabla f_1-\omega_{cr}^2\nabla\cdot(f_1\nabla f_1)=0,$$

(2.97b) $$f_4=(1-z)c_4-zc_1f_3-zc_2f_2-zc_3f_1+\widetilde{D_f}\nabla^2_{\chi,\eta}f_2.$$

Let us show that the first equation (2.97a) is satisfied. Using (2.95) and (2.81) it simplifies to

$$(g-\omega_{cr})\nabla^2_{\chi,\eta}(-zf_1c_1)+\nabla^2_{\chi,\eta}[a(c_1,f_1)]-\omega_{cr}^2\nabla\cdot(f_1\nabla f_1)=0.$$

Then using (2.94) and simplifying we get

$$\left[z(1-g)+a(1,1-z)-\frac{1}{2}\omega_{cr}^2(1-z)^2\right]\nabla^2_{\chi,\eta}(c_1^2)=0,$$

which is satisfied due to (2.92).

At $O(\varepsilon^5)$ we obtain the following equation for c_1:

(2.98) $$\frac{\partial c_1}{\partial T}=\nabla^2_{\chi,\eta}[(1-g)c_3+(g-\omega_{cr})f_3]+\nabla^2_{\chi,\eta}[b(c_1,f_1)]+$$

$$\nabla^2_{\chi,\eta}[(g^2-g)c_1c_2+(g^2-2g)f_1f_2+(2g-g^2)c_1f_2+(2g-g^2)c_2f_1]-\mu\nabla^2_{\chi,\eta}f_1-$$

$$\omega_{cr}\nabla_{\chi,\eta}\cdot\{[(1-g)c_2+(g-\omega_{cr})f_2+a(c_1,f_1)]\nabla_{\chi,\eta}f_1\}-\omega_{cr}^2\nabla\cdot(f_1\nabla f_2)-\omega_{cr}^2\nabla\cdot(f_2\nabla f_1).$$

Simplifying this expression we finally obtain the Cahn-Hilliard equation:

(2.99) $$\frac{\partial c_1}{\partial T}=-\frac{1}{z^2}\left(z^2+z-\frac{1}{2}\right)\widetilde{D_f}\nabla^4_{\chi,\eta}c_1-\mu(1-z)\nabla^2_{\chi,\eta}c_1+Q\nabla^2_{\chi,\eta}(c_1^3),$$

where the coefficient Q is shown in Fig. 2.18 and given by

$$Q=-z^2(1-g)+gz^2(1-z)(g-2)+b(1,1-z)-$$

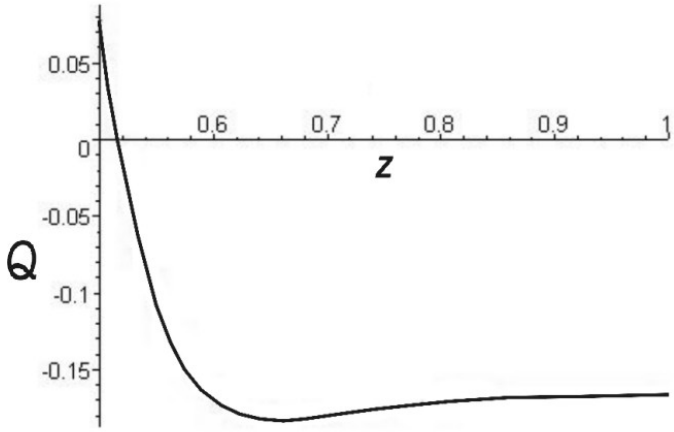

FIGURE 2.18. Dependence of the coefficient Q of the Cahn-Hilliard equation (2.99) on z.

$$\frac{1}{3}\omega_{cr}(1-z)[a(1,1-z)+z(1-g)]+\omega_{cr}^2 z(1-z)^2 =$$

$$\frac{1}{24z^6}(12z^7-80z^6+216z^5-276z^4+195z^3-81z^2+21z-3).$$

2.10. Numerical results

To solve this problem numerically we first used finite difference approximation in time and space. We applied periodic boundary conditions for the cell density c and for the growth factor density f. We used a uniform rectangular grid on the computational domain $x \in [0,\ell]$, $y \in [0,\ell]$, were x and y were the nondimensional spatial variables. Using this method required small grid spacings in x and y (of the order of 10^{-5} – 10^{-6}), and in order to maintain stability of the scheme the time stepsize needed to be extremely small (of the order of 10^{-10} – 10^{-12}) because of the quadratic timestep condition for parabolic equations.

To speed up our calculations and increase the order of accuracy we solved the problem using the Crank-Nicolson numerical scheme combined with operator splitting and alternation in application of splitting in order to maintain second order accuracy in time [196]. This implicit scheme was applied only for the diffusion terms in both equations and the rest of the terms were treated explicitly. We have used the same boundary conditions (periodic for c and f) and performed simulations on the same computational domain $x \in [0, \ell]$, $y \in [0, \ell]$. The method was stable for relatively large time stepsize (of the order of 10^{-4}). We performed simulations for parameter values where stable hexagon structures were expected and we were able to obtain stable hexagons in our simulations starting with initial data that represented a small deviation of the densities c and f from the steady states. This result is shown in Fig. 19(a) for the new form of the diffusion coefficient.

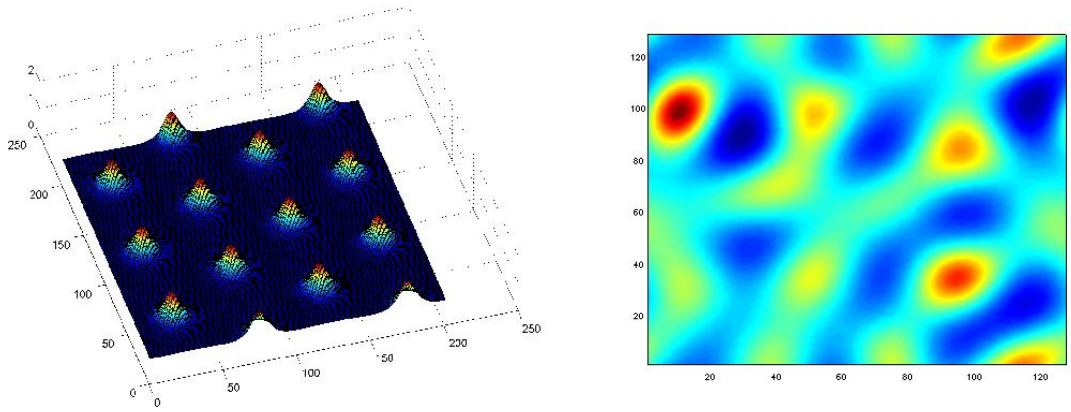

(a) Proliferating system

(b) Non-proliferating system

FIGURE 2.19. Left: Hexagon pattern. Here $q_c = 0.25$, $g = 0.8$, $\omega = 1.5$, $z = 15$, $\zeta = 35$, $D_f = 4.25$. Right: Cell pattern formed in a non-proliferating system. Here $\omega = 3.225$, $q_c = 0.25$, $D_f = 1$, $z = 0.8$, $g = 0.48$.

For numerical analysis of the model without cell proliferation we used a pseudo-spectral numerical scheme with periodic boundary conditions. We again used a semi-implicit approach with the

Crank-Nicolson scheme to handle the linear terms and the Adams-Bashforth scheme for the nonlinear terms. Figure 19(b) depicts the cell concentration at a fixed time. With time the cell structure becomes more coarse which is typical of the Cahn-Hilliard dynamics.

2.11. Discussion

We have developed a mathematical model of angiogenesis which governs spatio-temporal behavior of five continuous variables: the densities of endothelial cells, growth factor, proteases, focal adhesion complexes and active adhesion sites of the extracellular matrix. Our initial model consisted of five PDEs for these five unknown quantities. Using a steady state assumption we reduced it to the system of two nonlinear coupled PDEs for the densities of the endothelial cells and the growth factor. We have also introduced two different forms of the endothelial cell diffusion coefficient and analyzed the model in both cases. We studied the model analytically, first by performing linear stability analysis and then by doing weakly nonlinear analysis to determine what types of structures can be formed near the instability threshold when steady states lose their stability. In particular, we studied possibilities of appearance of stripes, squares and hexagons. We derived a system of amplitude equations and analyzed it. As a result we found parameter ranges in which stable hexagons, stripes and squares can exist in the system as well as coexist with one another.

We also studied our system in absence of endothelial cell proliferation, the case that is of particular interest for experimentalists [184]. For this case we also performed a linear stability analysis. Our weakly nonlinear analysis was based on the assumption of longwave solutions and resulted in the derivation of the Sivashinsky and Cahn-Hilliard equations.

We have performed numerical simulations of the system using several numerical schemes based on finite difference approximations as well as on pseudo-spectral approximations. We were able to obtain stable hexagonal structures for parameter values predicted by the analytical investigation. We have also performed simulations of the system in absence of endothelial cells proliferation in the Cahn-Hilliard parameter range which was derived in our analytical investigations. In this simulation we obtained labyrinth structures typical of systems described by the Cahn-Hilliard equation.

Appendix

Calculations with $D = D_0 \exp\left(-\frac{k_*}{cf}\right)$: hexagons and stripes

The right-hand sides in the $O(\varepsilon^3)$ problem are given by

$$R_{c3} = -\widetilde{\nabla}^2 \Big[g^2 c_1 c_2 + g^2 c_1 f_2 + g^2 c_2 f_1 + (g^2 - 2g) f_1 f_2 +$$

$$\left(\frac{1}{6}g^3 - \frac{1}{2}g^2\right) c_1^3 + \left(\frac{1}{2}g^3 - g^2\right) c_1^2 f_1 + \left(\frac{1}{2}g^3 - \frac{3}{2}g^2\right) c_1 f_1^2 + \left(\frac{1}{6}g^3 - g^2 + g\right) f_1^3 \Big] +$$

$$w\widetilde{\nabla} \cdot \Big\{ \left[(g+1)c_1 + g f_1\right] \widetilde{\nabla} f_2 \Big\} + w\widetilde{\nabla} \cdot \Big\{ \Big[(g+1)c_2 + g f_2 + \frac{1}{2} g^2 c_1^2 +$$

$$\left(\frac{1}{2}g^2 - g\right) f_1^2 + g^2 c_1 f_1 \Big] \widetilde{\nabla} f_1 \Big\} + f_1 c_2 + f_2 c_1 + f_1 c_1^2 + 2(1 - q_c) c_1 c_2 + \frac{\partial c_1}{\partial T},$$

$$R_{f3} = -\mu \widetilde{\nabla}^2 f_1 + z f_1 c_2 + z f_2 c_1 + \frac{\partial f_1}{\partial T}.$$

The coefficients K_j appearing on right-hand side R_{c2} of the $O(\varepsilon^2)$ problem have the form

$$K_1 = 2\alpha_{cr}^2[g^2a^2 + (g^2 - 2g)b^2 + 2g^2ab - w(g+1)ab - wgb^2] + ab + (1-q_c)a^2,$$

$$K_2 = ab + (1-q_c)a^2,$$

$$K_3 = 3\alpha_{cr}^2[g^2a^2 + (g^2 - 2g)b^2 + 2g^2ab - w(g+1)ab - wgb^2] + 2ab + 2(1-q_c)a^2,$$

$$K_4 = \alpha_{cr}^2[g^2a^2 + (g^2 - 2g)b^2 + 2g^2ab - w(g+1)ab - wgb^2] + 2ab + 2(1-q_c)a^2.$$

The coefficients c_{2j}, f_{2j} appearing in the solution c_2, f_2 of the $O(\varepsilon^2)$ problem have the form

$$c_{21} = -\frac{1}{D_1}\left\{4\alpha_{cr}^2[zab(\omega - g) + K_1\widetilde{D_{f\,cr}}] + K_1(\zeta + z)\right\},$$

$$f_{21} = -\frac{1}{D_1}\left[4\alpha_{cr}^2 zab(1+g) + zab(1-q_c) + \zeta K_1\right],$$

$$D_1 = 16\alpha_{cr}^4\widetilde{D_{f\,cr}}(1+g) + (1-q_c)(\zeta + z) +$$

$$4\alpha_{cr}^2[\widetilde{D_{f\,cr}}(1-q_c) + (1+g)(\zeta + z) - \zeta(\omega - g)],$$

$$c_{22} = -\frac{K_2}{1-q_c}, \quad f_{22} = -\frac{\zeta K_2}{(1-q_c)(\zeta + z)} - \frac{zab}{\zeta + z},$$

$$c_{23} = -\frac{1}{D_3}\left\{3\alpha_{cr}^2[2zab(\omega - g) + K_3\widetilde{D_{f\,cr}}] + K_3(\zeta + z)\right\},$$

$$f_{23} = -\frac{1}{D_3}\left[6\alpha_{cr}^2 zab(1+g) + 2zab(1-q_c) + \zeta K_3\right],$$

$$D_3 = 9\alpha_{cr}^4 \widetilde{D_{f\,cr}}(1+g) + (1-q_c)(\zeta+z)+$$

$$3\alpha_{cr}^2[\widetilde{D_{f\,cr}}(1-q_c) + (1+g)(\zeta+z) - \zeta(\omega-g)].$$

The coefficients C_k, $k = 1, 2, 3, 4$ appearing in the amplitude equations are given by

$$C_1 = b\alpha_{cr}^2 c_5/c_0, \quad C_2 = -(\zeta K_4 + 2zabc_5)/c_0,$$

$$C_3 = -\{\zeta R_1 + zc_5[b(c_{21}+2c_{22}) + a(f_{21}+2f_{22})]\}/c_0,$$

$$C_4 = -\{\zeta R_2 + zc_5[b(2c_{22}+c_{23}) + a(2f_{22}+f_{23})]\}/c_0,$$

where

$$c_0 = b(a+c_5), \quad c_5 = (1+g)\alpha_{cr}^2 + 1 - q_c,$$

$$R_1 = \alpha_{cr}^2[g^2a(c_{21}+f_{21})+2g^2a(c_{22}+f_{22})+2g^2bc_{21}+(g^2-2g)bf_{21}+2(g^2-2g)bf_{22}+(\frac{1}{2}g^3-\frac{3}{2}g^2)a^3$$

$$+(\frac{3}{2}g^3-3g^2)a^2b+(\frac{3}{2}g^3-\frac{9}{2}g^2)ab^2+(\frac{1}{2}g^3-3g^2+3g)b^3-2af_{21}\omega(1+g)-2bf_{21}\omega g+$$

$$\omega(1+g)b(c_{21}+2c_{22})-\omega gb(f_{21}+2f_{22})-\frac{1}{2}\omega b(g^2a^2+2g^2ab+(g^2-2g)b^2)]+$$

$$b(c_{21}+2c_{22})+a(f_{21}+2f_{22})+3a^2b+2(1-q_c)a(c_{21}+2c_{22}),$$

$$R_2 = \alpha_{cr}^2[2g^2a(c_{22}+f_{22}) + g^2a(c_{23}+f_{23}) + g^2b(2c_{22}+c_{23}) + (g^2-2g)b(2f_{22}+f_{23})+$$

$$g^3(a+b)^3 - 3g^2a^3 - 6g^2a^2b - 9g^2ab^2 - 6(g^2-g)b^3$$

$$-\frac{3}{2}af_{23}\omega(1+g) - \frac{3}{2}bf_{23}\omega g + \omega(1+g)b(\frac{1}{2}c_{23} - 2c_{22})+$$

$$\omega gb(\frac{1}{2}f_{23} - 2f_{22}) - \omega b(g^2a^2 + 2g^2ab + (g^2-2g)b^2)]+$$

$$b(c_{23}+2c_{22}) + a(f_{23}+2f_{22}) + 6a^2b + 2(1-q_c)a(c_{23}+2c_{22}).$$

Calculations with $D = D_0 \exp\left(-\frac{k_*}{cf}\right)$: squares

The right-hand sides in the $O(\varepsilon^3)$ problem are given by

$$R_{c3} = -\widetilde{\nabla}^2\left[(g^2-2g)(f_1-c_1)(f_2-c_2) + gf_1(f_1-c_1)^2+\right.$$

$$\left. g^2\left(\frac{1}{2}c_1 - f_1\right)(f_1-c_1)^2 + \frac{1}{6}g^3(f_1-c_1)^3\right] +$$

$$w\widetilde{\nabla}\cdot\left\{[(1-g)c_1 + gf_1]\,\widetilde{\nabla}f_2\right\} +$$

$$w\widetilde{\nabla}\cdot\left\{\left[(1-g)c_2 + gf_2 + \left(\frac{1}{2}g^2 - g\right)(f_1-c_1)^2\right]\widetilde{\nabla}f_1\right\} +$$

$$f_1c_2 + f_2c_1 + f_1c_1^2 + 2(1-q_c)c_1c_2 + \frac{\partial c_1}{\partial T},$$

$$R_{f3} = \mu\widetilde{\nabla}^2 f_1 + z f_1 c_2 + z f_2 c_1 + \frac{\partial f_1}{\partial T}$$

The coefficients K_j appearing on right-hand side R_{c2} of the $O(\varepsilon^2)$ problem have the form

$$K_1 = 2\alpha_{cr}^2[g^2a^2 + (g^2-2g)b^2 + 2g^2ab - w(g+1)ab - wgb^2] + ab + (1-q_c)a^2,$$

$$K_2 = ab + (1-q_c)a^2,$$

$$K_3 = 2\alpha_{cr}^2[g^2a^2 + (g^2-2g)b^2 + 2g^2ab - w(g+1)ab - wgb^2] + 2ab + 2(1-q_c)a^2,$$

The coefficients c_{2j}, f_{2j} appearing in the solution c_2, f_2 of the $O(\varepsilon^2)$ problem have the form

$$c_{21} = -\frac{1}{D_1}\left\{4\alpha_{cr}^2[zab(\omega-g) + K_1\widetilde{D_{f\,cr}}] + K_1(\zeta+z)\right\},$$

$$f_{21} = -\frac{1}{D_1}\left[4\alpha_{cr}^2 zab(1+g) + zab(1-q_c) + \zeta K_1\right],$$

$$D_1 = 16\alpha_{cr}^4\widetilde{D_{f\,cr}}(1+g) + (1-q_c)(\zeta+z) +$$

$$4\alpha_{cr}^2[\widetilde{D_{f\,cr}}(1-q_c) + (1+g)(\zeta+z) - \zeta(\omega-g)],$$

$$c_{22} = -\frac{K_2}{1-q_c}, \quad f_{22} = -\frac{\zeta K_2}{(1-q_c)(\zeta+z)} - \frac{zab}{\zeta+z},$$

$$c_{23} = -\frac{1}{D_3}\left\{3\alpha_{cr}^2[2zab(\omega-g) + K_3\widetilde{D_{f\,cr}}] + K_3(\zeta+z)\right\},$$

$$f_{23} = -\frac{1}{D_3}\left[6\alpha_{cr}^2 zab(1+g) + 2zab(1-q_c) + \zeta K_3\right],$$

$$D_3 = 9\alpha_{cr}^4 \widetilde{D_{f\,cr}}(1+g) + (1-q_c)(\zeta+z) +$$

$$3\alpha_{cr}^2[\widetilde{D_{f\,cr}}(1-q_c) + (1+g)(\zeta+z) - \zeta(\omega-g)].$$

The coefficients C_k, $k = 1, 3, 4$ appearing in the amplitude equations are given by

$$C_1 = b\alpha_{cr}^2 c_5/c_0, \quad C_3 = -\{\zeta R_1 + zc_5[b(c_{21}+2c_{22}) + a(f_{21}+2f_{22})]\}/c_0,$$

$$C_4 = -\{\zeta R_2 + 2zc_5[b(c_{22}+c_{23}) + a(f_{22}+f_{23})]\}/c_0,$$

where

$$c_0 = a\zeta + bc_5, \quad c_5 = (1+g)\alpha_{cr}^2 + 1 - q_c,$$

$$R_1 = \alpha_{cr}^2[g^2 a(c_{21}+f_{21}) + 2g^2 a(c_{22}+f_{22}) + 2g^2 bc_{21} +$$

$$(g^2-2g)bf_{21} + 2(g^2-2g)bf_{22} + (\frac{1}{2}g^3 - \frac{3}{2}g^2)a^3 +$$

$$(\frac{3}{2}g^3 - 3g^2)a^2 b + (\frac{3}{2}g^3 - \frac{9}{2}g^2)ab^2 + (\frac{1}{2}g^3 - 3g^2 + 3g)b^3 -$$

$$2af_{21}\omega(1+g) - 2bf_{21}\omega g + \omega(1+g)b(c_{21}+2c_{22}) -$$

$$\omega gb(f_{21}+2f_{22}) - \frac{1}{2}\omega b(g^2a^2 + 2g^2 ab + (g^2-2g)b^2)] +$$

$$b(c_{21}+2c_{22})+a(f_{21}+2f_{22})+3a^2b+2(1-q_c)a(c_{21}+2c_{22}),$$

$$R_2=\alpha_{cr}^2\{2g^2a(c_{22}+f_{22}+c_{23}+f_{23})+2g^2b(c_{22}+c_{23})+4b(g^2-2g)\}+$$

$$(g^3-3g^2)a^3-3(g^3-2g^2)a^2b+3(g^3-9g^2)ab^2+(g^3-6g^2+6g)b^3$$

$$-2\omega\alpha_{cr}^2\{f_{23}[(1+g)a+gb]+b(1+g)c_{22}+bgf_{22}+abg^2\left(\frac{1}{2}a+b\right)+b^3\left(\frac{1}{2}g^2-g\right)\}+$$

$$2b(c_{22}+c_{23})+2a(f_{22}+2f_{23})+6a^2b+4a(1-q_c)(c_{22}+c_{23}).$$

Calculations with $D=D_0\exp\left(-\frac{k_*c}{f}\right)$: hexagons and stripes

The right-hand sides in the $O(\varepsilon^3)$ problem are given by

$$R_{c3}=-\widetilde{\nabla}^2\left[(g^2-2g)(f_1-c_1)(f_2-c_2)+gf_1(f_1-c_1)^2+\right.$$

$$\left.g^2\left(\frac{1}{2}c_1-f_1\right)(f_1-c_1)^2+\frac{1}{6}g^3(f_1-c_1)^3\right]+w\widetilde{\nabla}\cdot\left\{\left[(1-g)c_1+gf_1\right]\widetilde{\nabla}f_2\right\}+$$

$$w\widetilde{\nabla}\cdot\left\{\left[(1-g)c_2+gf_2+\left(\frac{1}{2}g^2-g\right)(f_1-c_1)^2\right]\widetilde{\nabla}f_1\right\}+$$

$$f_1c_2+f_2c_1+f_1c_1^2+2(1-q_c)c_1c_2+\frac{\partial c_1}{\partial T},$$

$$R_{f3}=\mu\widetilde{\nabla}^2f_1+zf_1c_2+zf_2c_1+\frac{\partial f_1}{\partial T}$$

The coefficients K_j appearing on right-hand side R_{c2} of the $O(\varepsilon^2)$ problem have the form

$$K_1 = 2\alpha_{cr}^2[(g^2-2g)(b-a)^2 - w(1-g)ab - wgb^2] + ab + (1-q_c)a^2,$$

$$K_2 = ab + (1-q_c)a^2,$$

$$K_3 = 3\alpha_{cr}^2[(g^2-2g)(b-a)^2 - w(1-g)ab - wgb^2] + 2ab + 2(1-q_c)a^2,$$

$$K_4 = \alpha_{cr}^2[(g^2-2g)(b-a)^2 - w(1-g)ab - wgb^2] + 2ab + 2(1-q_c)a^2.$$

The coefficients c_{2j}, f_{2j} appearing in the solution c_2, f_2 of the $O(\varepsilon^2)$ problem have the form

$$c_{21} = -\frac{1}{D_1}\left\{4\alpha_{cr}^2[zab(\omega-g) + K_1\widetilde{D_{f\,cr}}] + K_1(\zeta+z)\right\},$$

$$f_{21} = -\frac{1}{D_1}\left[4\alpha_{cr}^2 zab(1-g) + zab(1-q_c) + \zeta K_1\right],$$

$$D_1 = 15\alpha_{cr}^4\widetilde{D_{f\,cr}}(1-g) + 3\alpha_{cr}^2[\widetilde{D_{f\,cr}}(1-q_c) + (1-g)(\zeta+z) - \zeta(\omega-g)],$$

$$c_{22} = -\frac{K_2}{1-q_c}, \quad f_{22} = -\frac{\zeta K_2}{(1-q_c)(\zeta+z)} - \frac{zab}{\zeta+z},$$

$$c_{23} = -\frac{1}{D_3}\left\{3\alpha_{cr}^2[2zab(\omega-g) + K_3\widetilde{D_{f\,cr}}] + K_3(\zeta+z)\right\},$$

$$f_{23} = -\frac{1}{D_3}\left[6\alpha_{cr}^2 zab(1-g) + 2zab(1-q_c) + \zeta K_3\right],$$

$$D_3 = 8\alpha_{cr}^4 \widetilde{D}_{f\,cr}(1-g) + 2\alpha_{cr}^2[\widetilde{D}_{f\,cr}(1-q_c) + (1-g)(\zeta+z) - \zeta(\omega-g)].$$

The coefficients C_k, $k = 1, 2, 3, 4$ appearing in the amplitude equations are given by

$$C_1 = b\alpha_{cr}^2 c_5/c_0, \quad C_2 = -(\zeta K_4 + 2zabc_5)/c_0,$$

$$C_3 = -\{\zeta R_1 + zc_5[b(c_{21}+2c_{22}) + a(f_{21}+2f_{22})]\}/c_0,$$

$$C_4 = -\{\zeta R_2 + zc_5[b(2c_{22}+c_{23}) + a(2f_{22}+f_{23})]\}/c_0,$$

where

$$c_0 = a\zeta + bc_5, \quad c_5 = (1-g)\alpha_{cr}^2 + 1 - q_c,$$

$$R_1 = \alpha_{cr}^2[(g^2-2g)(b-a)(f_{21}-c_{21}+2f_{22}-2c_{22})+$$

$$3g(b-a)^2\left(b + g\left(\frac{1}{2}a - b\right) + \frac{1}{6}g^2(b-a)\right) -$$

$$\omega\{2f_{21}((1-g)a+gb) + \left(\frac{1}{2}g^2 - g\right)b(b-a)^2 -$$

$$b((1-g)c_{21} + gf_{21} - 2(1-g)c_{22} - 2gf_{22})\}]+$$

$$(2(1-q_c)a + b)(c_{21}+2c_{22}) + f_{21}a + 2f_{22}a + 3a^2b,$$

$$R_2 = \alpha_{cr}^2[(g^2-2g)(b-a)(2f_{22}-2c_{22}+f_{23}-c_{23})+$$

$$6g(b-a)^2\left(b+g\left(\frac{1}{2}a-b\right)+\frac{1}{6}g^2(b-a)\right)+$$

$$\omega\{-\frac{3}{2}f_{23}((1-g)a+gb)-(g^2-2g)b(b-a)^2-$$

$$b\left(2(1-g)c_{22}+2gf_{22}-\frac{1}{2}(1-g)c_{23}-\frac{1}{2}gf_{23}\right)\}]+$$

$$(2(1-q_c)a+b)(2c_{22}+c_{23})+2af_{22}+af_{23}+6a^2b.$$

Calculations with $D=D_0\exp\left(-\frac{k_*c}{f}\right)$: squares

The right-hand sides in the $O(\varepsilon^3)$ problem are given by

$$R_{c3}=-\widetilde{\nabla}^2\left[(g^2-2g)(f_1-c_1)(f_2-c_2)+gf_1(f_1-c_1)^2+\right.$$

$$\left.g^2\left(\frac{1}{2}c_1-f_1\right)(f_1-c_1)^2+\frac{1}{6}g^3(f_1-c_1)^3\right]+w\widetilde{\nabla}\cdot\left\{\left[(1-g)c_1+gf_1\right]\widetilde{\nabla}f_2\right\}+$$

$$w\widetilde{\nabla}\cdot\left\{\left[(1-g)c_2+gf_2+\left(\frac{1}{2}g^2-g\right)(f_1-c_1)^2\right]\widetilde{\nabla}f_1\right\}+$$

$$f_1c_2+f_2c_1+f_1c_1^2+2(1-q_c)c_1c_2+\frac{\partial c_1}{\partial T},$$

$$R_{f3}=\mu\widetilde{\nabla}^2f_1+zf_1c_2+zf_2c_1+\frac{\partial f_1}{\partial T}.$$

The coefficients K_j appearing on right-hand side R_{c2} of the $O(\varepsilon^2)$ problem have the form

$$K_1=2\alpha_{cr}^2[(g^2-2g)(b-a)^2-w(1-g)ab-wgb^2]+ab+(1-q_c)a^2,$$

$$K_2 = ab + (1 - q_c)a^2,$$

$$K_3 = 2\alpha_{cr}^2[(g^2 - 2g)(b - a)^2 - w(1 - g)ab - wgb^2] + 2ab + 2(1 - q_c)a^2.$$

The coefficients c_{2j}, f_{2j} appearing in the solution c_2, f_2 of the $O(\varepsilon^2)$ problem have the form

$$c_{21} = -\frac{1}{D_1}\left\{4\alpha_{cr}^2[zab(\omega - g) + K_1\widetilde{D_{f\,cr}}] + K_1(\zeta + z)\right\},$$

$$f_{21} = -\frac{1}{D_1}\left[4\alpha_{cr}^2 zab(1 - g) + zab(1 - q_c) + \zeta K_1\right],$$

$$D_1 = 15\alpha_{cr}^4\widetilde{D_{f\,cr}}(1 - g) + 3\alpha_{cr}^2[\widetilde{D_{f\,cr}}(1 - q_c) + (1 - g)(\zeta + z) - \zeta(\omega - g)],$$

$$c_{22} = -\frac{K_2}{1 - q_c}, \quad f_{22} = -\frac{\zeta K_2}{(1 - q_c)(\zeta + z)} - \frac{zab}{\zeta + z},$$

$$c_{23} = -\frac{1}{D_3}\left\{3\alpha_{cr}^2[2zab(\omega - g) + K_3\widetilde{D_{f\,cr}}] + K_3(\zeta + z)\right\},$$

$$f_{23} = -\frac{1}{D_3}\left[6\alpha_{cr}^2 zab(1 - g) + 2zab(1 - q_c) + \zeta K_3\right],$$

$$D_3 = 8\alpha_{cr}^4\widetilde{D_{f\,cr}}(1 - g) + 2\alpha_{cr}^2[\widetilde{D_{f\,cr}}(1 - q_c) + (1 - g)(\zeta + z) - \zeta(\omega - g)].$$

The coefficients C_k, $k = 1, 2, 3, 4$ appearing in the amplitude equations are given by

$$C_1 = b\alpha_{cr}^2 c_5/c_0, \quad C_3 = -\{\zeta R_1 + zc_5[b(c_{21} + 2c_{22}) + a(f_{21} + 2f_{22})]\}/c_0,$$

$$C_4 = -\{\zeta R_2 + 2zc_5[b(c_{22} + c_{23}) + a(f_{22} + f_{23})]\}/c_0,$$

where

$$c_0 = a\zeta + bc_5, \quad c_5 = (1-g)\alpha_{cr}^2 + 1 - q_c,$$

$$R_1 = \alpha_{cr}^2[(g^2-2g)(b-a)(f_{21}-c_{21}+2f_{22}-2c_{22})+$$

$$3g(b-a)^2\left(b+g\left(\frac{1}{2}a-b\right)+\frac{1}{6}g^2(b-a)\right)-$$

$$\omega\{2f_{21}((1-g)a+gb)+\left(\frac{1}{2}g^2-g\right)b(b-a)^2-$$

$$b((1-g)c_{21}+gf_{21}-2(1-g)c_{22}-2gf_{22})\}]+$$

$$(2(1-q_c)a+b)(c_{21}+2c_{22})+f_{21}a+2f_{22}a+3a^2b,$$

$$R_2 = \alpha_{cr}^2[2(g^2-2g)(b-a)(f_{22}-c_{22}+f_{23}-c_{23})+$$

$$6g(b-a)^2\left(b+g\left(\frac{1}{2}a-b\right)+\frac{1}{6}g^2(b-a)\right)-$$

$$\omega\{2f_{23}((1-g)a+gb)+(g^2-2g)b(b-a)^2+$$

$$2b((1-g)c_{22}+gf_{22})\}]+2[(c_{22}+c_{23})(b+2a(1-q_c))+a(f_{22}+f_{23}+3ab)].$$

CHAPTER 3

A hybrid discrete-continuous model of tumor-induced angiogenesis

3.1. Introduction

As discussed in Chapter 1, angiogenesis occurs during embryogenesis, wound healing, as well as in the course of many pathological processes such as rheumatoid arthritis [177, 181], psoriasis [50], cerebral ischemia [178], cardiovascular diseases [146], and growth of solid tumors [85].

Initially, solid tumors are avascular. They do not have their own blood supply and rely on simple diffusion to provide necessary oxygen and nutrition as well as to remove tumor cell waste products. As the tumor gets bigger, diffusion through the surface is not any longer capable of supplying the entire mass of cells. As a result, some of tumor cells start to die due to starvation and hypoxia (oxygen deprivation). Tumor stops growing and reaches steady state size $1-3$ mm, in which the number of dying cells counterbalances the number of proliferating cells. Growth can resume only if the tumor becomes vascularized, i.e. permeated by a vessel network, so that blood can perform transporting functions.

To achieve vascularization, tumors switch on enhanced production of growth factors that play the role of angiogenic signals. They diffuse from tumor to nearby primary vessels initiating a complicated cascade of events that results in formation of new capillaries extending from the primary vessels to the tumor [26, 59, 62, 65, 187]. Blood that starts circulating through newly formed vessels supplies the tumor with necessary nutrients and oxygen and may also serve as an easier escape route for metastatic cells [2, 4, 38, 44, 61, 169].

Thus angiogenesis is crucial for cancer invasion and understanding the mechanisms that control it will provide the basis for rational therapeutic intervention. In other words there is a hope that by blocking formation of new blood vessels through drugs it may be possible to suppress tumor growth and to prevent metastasis formation [11, 23, 54, 55, 62, 63, 84, 88, 92, 173, 208].

There are many mathematical works that intend to model and better understand the angiogenesis process. The models can be of quite diverse nature, including reaction-diffusion models, fluid dynamics type models, stochastic models and many others. Various stages of the angiogenesis process are described, from the first steps of initiation of angiogenesis to modeling the blood flow through the resulting vascular network.

In this chapter we describe the stage of the process in which endothelial cells move in response to chemical stimuli, growth factors, released in the system and form sprouts that later become capillaries. From the mathematical viewpoint, we employ a hybrid model, in which the cells are treated as discrete objects that move, proliferate, die, talk to each other, etc. according to prescribed rules [5, 40, 99, 100, 106, 138, 142, 161, 167, 168, 193, 194, 197, 215].

Let us discuss the phenomena that have been observed experimentally and are included in the model.

It has been observed that the growth of the sprout is guided and controlled by a small number of cells that are close to the front end of the sprout, i.e., by the tip of the sprout. The remaining cells in the sprout retain cell-cell contacts and follow in a more passive manner (see, e.g., [68] and the references therein). The shape of the sprout is determined by the trajectory of the tip. Thus, in our model we follow tip motion disregarding the rest of the cell body.

Deconstructing tip trajectories shows persistence in the direction of cell motion, so that tip trajectory can be thought of as a broken line [132]. The tip goes along a line segment for some

time, then stops, and after a period of hesitation chooses another direction of motion. This direction is that of the gradient of the growth factor field altered by a small random component.

Not only the direction of tip propagation but also all the other events of tip's motion depend on the local concentration of the growth factor and its gradient. Examples are the tip speed, the waiting time at the trajectory vertex, survival of the tip (if a local concentration of the growth factor is below a critical value, the tip ceases to exist). Under appropriate conditions the tip can split thus producing two separately propagating tips. In addition, two propagating tips can merge and form a loop. These events lead to the formation of a capillary network.

Growth factor field is affected by several things. First of all, the growth factor is released by the tumor cells and it diffuses through the surrounding tissue, the extracellular matrix. Next, the propagating tips also produce some amounts of growth factor. Indeed, this is a way for a tip to signal to another tip and eventually merge and form a loop.

Several more things that are taken into account are (i) in addition to the sources of growth factor in the system, there may be sinks, (ii) the growth factors are also known to be degraded by the environment, mainly through oxidation processes and (iii) there may be more than one type of chemical stimuli in the system.

3.2. Mathematical Model

In this section we focus on mass balances for the growth factor f and the repulsion factor r as well as discuss the rules that govern the motion of capillary tips.

3.2.1. Growth factor

Mass balance of the growth factor is modeled by the equation

$$\frac{\partial f}{\partial t} = D_f \nabla^2 f + F_c + F_t - F_s - \beta f. \tag{3.100}$$

Here the first term on the right-hand side describes diffusion of the factor with diffusion coefficient D_f, and ∇^2 is the Laplacian in two spatial dimensions, x and y. Next, second and third terms, F_c and F_t, are the rates of growth factor production by cancer cells and growing tips, respectively. Next term, F_s, is the rate of factor consumption by the sinks hidden in the ECM. The form of these terms, F_c, F_t, and F_s, is discussed later. Finally, the last term accounts for the natural decay of the factor with the rate constant β. We solve the Cauchy problem for this equation in the entire plane $-\infty < x, y < \infty$ for $t > 0$ under the assumption that initially, for $t = 0$, the growth factor is absent.

The solution of this problem can be conveniently written in terms of the fundamental solution

$$g_0(x, y, t|x_0, y_0, t_0) = \frac{H(t - t_0)e^{-\beta(t-t_0)}}{4\pi D_f(t - t_0)} \exp\left(-\frac{(x - x_0)^2 + (y - y_0)^2}{4D_f(t - t_0)}\right) \tag{3.101}$$

of the operator

$$\frac{\partial}{\partial t} - D_f \nabla^2 + \beta$$

as

$$f(x, y, t) = I_c(x, y, t) + I_t(x, y, t) - I_s(x, y, t). \tag{3.102}$$

Here I_c and I_t, given by

(3.103a) $$I_c(x,y,t) = \int_0^t \iint_{R^2} F_c(x_0,y_0,t_0) g_0(x,y,t|x_0,y_0,t_0)\, dx_0\, dy_0\, dt_0,$$

(3.103b) $$I_t(x,y,t) = \int_0^t \iint_{R^2} F_t(x_0,y_0,t_0) g_0(x,y,t|x_0,y_0,t_0)\, dx_0\, dy_0\, dt_0$$

are the contributions of the cancer cells and the tips, respectively, to the growth factor field. The quantity I_s, given by

(3.103c) $$I_s(x,y,t) = \int_0^t \iint_{R^2} F_s(x_0,y_0,t_0) g_0(x,y,t|x_0,y_0,t_0)\, dx_0\, dy_0\, dt_0,$$

characterizes the reduction of the growth factor field due to the presence of the sinks.

In this model we treat the cancer as a collection of M point sources of growth factor located at $(x_c^{(n)}, y_c^{(n)})$, $n = 1, \ldots, M$, each releasing the factor at a constant rate Q_c, so that

(3.104) $$F_c(x,y,t) = \sum_{n=1}^{M} Q_c \delta(x - x_c^{(n)}) \delta(y - y_c^{(n)}), \quad -\infty < x, y < \infty, \quad t > 0.$$

Thus, the cancer dependent part (3.103a) of the growth factor field (3.102) simplifies to

$$I_c(x,y,t) = Q_c \sum_{n=1}^{M} \int_0^t g_0(x,y,t|x_c^{(n)}, y_c^{(n)}, t_0)\, dt_0$$

$$= Q_c \sum_{n=1}^{M} \int_0^t \frac{e^{-\beta(t-t_0)}}{4\pi D_f (t-t_0)} \exp\left(-\frac{(x - x_c^{(n)})^2 + (y - y_c^{(n)})^2}{4D_f(t-t_0)} \right) dt_0.$$

The tips are also considered to be localized point sources that release the factor at the rate Q_t. However, the contribution I_t of the tips to the factor field is more difficult to compute, not only because the tips are moving, so that all the tip trajectories have to be traced, but also because new

tips can appear due to tip splitting, and some tips can disappear due to anastomosis. Suppose at time t there are N tips that either are alive at time t or have existed during the time interval $(0, t)$ but no longer exist at t. All such tips have contributed to the formation of the growth factor field and must be accounted for. For the purpose of computing the factor field, a convenient way to represent the tips is as follows. Suppose the n-th tip, $n = 1, \ldots, N$, first appeared at time $t_b^{(n)}$ and disappeared at $t_d^{(n)}$. We consider the tip as if it existed at all times but with the rate of factor production given by

$$Q_t^{(n)}(t) = \begin{cases} Q_t, & t_b^{(n)} < t < t_d^{(n)} \\ 0, & \text{otherwise} \end{cases}$$

where Q_t is a constant parameter of the problem. Note that for some tips $t_b^{(n)}$ can be equal to zero – these are the original tips that started the angiogenesis process. For other tips $t_b^{(n)} > 0$ – these are the secondary tips that appeared in the course of angiogenesis. Similarly, $t_d^{(n)}$ is equal to t for those tips that still exist at the time t, at which the factor field is computed, while $t_d^{(n)} < t$ for the tips that no longer exist at the time of the field calculation. Then

$$F_t(x, y, t) = \sum_{n=1}^{N} Q_t^{(n)}(t)\delta(x - \xi^{(n)}(t))\delta(y - \eta^{(n)}(t)), \quad -\infty < x, y < \infty, \quad t > 0, \tag{3.105}$$

and the tip dependent part (3.103b) of the growth factor field (3.102) simplifies to

$$I_t(x, y, t) = Q_t \sum_{n=1}^{N} \int_{t_b^{(n)}}^{t_d^{(n)}} g_0(x, y, t|\xi^{(n)}(t_0), \eta^{(n)}(t_0), t_0)\, dt_0$$

$$= Q_t \sum_{n=1}^{N} \int_{t_b^{(n)}}^{t_d^{(n)}} \frac{e^{-\beta(t-t_0)}}{4\pi D_f(t - t_0)} \exp\left(-\frac{(x - \xi^{(n)}(t_0))^2 + (y - \eta^{(n)}(t_0))^2}{4D_f(t - t_0)}\right) dt_0. \tag{3.106}$$

Here $(\xi^{(n)}(t), \eta^{(n)}(t))$ are the coordinates of the n-th tip at time t. Since the trajectory of a tip is a broken line, it is sufficient to know the location of its vertices, the times when the vertices are reached, and the time spent by the tip at each vertex. Thus, the movement history of the n-th tip that has K vertices with coordinates $(\xi_k^{(n)}, \eta_k^{(n)})$, $k = 1, \ldots, K$ at time t, is completely described by

$$(\xi_k^{(n)}, \eta_k^{(n)}), t_{a,k}^{(n)}, t_{d,k}^{(n)}, \quad k = 1, \ldots, K$$

where $t_{a,k}^{(n)}$ is the time of arrival of the tip to the k-th vertex, and $t_{d,k}^{(n)}$ is the time of departure from it (note that the difference $t_{d,k}^{(n)} - t_{a,k}^{(n)}$ is the waiting time at the k-th vertex, calculation of which is discussed in the next section). The factor release by the n-th tip in (3.106) can now be written as a sum of two terms, one governing factor release by the tip as it moves from one vertex to another, and the other governing factor release during the time that the tip stays at the vertices

$$Q_t \sum_{k=1}^{K-1} \int_{t_{d,k}^{(n)}}^{t_{a,k+1}^{(n)}} \frac{e^{-\beta(t-t_0)}}{4\pi D_f (t-t_0)} \exp\left(-\frac{(x-\xi^{(n)}(t_0))^2 + (y-\eta^{(n)}(t_0))^2}{4D_f(t-t_0)} \right) dt_0 +$$

$$Q_t \sum_{k=2}^{K} \int_{t_{a,k}^{(n)}}^{t_{d,k}^{(n)}} \frac{e^{-\beta(t-t_0)}}{4\pi D_f (t-t_0)} \exp\left(-\frac{(x-\xi_k^{(n)})^2 + (y-\eta_k^{(n)})^2}{4D_f(t-t_0)} \right) dt_0,$$

where

$$\xi^{(n)}(t_0) = \xi_k^{(n)} + \frac{\xi_{k+1}^{(n)} - \xi_k^{(n)}}{t_{a,k+1}^{(n)} - t_{d,k}^{(n)}}(t_0 - t_{d,k}^{(n)}), \quad \eta^{(n)}(t_0) = \eta_k^{(n)} + \frac{\eta_{k+1}^{(n)} - \eta_k^{(n)}}{t_{a,k+1}^{(n)} - t_{d,k}^{(n)}}(t_0 - t_{d,k}^{(n)}),$$

for $t_{d,k}^{(n)} < t_0 < t_{a,k+1}^{(n)}$. Note that if the n-th tip is in motion at time t, then $t = t_{a,K}^{(n)}$, while in the case that the tip is not moving at t, we have $t = t_{d,K}^{(n)}$.

The sink is as a collection of S localized point sinks, located at $(x_s^{(n)}, y_s^{(n)})$, $n = 1, \ldots, S$, each consuming the factor at a constant rate Q_s, so that

$$F_s(x, y, t) = \sum_{n=1}^{S} Q_s \delta(x - x_s^{(n)}) \delta(y - y_s^{(n)}), \quad -\infty < x, y < \infty, \quad t > 0. \tag{3.107}$$

Thus, the sink dependent part (3.103c) of the growth factor field (3.102) simplifies to

$$I_s(x, y, t) = Q_s \sum_{n=1}^{S} \int_0^t g_0(x, y, t | x_s^{(n)}, y_s^{(n)}, t_0)\, dt_0$$

$$= Q_s \sum_{n=1}^{S} \int_0^t \frac{e^{-\beta(t-t_0)}}{4\pi D_f (t - t_0)} \exp\left(-\frac{(x - x_s^{(n)})^2 + (y - y_s^{(n)})^2}{4 D_f (t - t_0)} \right) dt_0.$$

We remark that the presence of the sink can result in unphysical negative concentrations of the growth factor in some regions. They are treated as regions without growth factor which does not cause any problems. Indeed, the tips cannot penetrate into this regions because the tips die if the factor concentration drops below a critical value (see below).

3.2.2. Repulsion factor

Mass balance of the repulsion factor is modeled by the equation

$$\frac{\partial r}{\partial t} = D_r \nabla^2 r + G_t - \beta_r r. \tag{3.108}$$

Similar to (3.100), the first term on the right-hand side describes diffusion of the repulsion factor with diffusion coefficient D_r. The second term, G_t, is the rate of repulsion factor production by

the growing tips (cf. (3.105))

$$G_t(x,y,t) = \sum_{n=1}^{N} P_t^{(n)}(t)\delta(x-\xi^{(n)}(t))\delta(y-\eta^{(n)}(t)), \quad -\infty < x,y < \infty, \quad t > 0, \tag{3.109}$$

with

$$P_t^{(n)}(t) = \begin{cases} P_t, & t_b^{(n)} < t < t_d^{(n)} \\ 0, & \text{otherwise} \end{cases}$$

The last term accounts for the natural decay of the factor with the rate constant β_r. As before, we solve the Cauchy problem for this equation in the entire plane $-\infty < x,y < \infty$ for $t > 0$ under the assumption that initially, for $t = 0$, the repulsion factor is absent. The solution is

$$r(x,y,t) = P_t \sum_{n=1}^{N} \int_{t_b^{(n)}}^{t_d^{(n)}} \frac{e^{-\beta_r(t-t_0)}}{4\pi D_r(t-t_0)} \exp\left(-\frac{(x-\xi^{(n)}(t_0))^2 + (y-\eta^{(n)}(t_0))^2}{4D_r(t-t_0)}\right) dt_0.$$

It is treated numerically in the same way as (3.106).

3.2.3. Advancing, splitting and merging of tips

Rules of motion for a single tip are as follows:

- the tip waits for some time $\Delta\tau$ before starting to move,

$$\Delta\tau = t_0 + \frac{1}{a}\text{arctanh}[r - (1-r)\tanh(at_0)]$$

where r is a random variable uniformly distributed between 0 and 1, and t_0 and a are parameters of the problem;

- the absolute value of tip velocity is given by

$$v = \frac{\delta |\text{grad} f|}{(1 + f/f_*)^2},$$

where δ is cell chemotactic mobility and f is the value of growth factor field concentration at the point where the moving tip is located [67].

- the angle of tip movement is given by the direction of the growth factor and repulsive factor gradients at the point of interest and also contains a stochastic component. The stochastic angle is normally distributed with variance σ.

Tips can merge and branch according to the following rules:

- fusion occurs when the distance between two growing tips becomes smaller than a critical value. The necessary condition for fusion is that two tips themselves are or descend from two different initial vessels. In other words, close relatives are prohibited to fuse;
- splitting can occurs after a tip has moved ten times provided

$$r < \tanh\left[\frac{f}{f_0}\right]$$

where f is the growth factor concentration in the point of the growing tip and r is a random variable uniformly distributed between 0 and 1.

3.3. Numerical results and discussion

We have included two plots for each parameter set. The difference between the plots is due to the presence of stochastic components in the algorithm. In Fig. 3.1 we have plotted the structure of the vessel network for the base parameter values given in Table 1. In each of the two plots we

see five sprouts that propagate to the right, where the tumor cells are located. The sprouts branch, merge and eventually form a relatively complex network.

TABLE 1. Base parameter values

Parameter/Value	Parameter Definition
$D_f = 1$	diffusion coefficient of the growth factor
$\beta = 5$	decay rate of the growth factor
$Q_c = 0.4$	rate of growth factor release by tumor cells
$Q_t = 0.25$	rate of growth factor release by tips
$Q_s = 0$	rate of consumption of growth factor by sinks
$D_r = 1$	diffusion coefficient of the repulsion factor
$\beta_r = 5$	decay rate of the repulsion factor
$P_t = 45$	rate of repulsion factor release by tips
$a = 20$	waiting time parameter
$t_0 = 0.1$	waiting time parameter
$\delta = 0.15$	tip mobility parameter
$f_* = 1$	velocity sensitivity on growth factor concentration
$\sigma = 0.1$	variance (in calculation of tip motion angle)
$f_0 = 30$	splitting parameter

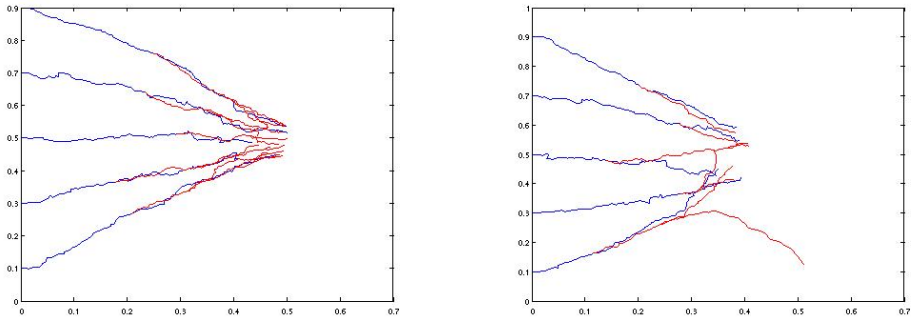

(a) (b)

FIGURE 3.1. Sprout structure for the base parameter values. The two figures are obtained for the same parameter values; the difference between the figures is due to the presence of stochastic components in the rules of tip motion.

In Fig. 3.2 we have plotted vessel network structure for the parameter values shown in the Table 1 but with an increased rate of the growth factor release by tip cells Q_t which is taken here to be equal to 0.35. If we compare Fig. 3.1 and Fig. 3.2 we can see that the growing vessels begin to branch earlier, which is due to the increased growth factor concentration in the system. Also in this case newly split vessels tend to attract to other vessels stronger than before since the amount of the growth factor released by tips is now greater. The vessels sense both repulsion and attraction forces but as it was discussed above, in the case when two tips are close to each other, attraction interactions are much weaker than repulsion and can be neglected. In other words, the tips are attracted mostly to the vessels that are not their immediate neighbors. Thus, increased rate of growth factor release yields increased branching coupled with stronger attraction towards distant vessels which leads to more elaborated network structure which is observed in Fig. 3.2.

In Fig. 3.3, a vessel network structure is shown for the parameter values given in Table 1 but with a decreased rate of decay of the growth factor β which is taken here to be 3. If we compare the results in this case with the results for the base parameter values (Fig. 3.1) we notice that the

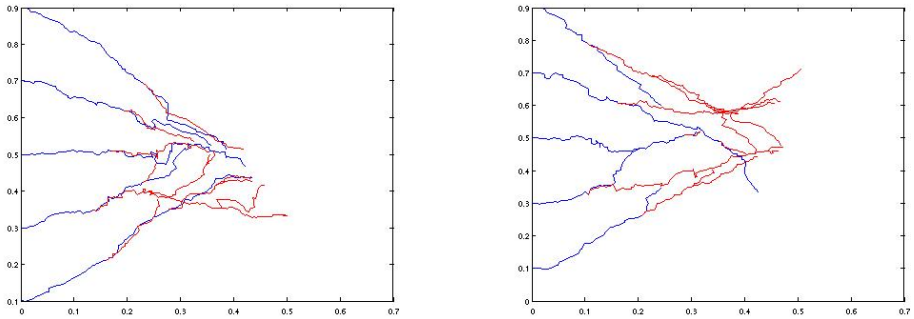

(a) (b)

FIGURE 3.2. Sprout structure for the base parameter values except $Q_t = 0.35$.

network structures are very similar and the only difference is that in Fig. 3.3 we observe increased vessel branching due to the fact that the growth factor concentration in the system is higher.

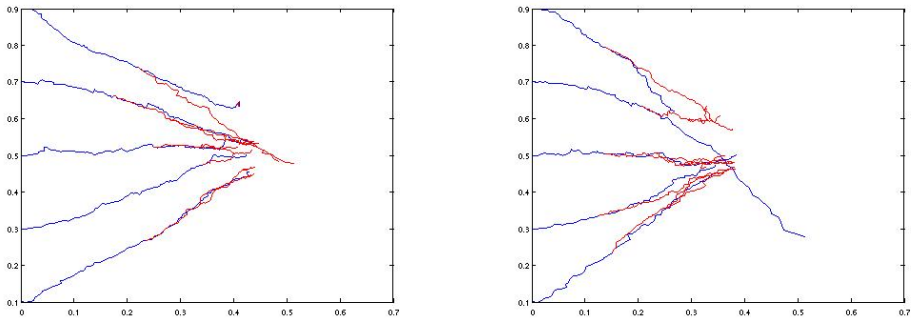

(a) (b)

FIGURE 3.3. Sprout structure for the base parameter values except $\beta = 3$.

In Fig. 3.4 we plot vessel network structure for the parameter values given in Table 1 but with an increased rate of the repulsion factor release by the tip cells P_t which is taken here to be 60. Comparing results in Fig. 3.1 and Fig. 3.4 we notice that in the second case newly split vessels tend to move farther apart from each other which can be explained by a stronger contribution of the repulsion factor to the growing tip dynamics.

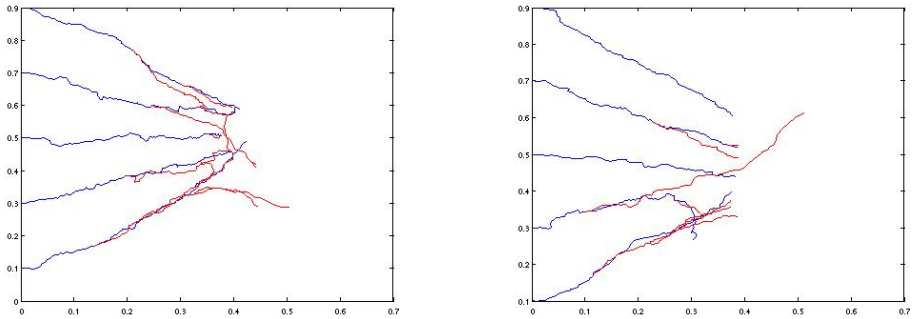

(a) (b)

FIGURE 3.4. Sprout structure for the base parameter values except $P_t = 60$.

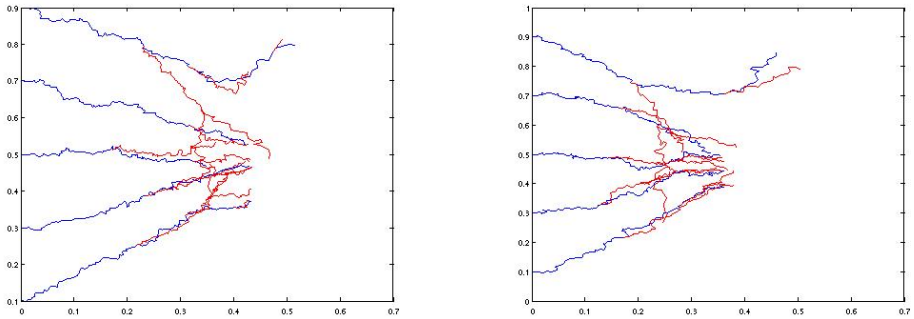

(a) (b)

FIGURE 3.5. Sprout structure for the base parameter values except $\sigma = 0.5$.

Finally, in Fig. 3.5 we have plotted vessel network structure for the parameter values given in Table 1 but with an increased variance σ that is used in the calculation of the random component of the turn angle of a moving tip. For these plots σ is taken to be 0.5. Comparing Fig. 3.1 with Fig. 3.5, we conclude that, as one could expect, the increase in the value of σ does not affect the vessel network structure, i.e. it does not influence branching or chemotactic component of the tip turn angle. However, it makes every single trajectory more random in the sense that the stochastic contribution to the turn angle increases.

3.4. Conclusions

We have developed a discrete-continuous mathematical model of angiogenesis, in which the growth factor concentration is a continuous variable while the propagating tips of each growing sprout are treated as discrete objects. The model incorporates many realistic features of the process such as the growth factor release by tumor and by endothelial cells, the natural decay of the growth factor, repulsion factor release by endothelial cells, chemotactic motion of the tip cells with stochastic component, the dependence of cell speed on the growth factor concentration, growing tip branching and fusion with other tips, sprout death due to an insufficient concentration of the growth factor.

We studied the model numerically by working out an algorithm for the tip cell motion and vessel network construction. We chose parameter values given in Table 1 based on experimental data [53, 67, 99, 100, 194, 217] and produced numerical results which demonstrated the dynamics of growing vessels and formation of networks. We varied computational parameters, one at a time, and we were able to show that changes in our computational results induced by the change of a certain parameter completely agree with our understanding of the contribution of this parameter to the cell motion, vessel growth and vessel network formation.

CHAPTER 4

Conclusions

Angiogenesis is formation of new blood vessels from the preexisting vasculature and it happens naturally inside the body. It also occurs under many pathological processes such as rheumatoid arthritis, psoriasis, cerebral ischemia, cardiovascular disease, growth of solid tumors, soft tissue sarcomas, chronic liver disease and others. Angiogenesis plays a crucial role in so many human diseases that scientists believe that angiogenic therapy will completely change the way the diseases are ultimately treated. Understanding of the fundamental mechanisms that govern angiogenesis can provide us with a powerful therapeutic tool that will enable us to combat a variety of severe pathological conditions. Our ability to manipulate new blood vessel growth, stimulating or preventing it according to patient's needs can become a triumph of modern medicine, significantly lengthening the list of curable diseases.

Since the walls of all blood vessels are built of endothelial cells, it is a natural conclusion that EC migration plays a central role in the process of angiogenesis and one can control new vessel growth by influencing EC migration. In order to study such a complicated process as cell migration, in-vitro experiments are performed. Behavior of endothelial cells cultured on biogel that resembles ECM structure can mimic some of key stages of angiogenesis (such as association in tube-like structures and subsequent capillary network formation), thus providing a powerful experimental tool for studying the possibilities of affecting different stages of angiogenesis.

The goal of our work was to propose and study a mathematical model that governs EC dynamics in in-vitro experiments and exhibits pattern formation. Existing mathematical models of

tumor-induced angiogenesis fall into three major categories: continuum models, mechanochemical models and discrete, cell-based models. These models deal with various stages of angiogenesis, can be deterministic or stochastic, focusing on detailed biochemical pathways or overall phenomenological description of the main stages of angiogenesis. Some models deal with in-vivo angiogenesis, while other models describe the results of in-vitro experiments with endothelial cell cultures grown on Matrigel. All these works were indispensable as a starting point of our modeling efforts. However, our model differs from the existing models by the dependent variables we introduce, by our treatment of cell motility, and by certain problems that we pose.

The model that we have proposed in Chapter 2 is a reaction-diffusion model that can be used for a description of various manifestations of angiogenesis. We use it to describe EC pattern formation on a two-dimensional gel matrix.

As it follows from the brief description given in Chapter 1, there is a number of molecular mechanisms that appear to be crucial during the early stages of angiogenesis, and by means of interfering with which angiogenesis can in principle be blocked. Namely,

- (i) VEGF and other growth factor interactions with their cell-surface receptors that trigger multiple intracellular signal pathways, in particular promoting survival and proliferation of immature ECs;
- (ii) formation of focal adhesion complexes on the leading edge of the cell;
- (iii) release of proteases by ECs;
- (iv) localized degradation of extracellular matrix components by proteases, creation of specific attachment sites in the extracellular matrix;
- (v) anchorage dependence of cell growth, survival, division and migration mediated mainly by focal adhesions via intracellular signals they generate;

- (vi) EC directional crawling through the ECM in response to chemotactic gradient of VEGF.

Thus, our mathematical model governs the spatio-temporal behavior of the following quantities:

- c the concentration of endothelial cells,
- f the growth factor concentration,
- r the concentration of focal adhesion sites,
- p the protease concentration,
- m the concentration of ECM active sites available for cell adhesion.

We began with a derivation of the reinforced random walk equation that governs chemotactic/diffusional behavior of the ECs and after that we formulated mass balance equations for f, p, r and m that govern the corresponding chemical reaction scheme. Then we employed a steady-state assumption with respect to the state variables p, r, and m, reducing the system of equations to two coupled nonlinear PDEs for two unknowns - c and f.

We found uniform steady states of the system and investigated their linear stability. Then we focused on nonlinear stability analysis of one of the basic states. In particular, we studied the possibility of the appearance of stripes, squares and hexagons. We derived a system of amplitude equations and analyzed it. As a result we found parameter ranges in which stable hexagons, stripes and squares can exist in the system as well as coexist with one another. It should be noted that the experimentally observed patterns are not necessarily spatially regular, so that hexagons, squares and stripes, can be perceived as regular counterparts of the experimental observations. These patterns can result from Turing instabilities which were studied in Chapter 2. We anticipate that these regular patterns may in turn become unstable leading to irregular polygonal structures similar

to those observed in experiments. Our study of the Turing patterns is useful as it determines the parameter regime where the irregular structures can appear as a secondary bifurcation and can be sought numerically.

We also studied our system in absence of endothelial cell proliferation, the case that is of particular interest for experimentalists. In this case we also performed a linear stability analysis. Our weakly nonlinear analysis was based on the assumption of longwave solutions and resulted in the derivation of the Sivashinsky and Cahn-Hilliard equations.

We were able to numerically obtain stable hexagonal structures for parameter values predicted by the analytical investigation. To solve this problem numerically we used Crank-Nicolson method combined with operator splitting and alternation in application of splitting. This implicit method was applied only for the diffusion terms in both equations and the rest of the terms we treated explicitly. We performed simulations for parameter values where stable hexagon structures were expected and we were able to obtain stable hexagons in our simulations starting with initial data that represented a small deviation of the densities c and f from the steady states.

When the model without cell proliferation was analyzed numerically, we have used a pseudo-spectral code with periodic boundary conditions. A semi-implicit scheme has been used with a Crank-Nicolson method to handle the linear terms and an Adams-Bashforth method for the non-linear terms. The results are typical for Cahn-Hilliard dynamics we observed phase separation and coarsening.

In Chapter 3 we have developed a hybrid model, in which the growth factor concentration f remained continuous, but the cells were treated as discrete objects that could move, proliferate, die, talk to each other, etc. according to prescribed rules. The direction of tip propagation and other events of tip's motion such as its speed, the waiting time at the trajectory vertex, survival of the

tip depended on the local concentration of the growth factor and its gradient. Under appropriate conditions growing tip could fuse with another growing capillary or split thus producing two separately propagating tips. Interplay of all these events leaded to the formation of a capillary network. We studied the model numerically by working out an algorithm for the tip cell motion and vessel network development. We varied computational parameters, one at a time, and we were able to show that changes in our computational results induced by the change of a certain parameter completely agree with our understanding of the contribution of this parameter to the cell motion, vessel growth and vessel network formation. Our numerical results are reminiscent of those seen in the actual experiments.

In the present work we have developed two different modeling approaches in an attempt to elucidate the key features of the complicated process of angiogenesis. The first, continuous model allows us explore the logic of pattern formation during in-vitro experiments with endothelial cells. The second model has to do with in-vivo angiogenesis and employs discrete-continuous formulation. There is a long way to being able to reliably simulate actual experimental scenarios, which are not necessarily well understood and cannot be easily reproduced. However, we are sure that exploring the logic of biological processes is worthwhile even at our present state of knowledge. It allows one to take a hypothetical mechanism and examine its consequences in the form of a mathematical model, making predictions and suggesting experiments that would verify or invalidate the model. We believe that collaboration between experimentalists and applied mathematicians will lead towards a better understanding of the biological processes involved in angiogenesis and a vast array of medical problems where angiogenesis is important.

References

[1] A. ABRAMSSON, P. LINDBLOM, AND C. BETSHOLTZ, *Endothelial and nonendothelial sources of pdgf-b regulate pericyte recruitment and influence vascular pattern formation in tumors*, J. Clin. Invest., 112 (2003), pp. 1142–1151.

[2] T. ACKER AND K. H. PLATE, *Role of hypoxia in tumor angiogenesis - molecular and cellular angiogenic crosstalk*, Cell Tissue Res., 314 (2003), pp. 145–155.

[3] L. AIELLO, E. PIERCE, E. FOLEY, H. TAKAGI, H. CHEN, L. RIDDLE, N. FERRARA, G. KING, AND L. SMITH, *Suppression of retinal neovascularization in vivo by inhibition of vascular endothelial growth factor (vegf) using soluble vegf-receptor chimeric proteins*, Proc. Natl. Acad. Sci. U S A, 92 (1995), pp. 10457–61.

[4] B. ALBERTS, D. BRAY, J. LEWIS, M. RAFF, K. ROBERTS, AND J. WATSON, *Molecular biology of the cell*, Garland Science, New York, 4 ed., 2002.

[5] A. R. A. ANDERSON AND M. A. J. CHAPLAIN, *Continuous and discrete mathematical models of tumor-induced angiogenesis*, Bull. Math. Biol, 60 (1998), pp. 857–899.

[6] ——, *A mathematical model for capillary network formation in the absence of endothelial cell proliferation*, Appl. Math. Lett., 11 (1998), pp. 109–114.

[7] A. R. A. ANDERSON, M. A. J. CHAPLAIN, C. GARCIA-REIMBERT, AND C. A. VARGAS, *A gradient-driven mathematical model of antiangiogenesis*, Math. Comput. Model., 32 (2000), pp. 1141–1152.

[8] L. ARAKELYAN, Y. MERBL, AND Z. AGUR, *Vessel maturation effects on tumour growth: Validation of a computer model in implanted human ovarian carcinoma spheroids*, Eur. J. Cancer, 41 (2005), pp. 159–167.

[9] T. ASAHARA, D. CHEN, T. TAKAHASHI, K. FUJIKAWA, M. KEARNEY, M. MAGNER, AND G. YANCOPOULOS, *Tie2 receptor ligands, angiopoietin-1 and angiopoietin-2, modulate vegf-induced postnatal neovascularization.*, Circ. Res., 83 (1998), pp. 233–240.

[10] R. AUERBACH, R. LEWIS, B. SHINNERS, L. KUBAI, AND N. AKHTAR, *Angiogenrsis assays: a critical overview.*, Clin. Chem., 49 (2003), pp. 32–40.

[11] H. AUGUSTIN, *Translating angiogenesis research into the clinic: the challenges ahead.*, Br J Radiol, 76 (2003), p. S3.

[12] D. AUSPRUNK AND J. FOLKMAN, *Migration and proliferation of endothelial cells in preformed and newly formed blood vessels during tumor angiogenesis.*, Microvasc Res., 14 (1977), pp. 53–65.

[13] H. K. AVRAHAM, T. H. LEE, Y. H. KOH, T. A. KIM, S. X. JIANG, M. SUSSMAN, A. M. SAMAREL, AND S. AVRAHAM, *Vascular endothelial growth factor regulates focal adhesion assembly in human brain microvascular endothelial cells through activation of the focal adhesion kinase and related adhesion focal tyrosine kinase*, J. Biol. Chem., 278 (2003), pp. 36661–36668.

[14] S. BAIGUERA, M. CONCONI, D. GUIDOLIN, G. MAZZOCCHI, L. MALENDOWICZ, P. PARNIGOTTO, R. SPINAZZI, AND G. NUSSDORFER, *Ghrelin inhibits in vitro angiogenic activity of rat brain microvascular endothelial cells.*, Int. J. Mol. Med., 14 (2004), pp. 849–54.

[15] M. BAILLY AND J. CONDEELIS, *Cell motility: Insights from the backstage*, Nat. Cell Biol., 4 (2002), pp. E292–E294.

[16] M. BARIAGA, *Shedding light on blindness*, Science, 267 (1995), pp. 452–453.

[17] D. R. BEIL AND L. M. WEIN, *Analysis and comparison of multimodal cancer treatments*, IMA J. Math. Appl. Med. Biol., 18 (2001), pp. 343–376.

[18] L. BENJAMIN, D. GOLIJANIN, A. ITIN, D. PODE, AND E. KESHET, *Selective ablation of immature blood vessels in established human tumors follows vascular endothelial growth factor withdrawal.*, J. Clin. Invest., 103 (1999), pp. 159–165.

[19] A. BERNOFF AND A. BERTOZZI, *Singularities in a modified Kuramoto-Sivashinsky equation describing interface motion for phase transition*, Physica D, 85 (1995), pp. 375–404.

[20] W. BIRKENHAGER AND J. STAESSEN, *Is angigenesis a plausible hypothesis in Alzheimer's disease?*, J. Hypertens., 21 (2003), pp. 1426–7.

[21] G. BREIER, *Endothelial receptor tyrosine kinases involved in blood vessel development and tumor angiogenesis.*, Adv. Exp. Med. Biol., 476 (2000), pp. 57–66.

[22] ——, *Functions of the VEGF/VEGF receptor system in the vascular system.*, Semin. Thromb. Hemost., 26 (2000), pp. 553–9.

[23] R. A. BREKKEN, C. G. LI, AND S. KUMAR, *Strategies for vascular targeting in tumors*, Int. J. Cancer, 100 (2002), pp. 123–130.

[24] P. BROOKS, R. CLARK, AND D. CHERESH, *Requirement of vascular integrin $\alpha 5 \beta 3$ for angiogenesis.*, Science, 264 (1994), pp. 569–571.

[25] P. BROOKS, A. MONTGOMERY, M. ROSENFELD, T. HU, G. KLIER, AND D. CHERESH, *Integrin $\alpha 5\beta 3$ antagonists promote tumor regression by inducing apoptosis of angiogenic blood vessels.*, Cell, 79 (1994), pp. 1157–1164.

[26] T. BROWDER, J. FOLKMAN, P. HAHNFELDT, J. HEYMACH, L. HLATKY, M. KIERAN, AND M. S. ROGERS, *Antiangiogenic therapy and p53*, Science, 297 (2002), pp. U1–U2.

[27] L. BROWN, M. D. M, K. CLAFFEY, J. NAGY, D. FENG, A. DVORAK, AND H. DVORAK, *Vascular permeability factor/vascular endothelial growth factor: a multifunctional angiogenic cytokine*, EXS., 79 (1997), pp. 233–269.

[28] K. BURRIDGE AND M. CHRZANOWSKA-WODNICKA, *Focal adhesions, contractility, and signaling.*, Ann. Rev. Cell Dev. Biol., 12 (1996), pp. 463–518.

[29] H. M. BYRNE AND M. A. J. CHAPLAIN, *Explicit solutions of a simplified model of capillary sprout growth during tumor angiogenesis*, Appl. Math. Lett., 8 (1995), pp. 71–76.

[30] ——, *Growth of nonnecrotic tumors in the presence and absence of inhibitors*, Math. Biosci., 130 (1995), pp. 151–181.

[31] ——, *Mathematical-models for tumor angiogenesis - numerical simulations and nonlinear-wave solutions*, Bull. Math. Biol, 57 (1995), pp. 461–486.

[32] ——, *Explicit solutions of a simplified model of capillary sprout growth during tumor angiogenesis*, Appl. Math. Lett., 9 (1996), pp. 69–74.

[33] T. BYZOVA, C. GOLDMAN, N. PAMPORI, K. THOMAS, A. BETT, S. SHATTIL, AND E. PLOW, *A mechanism for modulation of cellular responses to VEGF: activation of the integrins*, Mol. Cell, 6 (2000), pp. 851–860.

[34] J. CAHN AND J. HILLIARD, *Free energy of a nonuniform system. 1. Interfacial free energy*, J. Chem. Phys., 28 (1958), pp. 258–267.

[35] P. CARMELIET, *Manipulating angiogenesis in medicine*, J. Internal Med., 255 (2004), pp. 538–561.

[36] ——, *VEGF as a key mediator of angiogenesis in cancer*, Oncology, 69 Suppl 3 (2005), pp. 11–16.

[37] M. A. J. CHAPLAIN, *The mathematical modelling of tumour angiogenesis and invasion*, Acta Biotheor., 43 (1995), pp. 387–402.

[38] ——, *Avascular growth, angiogenesis and vascular growth in solid tumours: the mathematical modelling of the stages of tumour development*, Math. Comput. Model., 23 (1996), pp. 47–87.

[39] ——, *Mathematical modelling of angiogenesis*, J. Neuro-Oncol., 50 (2000), pp. 37–51.

[40] M. A. J. CHAPLAIN AND A. R. A. ANDERSON, *Mathematical modelling, simulation and prediction of tumour-induced angiogenesis*, Invasion Metastasis, 16 (1996), pp. 222–234.

[41] M. A. J. CHAPLAIN AND H. M. BYRNE, *Mathematical modeling of wound healing and tumor growth: Two sides of the same coin*, Wounds-Compend. Clin. Res. Pract., 8 (1996), pp. 42–48.

[42] M. A. J. CHAPLAIN, S. M. GILES, B. D. SLEEMAN, AND R. J. JARVIS, *A mathematical analysis of a model for tumor angiogenesis*, J. Math. Biol., 33 (1995), pp. 744–770.

[43] M. A. J. CHAPLAIN AND B. D. SLEEMAN, *A mathematical model for the production and secretion of tumor angiogenesis factor in tumors*, IMA J. Math. Appl. Med. Biol., 7 (1990), p. 93.

[44] M. A. J. CHAPLAIN AND A. M. STUART, *A mathematical model for the diffusion of tumor angiogenesis factor into the surrounding host tissue*, IMA J. Math. Appl. Med. Biol., 8 (1991), pp. 191–220.

[45] ——, *A model mechanism for the chemotactic response of endothelial-cells to tumor angiogenesis factor*, IMA J. Math. Appl. Med. Biol., 10 (1993), pp. 149–168.

[46] E. CHAVAKIS AND S. DIMMELER, *Regulation of endothelial cell survival and apoptosis during angiogenesis*, Arterioscl. Thromb. Vasc. Bio., 22 (2002), pp. 887–893.

[47] G. CHRISTOFORI, *The role of fibroblast growth factors in tumor progression and angiogenesis.*, in Tumor Angiogenesis, R. Bicknell, C. Lewis, and N. Ferrara, eds., Oxford University Press., 1996.

[48] G. CHRISTOFORI, P. NAIK, AND D. HANAHAN, *Vascular endothelial growth factor and its receptors, flt-1 and flk-1, are expressed in normal pancreatic islets and throughout islet cell tumorigenesis.*, Mol. Endocrinol., 9 (1995), pp. 1760–70.

[49] E. CLARK AND J. BRUGGE, *Integrins and signal transduction pathways: the road taken.*, Science., 268 (1995), pp. 233–9.

[50] D. CREAMER, D. SULLIVAN, R. BICKNELL, AND J. BARKER, *Angiogenesis in psoriasis*, Angiogenesis, 5 (2002), pp. 231–236.

[51] G. DAVIS AND C. CAMARILLO, *An $\alpha 2\beta 1$ integrin-dependent pinocytic mechanism involving intracellular vacuole formation and coalescence regulates capillary lumen and tube formation in three-dimensional collagen matrix.*, Exp. Cell Res., 224 (1996), pp. 39–51.

[52] Z. N. DEMOU AND L. V. MCINTIRE, *Fully automated three-dimensional tracking of cancer cells in collagen gels: Determination of motility phenotypes at the cellular level*, Cancer Res., 62 (2002), pp. 5301–5307.

[53] S. DI TALIA, A. GAMBA, F. LAMBERTI, AND G. SERINI, *Role of repulsive factors in vascularization dynamics*, Phys. Rev. E, 73 (2006), pp. 481–490.

[54] R. P. M. DINGS, D. W. J. VAN DER SCHAFT, B. HARGITTAI, J. HASEMAN, A. W. GRIFFIOEN, AND K. H. MAYO, *Anti-tumor activity of the novel angiogenesis inhibitor anginex*, Cancer Lett., 194 (2003), pp. 55–66.

[55] S. G. ECKHARDT, *Angiogenesis inhibitors as cancer therapy*, Hosp. Pract., 34 (1999), p. 63.

[56] N. FERRARA, H. GERBER, AND J. LECOUTER, *The biology of VEGF and its receptors*, Nat. Med., 9 (2003), pp. 669–676.

[57] N. FERRARA AND B. KEYT, *Vascular endothelial growth factor: basic biology and clinical implications*, EXS., 79 (1997), pp. 209–32.

[58] I. FERRENQ, L. TRANQUI, B. VAILHE, P. GUMERY, AND P. TRACQUI, *Modelling biological gel contraction by cells: mechanocellular formulation and cell traction force quantification*, Acta Biotheoretica, 45 (1997), pp. 267–293.

[59] J. FOLKMAN, *Tumor angiogenesis: therapeutic implications*, New Engl. J. Med., 285 (1971), pp. 1182–1186.

[60] ——, *Tumor angiogenesis*, in Cancer medicine, B.C.Decker, Ontario, Canada, 2000, pp. 132–152.

[61] ——, *Angiogenesis and apoptosis*, Seminars Cancer Bio., 13 (2003), pp. 159–167.

[62] ——, *Angiogenesis inhibitors - a new class of drugs*, Cancer Biol. Therapy, 2 (2003), pp. S127–S133.

[63] J. FOLKMAN, P. HAHNFELDT, AND L. HLATKY, *Cancer: Looking outside the genome*, Nat. Rev. Mol. Cell Biol., 1 (2000), pp. 76–79.

[64] J. FOLKMAN AND C. HAUDENSCHILD, *Angiogenesis in vitro.*, Nature, 288 (1980), pp. 551–556.

[65] J. FOLKMAN, E. MERLER, C. ABERNATHY, AND G. WILLIAMS, *Isolation of a tumor factor responsible for angiogenesis*, J. Exper. Med., 133 (1971), pp. 275–288.

[66] M. A. FONTELOS, A. FRIEDMAN, AND B. HU, *Mathematical analysis of a model for the initiation of angiogenesis*, SIAM J. Math. Anal., 33 (2002), pp. 1330–1355.

[67] R. FORD AND D. A. LAUFFENBURGER, *Measurement of bacterial random motility and chemotaxis coefficients. 2. Application of single-cell-based mathematical-model*, Biotechnology and Bioengineering, 37 (1991), pp. 661–672.

[68] P. FRIEDL, *Dynamic imaging of cellular interactions with extracellular matrix*, Histochemistry Cell Bio., 122 (2004), pp. 183–190.

[69] T. FUJIWARA AND Y. UEHARA, *The cytoarchitecture of the wall and the innervation pattern of the microvessels in the rat mammary-gland - a scanning electron-microscopic observation*, Amer. J. Anatomy, 170 (1984), pp. 39–54.

[70] S. FUKUDA, S. YOSHII, S. KAGA, M. MATSUMOTO, K. KUGIYAMA, AND N. MAULIK, *Therapeutic angiogenesis for severe ischemic heart diseases by autologous bone marrow cells transplantation*, Mol. Cell. Biochem., 264 (2004), pp. 143–149.

[71] T. FUNADA, *Nonlinear surface-waves driven by the Marangoni instability in a heat-transfer system*, J. Phys. Soc. Jpn., 56 (1987), pp. 2031–2038.

[72] B. G. GALVEZ, S. MATIAS-ROMAN, J. P. ALBAR, F. SANCHEZ-MADRID, AND A. G. ARROYO, *Membrane type 1-matrix metalloproteinase is activated during migration of human endothelial cells and modulates endothelial motility and matrix remodeling*, J. Biol. Chem., 276 (2001), pp. 37491–37500.

[73] A. GAMBA, D. AMBROSI, A. CONIGLIO, A. DE CANDIA, S. DI TALIA, E. GIRAUDO, G. SERINI, L. PREZIOSI, AND F. BUSSOLINO, *Percolation, morphogenesis, and Burgers dynamics in blood vessels formation*, Phys. Rev. Lett., 90 (2003), p. 118101.

[74] D. GAMMACK, H. M. BYRNE, AND C. E. LEWIS, *Estimating the selective advantage of mutant p53 tumour cells to repeated rounds of hypoxia*, Bull. Math. Biol, 63 (2001), pp. 135–166.

[75] H. P. GERBER, *Anti-angiogenesis: Biology is the foundation for therapy*, Drug Discovery Today, 8 (2003), pp. 344–346.

[76] H. GERHARDT, M. GOLDING, M. FRUTTIGER, C. RUHRBERG, A. LUNDKVIST, A. ABRAMSSON, M. JELTSCH, C. MITCHELL, K. ALITALO, D. SHIMA, AND C. BETSHOLTZ, *VEGF guides angiogenic sprouting utilizing endothelial tip cell filopodia*, J. Cell Bio., 161 (2003), pp. 1163–1177.

[77] P. K. GHOSH, A. VASANJI, G. MURUGESAN, S. J. EPPELL, L. M. GRAHAM, AND P. L. FOX, *Membrane microviscosity regulates endothelial cell motility*, Nat. Cell Biol., 4 (2002), pp. 894–900.

[78] R. GODDE AND H. KURZ, *Structural and biophysical simulation of angiogenesis and vascular remodeling*, Dev. Dyn., 220 (2001), pp. 387–401.

[79] A. GOLOVIN, A. NEPOMNYASHCHY, AND L. PISMEN, *Nonpotential effects in nonlinear dynamics of Marangoni convection.*, Int. J. Bifurcation. Chaos, 12 (2002), pp. 2487–2500.

[80] M. GRACHEVA AND H. OTHMER, *A continuum model of motility in ameboid cells*, Bull. Math. Biol., 66 (2004), pp. 167–193.

[81] A. GRIFFIOEN AND J. MOLEMA, *Angiogenesis: Potentials for pharmacologic intervention in the treatment of cancer, cardiovascular diseases, and chronic inflammation*, Pharm. Revs., 52 (2000), pp. 237–268.

[82] H. P. GRIMM, A. B. VERKHOVSKY, A. MOGILNER, AND J. J. MEISTER, *Analysis of actin dynamics at the leading edge of crawling cells: Implications for the shape of keratocyte lamellipodia*, Eur. Biophys. J., 32 (2003), pp. 563–577.

[83] W. J. G. HACKING, E. VANBAVEL, AND J. A. E. SPAAN, *Shear stress is not sufficient to control growth of vascular networks: a model study*, Am. J. Physiol.-Heart Circul. Physiol., 39 (1996), pp. H364–H375.

[84] P. HAHNFELDT, J. FOLKMAN, AND L. HLATKY, *Minimizing long-term tumor burden: the logic for metronomic chemotherapeutic dosing and its antiangiogenic basis*, J. Theor. Biol., 220 (2003), pp. 545–554.

[85] P. HAHNFELDT, D. PANIGRAHY, J. FOLKMAN, AND L. HLATKY, *Tumor development under angiogenic signaling: a dynamical theory of tumor growth, treatment response, and postvascular dormancy*, Cancer Res., 59 (1999), pp. 4770–4775.

[86] R. HATTORI AND H. MATSUBARA, *Therapeutic angiogenesis for severe ischemic heart diseases by autologous bone marrow cells transplantation*, Mol. Cell Biochem., 264 (2004), pp. 151–155.

[87] A. HELISCH AND J. WARE, *Therapeutic angiogenesis for ischemic heart disease.*, Adv. Exp. Med. Biol., 476 (2002), pp. 327–350.

[88] R. S. HERBST, M. HIDALGO, A. S. PIERSON, S. N. HOLDEN, M. BERGEN, AND S. G. ECKHARDT, *Angiogenesis inhibitors in clinical development for lung cancer*, Seminars Onco., 29 (2002), pp. 66–77.

[89] K. H. HERRMANN, S. V. M. SATYANARAYANA, V. SRIDHAR, AND K. P. N. MURTHY, *Monte Carlo simulation of actin filament based cell motility*, Int. J. Mod. Phys. B, 17 (2003), pp. 5597–5611.

[90] K. HIRSCHI AND P. D'AMORE, *Pericytes in the microvasculature.*, Cardiovasc. Res., 32 (1996), pp. 687–698.

[91] L. HLATKY, P. HAHNFELDT, AND J. FOLKMAN, *Clinical application of antiangiogenic therapy: Microvessel density, what it does and doesn't tell us*, J. Natl. Cancer Inst., 94 (2002), pp. 883–893.

[92] K. HOEKMAN AND H. PINEDO, *Angiogenesis: a potential target for therapy of soft tissue sarcomas*, Cancer Treat Res, 120 (2004), pp. 169–80.

[93] J. HOLASH, S. DAVIS, N. PAPADOPOULOS, S. D. CROLL, L. HO, M. RUSSELL, P. BOLAND, R. LEIDICH, D. HYLTON, E. BUROVA, E. IOFFE, T. HUANG, C. RADZIEJEWSKI, K. BAILEY, J. P. FANDL, T. DALY, S. J. WIEGAND, G. D. YANCOPOULOS, AND J. S. RUDGE, *VEGF-Trap: a VEGF blocker with potent antitumor effects*, PNAS, 99 (2002), pp. 11393–11398.

[94] M. J. HOLMES AND B. D. SLEEMAN, *A mathematical model of tumour angiogenesis incorporating cellular traction and viscoelastic effects*, J. Theor. Biol., 202 (2000), p. 95.

[95] A. HUTTENLOCHER, S. PALECEK, M. GINSBERG, D. LAUFFENBURGER, AND R. HORWITZ, *Regulation of integrin-mediated adhesive release during cell migration*, Mol. Biol. Cell, 9 (1998), p. 33A.

[96] T. INAI, M. MANCUSO, H. HASHIZUME, F. BAFFERT, A. HASKELL, P. BALUK, D. D. HU-LOWE, D. R. SHALINSKY, G. THURSTON, G. D. YANCOPOULOS, AND D. M. MCDONALD, *Inhibition of vascular endothelial growth factor (VEGF) signaling in cancer causes loss of endothelial fenestrations, regression of tumor vessels, and appearance of basement membrane ghosts*, Amer. J. Pathology, 165 (2004), pp. 35–52.

[97] D. E. INGBER, *Mechanosensation through integrins: Cells act locally but think globally*, PNAS, 100 (2003), pp. 1472–1474.

[98] D. J. IRVINE, K. A. HUE, A. M. MAYES, AND L. G. GRIFFITH, *Simulations of cell-surface integrin binding to nanoscale-clustered adhesion ligands*, Biophys. J., 82 (2002), pp. 120–132.

[99] E. JABBARZADEH AND C. F. ABRAMS, *Chemotaxis and random motility in unsteady chemoattractant fields: a computational study*, J. Theor. Biol, 235 (2005), pp. 221–232.

[100] ——, *Simulations of chemotaxis and random motility in 2d random porous domains*, Bull. Math. Biol, 69 (2007), pp. 747–764.

[101] R. JAIN, L. MUNN, AND D. FUKUMURA, *Dissecting tumor patho-physiology using intravital microscopy*, Nat. Rev. Cancer, 2 (2002), pp. 266–76.

[102] R. JAIN, K. SCHLENGER, M. HOCKEL, AND F. YUAN, *Quantitative angiogenesis assays: progress and problems*, Nat. Med., 3 (1997), pp. 1203–8.

[103] R. KALLURI, *Basement membranes: Structure, assembly and role in tumour angiogenesis*, Nat. Rev. Cancer, 3 (2003), pp. 422–433.

[104] J. A. KANG, J. T. KIM, H. S. SONG, M. K. BAE, E. Y. YI, K. W. KIM, AND Y. J. KIM, *Anti-angiogenic and anti-tumor invasive activities of tissue inhibitor of metalloproteinase-3 from shark, scyliorhinus torazame*, Biochim. Biophys. Acta, 1620 (2003), pp. 59–64.

[105] B. Z. KATZ, E. ZAMIR, A. BERSHADSKY, Z. KAM, K. M. YAMADA, AND B. GEIGER, *Physical state of the extracellular matrix regulates the structure and molecular composition of cell-matrix adhesions*, Mol. Biol. Cell, 11 (2000), pp. 1047–1060.

[106] P. G. KEVREKIDIS, N. WHITAKER, D. J. GOOD, AND G. J. HERRING, *Minimal model for tumor angiogenesis*, Phys. Rev. E, 73 (2006), pp. 10889–10894.

[107] K. KIM, B. LI, J. WINER, M. ARMANINI, N. GILLETT, H. PHILLIPS, AND N. FERRARA, *Inhibition of vascular endothelial growth factor-induced angiogenesis suppresses tumour growth in vivo.*, Nature, 362 (1993), pp. 841–844.

[108] W. KIOSSES, S. SHATTIL, N. PAMPORI, AND M. SCHWARTZ, *Rac recruits high-affinity integrin $\alpha v \beta 3$ to lamellipodia in endothelial cell migration.*, Nat. Cell Biol., 3 (2001), pp. 316–320.

[109] C. KIRKPATRICK, V. KRUMP-KONVALINKOVA, R. UNGER, F. BITTINGER, M. OTTO, AND K. PETERS, *Tissue response and biomaterial integration: the efficacy of in vitro methods.*, Biomol. Eng., 19 (2002), pp. 211–217.

[110] C. KIRKPATRICK, M. OTTO, T. KOOTEN, V. KRUMP, J. KRIEGSMANN, AND F. BITTINGER, *Endothelial cell cutures as a tool in biomaterial research*, J. Mater. Sci. Mater. Med., 10 (1999), pp. 589–594.

[111] C. KIRKPATRICK, R. UNGER, V. KRUMP-KONVALINKOVA, K. PETERS, H. SCHMIDT, AND G. KAMP, *Experimental approaches to study vascularization in tissue engineerin and biomaterial applications*, J. Mater. Sci. Mater. Med., 14 (2003), pp. 677–681.

[112] T. KITAHARA, K. HIROMURA, H. IKEUCHI, S. YAMASHITA, S. KOBAYASHI, T. KUROIWA, Y. KANEKO, K. UEKI, AND Y. NOJIMA, *Mesangial cells stimulate differentiation of endothelial cells to form capillary-like networks in a three-dimensional culture system.*, Nephrol. Dial. Transplant., 20 (2005), pp. 42–9.

[113] D. KNIGHTON, I. SILVER, AND T. HUNT, *Regulation of wound-healing angiogenesis-effect of oxygen gradients and inspired oxygen concentration.*, Surgery, 90 (1981), pp. 262–270.

[114] T. KOBLIZEK, C. WEISS, G. YANCOPOULOS, U. DEUTSCH, AND W. RISAU, *Angiopoietin-1 induces sprouting angiogenesis in vitro.*, Curr. Biol., 8 (1998), pp. 529–532.

[115] P. KOOLWIJK, R. HANEMAAIJER, AND V. V. HINSBERGH, *Proteases and angiogenesis: Regulation of plasminogen activators and matrix metalloproteases by endothelial cells.*, NATO ASI series. Series A, Life sciences, 298 (1998).

[116] S. KOUVROUKOGLOU, K. C. DEE, R. BIZIOS, L. V. MCINTIRE, AND K. ZYGOURAKIS, *Endothelial cell migration on surfaces modified with immobilized adhesive peptides*, Biomater., 21 (2000), pp. 1725–1733.

[117] K. A. LANDMAN, G. J. PETTET, AND D. F. NEWGREEN, *Chemotactic cellular migration: Smooth and discontinuous travelling wave solutions*, SIAM J. Appl. Math., 63 (2003), pp. 1666–1681.

[118] ——, *Mathematical models of cell colonization of uniformly growing domains*, Bull. Math. Biol, 65 (2003), pp. 235–262.

[119] D. A. LAUFFENBURGER AND A. F. HORWITZ, *Cell migration: a physically integrated molecular process*, Cell, 84 (1996), pp. 359–369.

[120] T. LEONG, U. FEARON, AND D. VEALE, *Angiogenesis in psoriasis and psoriatic arthritis: clues to disease pathogenesis.*, Curr. Rheumatol. Rep., 7 (2005), pp. 325–329.

[121] H. A. LEVINE, S. PAMUK, B. D. SLEEMAN, AND M. NILSEN-HAMILTON, *Mathematical modeling of capillary formation and development in tumor angiogenesis: Penetration into the stroma*, Bull. Math. Biol, 63 (2001), pp. 801–863.

[122] ——, *Mathematical modeling of capillary formation and development in tumor angiogenesis: Penetration into the stroma. (vol 63, pg 801, 2001)*, Bull. Math. Biol, 64 (2002), p. 423.

[123] H. A. LEVINE, B. D. SLEEMAN, AND M. NILSEN-HAMILTON, *A mathematical model for the roles of pericytes and macrophages in the initiation of angiogenesis. I. the role of protease inhibitors in preventing angiogenesis*, Math. Biosci., 168 (2000), p. 77.

[124] ——, *Mathematical modeling of the onset of capillary formation initiating angiogenesis*, J. Math. Biol., 42 (2001), pp. 195–238.

[125] H. A. LEVINE, A. TUCKER, AND M. NILSEN-HAMILTON, *A mathematical model for the role of cell signal transduction in the initiation and inhibition of angiogenesis*, Growth Factors, 20 (2002), pp. 155–175.

[126] W. LIU AND ET AL., *Endothelial cell survival and apoptosis in the tumor vasculature.*, Apoptosis, 5 (2000), pp. 323–8.

[127] D. LU, X. JIMENEZ, H. F. ZHANG, Y. WU, P. BOHLEN, L. WITTE, AND Z. P. ZHU, *Complete inhibition of vascular endothelial growth factor (vegf) activities with a bifunctional diabody directed against both vegf kinase receptors, fms-like tyrosine kinase receptor and kinase insert domain-containing receptor*, Cancer Res., 61 (2001), pp. 7002–7008.

[128] S. A. MAGGELAKIS, *The effects of tumor angiogenesis factor (taf) and tumor inhibitor factors (tifs) on tumor vascularization: a mathematical model*, Math. Comput. Model., 23 (1996), pp. 121–133.

[129] ——, *A mathematical model of tissue replacement during epidermal wound healing*, Appl. Math. Model., 27 (2003), pp. 189–196.

[130] S. A. MAGGELAKIS AND A. E. SAVAKIS, *A mathematical model of growth factor induced capillary growth in the retina*, Math. Comput. Model., 24 (1996), pp. 33–41.

[131] ——, *A mathematical model of retinal neovascularization*, Math. Comput. Model., 29 (1999), pp. 91–97.

[132] G. MAHESHWARI AND D. A. LAUFFENBURGER, *Deconstructing (and reconstructing) cell migration*, Microscopy Res. Tech., 43 (1998), pp. 358–368.

[133] P. K. MAINI, L. OLSEN, AND J. A. SHERRATT, *Mathematical models for cell-matrix interactions during dermal wound healing*, Int. J. Bifurcation Chaos, 12 (2002), pp. 2021–2029.

[134] A. MALLAVARAPU AND T. J. MITCHISON, *Actin dynamics in filopodia*, Mol. Biol. Cell, 7 (1996), p. 3255.

[135] I. V. MALY AND G. G. BORISY, *Self-organization of a propulsive actin network as an evolutionary process*, PNAS, 98 (2001), pp. 11324–11329.

[136] D. MANOUSSAKI, *A mechanochemical model of angiogenesis and vasculogenesis*, ESAIM-mathematical modeling and numerical analysis-Modelisation mathematique et analyse numerique, 37 (2003), pp. 581–599.

[137] D. MANOUSSAKI, S. LUBKIN, R. VERNON, AND J. MURRAY, *A mechanical model of vascular network in vitro*, Acta Biotheoretica, 44 (1996), pp. 271–282.

[138] N. MANTZARIS, S. WEBB, AND H. OTHMER, *Mathematical modeling of tumor-induced angiogenesis.*, J Math Biol., 49 (2004), pp. 111–187.

[139] K. H. MARTIN, J. K. SLACK, S. A. BOERNER, C. C. MARTIN, AND J. T. PARSONS, *Integrin connections map: To infinity and beyond*, Science, 296 (2002), pp. 1652–1653.

[140] B. MAST, *The skin*, in Wound healing: Biochemical and Clinical Aspects, Saunders, Philadelphia, 1992, pp. 344–355.

[141] J. MEDINA, A. G. ARROYO, F. SANCHEZ-MADRID, AND R. MORENO-OTERO, *Angiogenesis in chronic inflammatory liver disease*, Hepatology, 39 (2004), pp. 1185–1195.

[142] R. M. H. MERKS, S. A. NEWMAN, AND J. A. GLAZIER, *Cell-oriented modeling of in vitro capillary development*, Cell. Automata, 3305 (2004), pp. 425–434.

[143] T. J. MITCHISON AND L. P. CRAMER, *Actin-based cell motility and cell locomotion*, Cell, 84 (1996), pp. 371–379.

[144] A. MOGILNER AND L. EDELSTEIN-KESHET, *Regulation of actin dynamics in rapidly moving cells: a quantitative analysis*, Biophys. J., 83 (2002), pp. 1237–1258.

[145] A. MOGILNER AND G. OSTER, *Polymer motors: Pushing out the front and pulling up the back*, Curr. Bio., 13 (2003), pp. R721–R733.

[146] D. MUKHERJEE, *Current clinical perspectives on myocardial angiogenesis*, Mol. Cell Biochem., 264 (2004), pp. 157–67.

[147] R. MUNOZ-CHAPULI, A. R. QUESADA, AND M. A. MEDINA, *Angiogenesis and signal transduction in endothelial cells*, Cell. Mol. Life Sci., 61 (2004), pp. 2224–2243.

[148] J. MURRAY, D. MANOUSSAKI, S. LUBKIN, AND R. VERNON, *A mechanical theory of in vitro vascular network formation*, in Vascular Morphogenesis: In vivo, In Vitro and In Mente, C. Little, V. Mironov, and E. Sage, eds., Birkhauser, Boston, 1998, pp. 173–188.

[149] J. D. MURRAY, *Pattern formation in integrative biology – a marriage of theory and experiment*, Comptes Rendus Acad. Sci. Ser. III-Sci. Vie-Life Sci., 323 (2000), p. 5.

[150] ——, *On the mechanochemical theory of biological pattern formation with application to vasculogenesis*, Comptes Rendus Biologies, 326 (2003), pp. 239–252.

[151] P. NAMI, J. OHAYON, AND P. TRACQUI, *Critical conditions for pattern formation and in vitro tubulogenesis driven by cellular traction fields*, J. Theor. Biol., 227 (2004), pp. 103–120.

[152] A. NEPOMNYASHCHY, *Order parameter equations for long-wavelength instabilities*, Physica D, 86 (1995), pp. 90–95.

[153] Y. NG AND P. D'AMORE, *Therapeutic angiogenesis for cardiovascular disease*, Curr. Control Trials Cardiovasc. Med., 2 (2001), pp. 278–285.

[154] M. NOVATCHKOVA AND F. EISENHABER, *Can molecular mechanisms of biological processes be extracted from expression profiles? Case study: Endothelial contribution to tumor-induced angiogenesis*, Bioessays, 23 (2001), pp. 1159–1175.

[155] L. OLSEN, J. A. SHERRATT, P. K. MAINI, AND F. ARNOLD, *A mathematical model for the capillary endothelial cell-extracellular matrix interactions in wound-healing angiogenesis*, IMA J. Math. Appl. Med. Biol., 14 (1997), pp. 261–281.

[156] M. E. ORME AND M. A. J. CHAPLAIN, *A mathematical model of the first steps of tumour-related angiogenesis: Capillary sprout formation and secondary branching*, IMA J. Math. Appl. Med. Biol., 13 (1996), pp. 73–98.

[157] ——, *Two-dimensional models of tumour angiogenesis and anti-angiogenesis strategies*, IMA J. Math. Appl. Med. Biol., 14 (1997), pp. 189–205.

[158] A. ORON, S. DAVIS, AND S. BANKOFF, *Long-scale evolution of thin liquid films*, Rev. Mod. Phys., 69 (1997), pp. 931–980.

[159] H. G. OTHMER AND A. STEVENS, *Aggregation, blowup, and collapse: the abc's of taxis in reinforced random walks*, SIAM J. Appl. Math., 57 (1997), pp. 1044–1081.

[160] S. P. PALECEK, C. E. SCHMIDT, D. A. LAUFFENBURGER, AND A. F. HORWITZ, *Integrin dynamics on the tail region of migrating fibroblasts*, J. Cell Sci., 109 (1996), pp. 941–952.

[161] E. PALSSON, *A three-dimensional model of cell movement in multicellular systems*, Future Gener. Comp. Syst., 17 (2001), pp. 835–852.

[162] S. PAMUK, *Qualitative analysis of a mathematical model for capillary formation in tumor angiogenesis*, Math. Models Meth. Appl. Sci., 13 (2003), pp. 19–33.

[163] A. J. PERUMPANANI, J. A. SHERRATT, J. NORBURY, AND H. M. BYRNE, *Biological inferences from a mathematical model for malignant invasion*, Invasion Metastasis, 16 (1996), pp. 209–221.

[164] G. PETTET, M. A. J. CHAPLAIN, D. L. S. MCELWAIN, AND H. M. BYRNE, *On the role of angiogenesis in wound healing*, Proc. R. Soc. Lond. Ser. B-Biol. Sci., 263 (1996), pp. 1487–1493.

[165] G. J. PETTET, H. M. BYRNE, D. L. S. MCELWAIN, AND J. NORBURY, *A model of wound-healing angiogenesis in soft tissue*, Math. Biosci., 136 (1996), pp. 35–63.

[166] P. G. PHILLIPS, L. M. BIRNBY, A. NARENDRAN, AND W. L. MILONOVICH, *Modulation of angiogenesis: Experimental strategies and potential therapeutic applications*, Bladder Disease, 539 (2003), pp. 803–829.

[167] M. J. PLANK AND B. D. SLEEMAN, *A reinforced random walk model of tumour angiogenesis and anti-angiogenic strategies*, Math. Med. Bio., 20 (2003), pp. 135–181.

[168] ——, *Lattice and non-lattice models of tumour angiogenesis*, Bull. Math. Biol, 66 (2004), pp. 1785–1819.

[169] M. J. PLANK, B. D. SLEEMAN, AND P. F. JONES, *A mathematical model of tumour anglogenesis, regulated by vascular endothelial growth factor and the angiopoietins*, J. Theor. Biol., 229 (2004), pp. 435–454.

[170] T. D. POLLARD, *The cytoskeleton, cellular motility and the reductionist agenda*, Nature, 422 (2003), pp. 741–745.

[171] T. D. POLLARD AND G. G. BORISY, *Cellular motility driven by assembly and disassembly of actin filaments*, Cell, 112 (2003), pp. 453–465.

[172] L. PREZIOSI, ed., *Cancer modelling and simulation*, Chapman and Hall/ CRC, 2003.

[173] M. A. RAHMAN AND M. TOI, *Anti-angiogenic therapy in breast cancer*, Biomed. Pharmocother., 57 (2003), pp. 463–470.

[174] K. RAJANGAM, H. BEHANNA, M. HUI, X. HAN, J. HULVAT, J. LOMASNEY, AND S. STUPP, *Heparin binding nanostructures to promote growth of blood vessels*, Nano Lett., 6 (2006), pp. 2086–2090.

[175] J. RAJENDRAN AND K. KROHN, *Imaging hypoxia and angiogenesis in tumors*, Radiol. Clin. North Am., 43 (2005), pp. 169–187.

[176] S. RAMTANI, *Mechnical modelling of cell/ecm and cell/cell interactions during the contraction of a fibroblast-populated collagen microsphere: theory and model simulation*, J. Biomechanics, 37 (2004), pp. 1709–1718.

[177] A. ROCCARO, F. RUSSO, T. CIRULLI, G. D. PIETRO, A. VACCA, AND F. DAMMACCO, *Antiangiogenesis for rheumatoid arthritis*, Curr. Drug Targets Inflamm. Allergy, 4 (2005), pp. 27–30.

[178] A. ROSELL-NOVEL, J. MONTANER, AND J. ALVAREZ-SABIN, *Angiogenesis in human cerebral ischemia*, Rev. Neurol., 38 (2004), pp. 1076–1082.

[179] C. ROSELLO, P. BALLET, E. PLANUS, AND P. TRACQUI, *Model driven quantification of individual and collective cell migration*, Acta Biotheor., 52 (2004), pp. 343–363.

[180] S. ROUSSEAU, F. HOULE, H. KOTANIDES, L. WITTE, J. WALTENBERGER, J. LANDRY, AND J. HUOT, *Vascular endothelial growth factor (VEGF)-driven actin-based motility is mediated by VEGFR2 and requires concerted activation of stress-activated protein kinase 2 (SAPK2/p38) and geldanamycin-sensitive phosphorylation of focal adhesion kinase*, J. Biol. Chem., 275 (2000), pp. 10661–10672.

[181] E. RUDOLPH AND J. WOODS, *Chemokine expression and regulation of angiogenesis in rheumatoid arthritis*, Curr. Pharm. Design, 11 (2005), pp. 613–631.

[182] M. SEANDEL, K. NOACK-KUNNMANN, D. ZHU, R. AIMES, AND J. QUIGLEY, *Growth factor induced angiogenesis in vivo requires specific cleavage of fibrillar type I collagen*, Blood, 97 (2001), pp. 2323–2332.

[183] D. R. SENGER, K. P. CLAFFEY, J. E. BENES, C. A. PERRUZZI, A. P. SERGIOU, AND M. DETMAR, *Angiogenesis promoted by vascular endothelial growth factor: Regulation through $\alpha(1)\beta(1)$ and $\alpha(2)\beta(1)$ integrins*, PNAS, 94 (1997), pp. 13612–13617.

[184] G. SERINI, D. AMBROSI, E. GIRAUDO, A. GAMBA, L. PREZIOSI, AND F. BUSSOLINO, *Modeling the early stages of vascular network assembly*, The EMBO J., 22 (2003), pp. 1771–1779.

[185] M. SHEETZ, D. FELSENFELD, C. GALBRAITH, AND D. CHOQUET, *Cell migration as a five-step cycle*, Biochem. Soc. Symp., 65 (1999), pp. 233–243.

[186] M. M. SHOLLEY, G. FERGUSON, H. SEIBEL, J. MONTOUR, AND J. WILSON, *Mechanisms of neavascularization. Vascular sprouting can occur without proliferation of endothelial cells.*, Lab. Invest., 51 (1984), pp. 624–634.

[187] D. W. SIEMANN, D. J. CHAPLIN, AND M. R. HORSMAN, *Vascular-targeting therapies for treatment of malignant disease*, Cancer, 100 (2004), pp. 2491–2499.

[188] B. SIVAKUMAR, L. E. HARRY, AND E. M. PALEOLOG, *Modulating angiogenesis - more vs less*, J. Amer. Med. Assoc., 292 (2004), pp. 972–977.

[189] G. SIVASHINSKY, *On cellular instability in the solidification of a dilute binary alloy*, Physica D, 8 (1983), pp. 243–248.

[190] B. D. SLEEMAN, *Mathematical modelling of tumour growth and angiogenesis*, Adv. Exp. Med. Biol., 428 (1997), pp. 671–677.

[191] B. D. SLEEMAN, A. R. A. ANDERSON, AND M. A. J. CHAPLAIN, *A mathematical analysis of a model for capillary network formation in the absence of endothelial cell proliferation*, Appl. Math. Lett., 12 (1999), pp. 121–127.

[192] B. D. SLEEMAN AND H. A. LEVINE, *Partial differential equations of chemotaxis and angiogenesis*, Math. Meth. Appl. Sci., 24 (2001), pp. 405–426.

[193] B. D. SLEEMAN AND I. P. WALLIS, *Tumour induced angiogenesis as a reinforced random walk: Modelling capillary network formation without endothelial cell proliferation*, Math. Comput. Model., 36 (2002), pp. 339–358.

[194] C. L. STOKES AND D. A. LAUFFENBURGER, *Analysis of the roles of microvessel endothelial-cell random motility and chemotaxis in angiogenesis*, J. Theor. Biol., 152 (1991), pp. 377–403.

[195] K. V. STOLETOV, K. E. RATCLIFFE, S. C. SPRING, AND B. I. TERMAN, *NCK and PAK participate in the signaling pathway by which vascular endothelial growth factor stimulates the assembly of focal adhesions*, J. Biol. Chem., 276 (2001), pp. 22748–22755.

[196] G. STRANG, *On the construction and comparision of difference schemes*, SIAM J. Numer. Anal., 5 (1968), pp. 506–517.

[197] S. Y. SUN, M. F. WHEELER, M. OBEYESEKERE, AND C. W. PATRICK, *A deterministic model of growth factor-induced angiogenesis*, Bull. Math. Biol, 67 (2005), pp. 313–337.

[198] D. SZCZERBA AND G. SZEKELY, *A computational model of micro-vascular growth*, Comput. Sci., 3516 (2005), pp. 17–24.

[199] T. TARUI, M. MAJUMDAR, L. A. MILES, W. RUF, AND Y. TAKADA, *Plasmin-induced migration of endothelial cells - a potential target for the anti-angiogenic action of angiostatin*, J. Biol. Chem., 277 (2002), pp. 33564–33570.

[200] T. TENNANT, C. RINKER-SCHAEFFER, AND W. STADLER, *Angiogenesis inhibitors.*, Curr. Onco. Rpts., 2 (2000), pp. 11–16.

[201] G. THURSTON AND N. W. GALE, *Vascular endothelial growth factor and other signaling pathways in developmental and pathologic angiogenesis*, Int. J. Hematology, 80 (2004), p. 7.

[202] R. TOMANEK, *Assembly of the vasculature and its regulation*, Birkhauser, Boston, 2002.

[203] S. TONG AND F. YUAN, *Numerical simulations of angiogenesis in the cornea*, Microvasc. Res., 61 (2001), pp. 14–27.

[204] L. TRANQUI AND P. TRACQUI, *Mechanical signalling and angiogenesis. The integration of cell-extracellular matrix couplings*, Comptes Rendus Acad. Sci. Ser. III-Sci. Vie-Life Sci., 323 (2000), pp. 31–47.

[205] P. A. UNDERWOOD, P. A. BEAN, AND J. R. GAMBLE, *Rate of endothelial expansion is controlled by cell: Cell adhesion*, Int. J. Biochem. Cell Bio., 34 (2002), pp. 55–69.

[206] B. VAILHE, D. VITTET, AND J. FEIGE, *In vitro models of vasculogenesis and angiogenesis.*, Lab. Invest., 81 (2001), pp. 439–452.

[207] R. VISSE AND H. NAGASE, *Matrix metalloproteinases and tissue inhibitors of metalloproteinases*, Circ. Res., 92 (2003), pp. 827–839.

[208] E. E. VOEST, *Angiogenesis: From understanding to targeting*, Biochim. Biophys. Acta, 1654 (2004), p. 1.

[209] D. WALGRAEF, *Spatio-Temporal Pattern Formation*, Springer, New York, NY, 1996.

[210] L. WEI, C. KEOGH, V. WHITAKER, M. THEUS, AND S. YU, *Angiogenesis and stem cell transplantation as potentioal treatments of cerebral ischemic stroke*, Pathophysiology, 12 (2005), pp. 47–62.

[211] A. WENGER, A. STAHL, H. WEBER, G. FINKENZELLER, H. AUGUSTIN, G. STARK, AND U. KNESER, *Modulation of in vitro angiogenesis in a three-dimensional spheroidal coculture model for bone tissue engineering*, Tissue Eng., 10 (2004), pp. 1536–1547.

[212] G. YANCOPOULOS, S. DAVIS, N. GALE, J. RUDGE, S. WIEGAND, AND J. HOLASH, *Vascular-specific growth factors and blood vessel formation.*, Nature, 407 (2000), pp. 242–8.

[213] S. YANG, J. GRAHAM, J. KAHN, E. SCHWARTZ, AND M. GERRITSEN, *Functional roles for PECAM-1 (CD31) and VE-cadherin (cd144) in tube assembly and lumen formation in three-dimensional collagen gels*, Am. J. Pathology, 155 (1999), pp. 887–895.

[214] S.-O. YOON, S.-J. PARK, C.-H. YUN, AND A.-S. CHUNG, *Roles of matrix metalloproteinases in tumor metastasis and angiogenesis*, J. Biochem. Mol. Biol., 36 (2003), pp. 128–137.

[215] M. H. ZAMAN, R. D. KAMM, P. MATSUDAIRA, AND D. A. LAUFFENBURGER, *Computational model for cell migration in three-dimensional matrices*, Biophys. J., 89 (2005), pp. 1389–1397.

[216] E. ZAMIR AND B. GEIGER, *Molecular complexity and dynamics of cell-matrix adhesions*, J. Cell Sci., 114 (2001), pp. 3583–3590.

[217] S. ZIGMOND, *Ability of polymorphonuclear leukocytes to orient in gradients of chemotactic factors*, J. Cell Bio., 75 (1977), pp. 606–616.